Intrinsic kinetics of

clathrate hydrate formation

Sébastien Bergeron, B.Eng.

Department of Chemical Engineering, McGill University, Montreal

May 2009

A thesis submitted to McGill University in partial fulfilment of the requirements
of the degree of Doctor of Philosophy

hier, seul un rêve pouvait le contenir

aujourd'hui, quelques centaines de pages le détaillent

demain, trois lettres suffiront

...

Abstract

The present thesis focuses on the intrinsic kinetics of clathrate hydrate formation to provide the fundamental data and modeling needed to predict hydrate growth. A novel hydrate growth model based on particle size distribution measurements and a concentration driving force was proposed. The reaction rate constant of propane hydrate formation was determined using the aforementioned model. The mole fraction of carbon dioxide and methane in the bulk liquid phase was measured at the onset of hydrate growth and thereafter in a semi-batch stirred tank crystallizer. It was found that the guest mole fraction in the bulk liquid phase increases with pressure, decreases with temperature and remains constant during at least the first thirteen minutes of the growth stage. Based on such measurements, an alternate formulation of the hydrate growth model, independent of the dissolution rate at the vapor-liquid water interface, was suggested. As a result, the reaction rate constant of both carbon dioxide and methane clathrate formation was determined and found to follow an Arrhenius-type relationship, increasing with temperature over a four-degree interval, while being insensitive to pressure over the range investigated. The temperature trend of the reaction rate constant of hydrate formation yielded positive activation energies for both carbon dioxide and methane hydrate growth. The carbon dioxide and methane solubility dependency on temperature in water under hydrate-liquid water and vapor-liquid water equilibrium was also demonstrated using fundamental thermodynamics.

Résumé

La présente thèse traite de la cinétique de formation des hydrates de gaz afin d'établir les données et la modélisation nécessaires à l'étude de leur croissance. Un modèle cinétique pour la formation des hydrates de gaz, intégrant des mesures de taille de particules et une force d'entraînement de concentration, a été développé et utilisé pour calculer la constante de vitesse de réaction des hydrates de propane. Des mesures de la fraction molaire du composé gazeux dans la phase liquide, au moment de la formation des hydrates et tout au long de leur croissance, ont été obtenues pour le dioxyde de carbone et le méthane. Les résultats ont démontré que cette fraction molaire augmente avec la pression, diminue avec la température et demeure constante durant au moins les premières treize minutes de la phase de croissance. Ces mesures ont permis de modifier le modèle cinétique pour le rendre indépendant de l'interface vapeur-eau liquide. Également, il a été démontré que la constante de vitesse de réaction des hydrates de dioxyde de carbone et de méthane obéit à la loi d'Arrhénius, augmentant avec la température sur un intervalle de quatre degrés centigrades, en plus d'être constante pour l'écart de pression considéré. L'effet de la température sur la constante de vitesse de réaction a permis de calculer une énergie d'activation positive pour la croissance des hydrates de dioxyde de carbone et de méthane. Enfin, l'effet de la température sur la solubilité du dioxyde de carbone et du méthane dans l'eau, tant pour un équilibre hydrate-eau liquide que vapeur-eau liquide, a été démontré à l'aide de la thermodynamique.

Contents

List of Figures

List of Tables

Acknowledgements

First and foremost, I would like to express my gratitude to my supervisor, Prof. Phillip Servio. Over the years, we have developed a relationship that reaches well beyond academic duties and blossomed into a profound friendship. Once my professor, now my supervisor, and forever a friend, thank you very much Phillip.

I am also grateful toward Prof. Arturo Macchi for his humor and his thinking outside the box.

I could not overlook the support of my wife over these past four years. She recognized and understood my devotion for my work and took a step back at times, when needed. Marie-Hélène, tu as rayonné sur chacune de ces pages et je sais que tu continueras à le faire dans ma vie, pour les années à venir...

I would also like to thank my research colleagues, especially Juan Beltrán, with whom I had never-ending discussions about the subtleties of clathrate hydrates. Another mark of recognition to Frank Caporuscio, Lou Cusmich, Alain Gagnon and Melanie Gorman, who went beyond the call of duty to help in every way they could.

At last, I would like to express my sincere recognition to the various funding agencies who contributed to this very research project, including the Natural Sciences and Engineering Research Council of Canada (NSERC), the Canadian Foundation for Innovation (CFI), the Canada Research Chair program (CRC), the Faculty of Engineering of McGill University (McGill Engineering Doctoral Award, Les Vadasz Fellowship) and the Department of Chemical Engineering of McGill University (Eugenie Ulmer Lamothe NSERC bonus).

Contributions of Authors

The following thesis is a manuscript-based document containing four peer-reviewed articles published, as well as one article currently in press. The author of the present thesis is the first author for all five publications and was responsible for the experimental work, the data analysis, as well as the writing of each article. Co-authors contributed in the editing and reviewing process only.

1. **Bergeron S.**, Beltrán J.G., Servio P. (in press) *Reaction rate constant of methane clathrate formation*, Fuel.

2. **Bergeron S.**, Servio P. (2009) CO_2 *and* CH_4 *mole fraction measurements during hydrate growth in a semi-batch stirred tank reactor and its significance to kinetic modeling*, Fluid Phase Equilibria, 276:150-155.

3. **Bergeron S.**, Servio P. (2008) *Reaction rate constant of* CO_2 *hydrate formation and verification of old premises pertaining to hydrate growth kinetics*, AIChE J., 54:2964-2970.

4. **Bergeron S.**, Servio P. (2008) *Reaction rate constant of propane hydrate formation*, Fluid Phase Equilibria, 265:30-36.

5. **Bergeron S.**, Servio P. (2007) *Theoretical temperature dependency of gas hydrate former solubility under hydrate-liquid water equilibrium*, Journal of Chemical Thermodynamics, 39:737-741.

Original Contributions

The following are original contributions arising from the present thesis.

1. Development of a clathrate hydrate growth model based on a concentration driving force, particle size distribution measurements and the reaction rate constant of hydrate formation.

2. Determination of the reaction rate constant of C_3H_8 clathrate formation at 274 K.

3. Measurement of both CO_2 and CH_4 mole fraction in the bulk liquid phase during hydrate growth in a semi-batch stirred tank crystallizer. The results indicated that the guest mole fraction increases with pressure, decreases with temperature and remains constant over at least the first 13 minutes of the growth stage.

4. Determination of the reaction rate constant of CO_2 and CH_4 clathrate formation over a four-degree interval (275 to 279 K).

5. Demonstration that the reaction rate constant of CO_2 and CH_4 clathrate formation follows an Arrhenius-type relationship, increasing with temperature. Pressure did not have a significant effect over the range investigated (~ 600 kPa increase for CH_4).

6. Demonstration of a positive activation energy for CO_2 and CH_4 hydrate growth.

7. Confirmation of both CO_2 and CH_4 solubility dependency on temperature in water under hydrate-liquid water and vapor-liquid water equilibrium using fundamental thermodynamics.

Chapter 1

Introduction

1.1   Rationale and objectives

In the last half-century, focus on clathrate hydrates has departed from a purely
scientific curiosity and industrial nuisance to gain general recognition due to their
potential. Publications in scientific journals as well as popular press demonstrate
such a growing interest, as the number of publications increased exponentially over
the last decades. From the Malik Production Research Program in Canada to the
joint project by Mitsui Engineering Shipbuilding Co., Ltd. and Chugoku Electric
Power Co., Inc. to complete a natural gas hydrate pellet production plant in Japan,
clathrate hydrates have successfully entered large-scale industrial processes. Nev-
ertheless, considerable knowledge gaps subsist in various fundamental areas of gas
hydrate research, including thermodynamics and kinetics. As such, the broad goals
of the current thesis were to model and measure the intrinsic kinetics of clathrate
hydrate formation. These studies were aimed at providing the fundamental data
and modeling needed to predict hydrate growth *in situ*, as well as for proper reac-
tor design aimed at large-scale hydrate production. In particular, a hydrate growth
model was developed to describe the growth stage of hydrate formation and to allow
the determination of the reaction rate constant of clathrate hydrate formation. The
former is the sole parameter that remains constant upon scale up as both heat and

mass transfer effects vary, representing a key parameter for any industrial reactor design, but also for studying the growth of gas hydrates *in situ*. Pure-component structure II propane, structure I carbon dioxide and structure I methane hydrates were investigated as they are the main components of most multi-component hydrate systems.

1.2 Description

The present thesis comprises five manuscripts. Following this introduction, necessary background information regarding various aspects of clathrate hydrates is presented in Chapter 2, including among others phase equilibria and kinetics of formation. Chapter 3 includes the manuscript entitled *Reaction rate constant of propane hydrate formation* published in the journal Fluid Phase Equilibria. In addition to describing a novel hydrate growth model, it reports the reaction rate constant of structure II propane hydrate formation. The manuscript entitled *CO_2 and CH_4 mole fraction measurements during hydrate growth in a semi-batch stirred tank reactor and its significance to kinetic modeling* published in the journal Fluid Phase Equilibria is included in Chapter 4. These experimental studies provide significant insights on the supersaturation of the bulk liquid phase at the onset of hydrate growth and thereafter, resulting in an alternate formulation of the kinetic model proposed in Chapter 3. Chapter 5 includes the manuscript entitled *Reaction rate constant of CO_2 hydrate formation and verification of old premises pertaining to hydrate growth kinetics*, which was published in the American Institute of Chemical Engineers Journal and demonstrates the use of the model presented in Chapter 4 to determine the reaction rate constant of structure I carbon dioxide clathrate formation. Chapter 6, with the manuscript *Reaction rate constant of methane clathrate formation* submitted to the journal Fuel, describes a similar approach to the one used in Chapter 5 to measure the reaction rate constant of methane hydrate formation. Both the temperature and pressure dependency of the reaction rate constant of clathrate hydrate formation is evaluated, unlike in Chapter 5 where only the ef-

fect of temperature on the reaction rate constant was investigated. Chapter 7, with the manuscript *Theoretical temperature dependency of gas hydrate former solubility under hydrate liquid-water equilibrium* published in the Journal of Chemical Thermodynamics, demonstrates the effect of temperature on the solubility of carbon dioxide and methane in water under both vapor-liquid water and hydrate-liquid water equilibrium using fundamental thermodynamics, providing a better understanding of the driving force for clathrate hydrate growth.

Chapter 2

Background

2.1 Historical perspectives and applications

Clathrate hydrates are nonstoichiometric crystalline inclusion compounds where gas or volatile liquid molecules are trapped inside cavities of hydrogen-bounded water molecules. Their discovery is attributed to Sir Humphrey Davy (1811) who noted that a solid forms in an aqueous solution of chlorine above the freezing point of water. Historically, research efforts on clathrate hydrates can be classified into three landmark periods. During the first century following their discovery, gas hydrates were perceived as a scientific curiosity and much of the research was aimed at identifying the components forming gas hydrates, as well as describing quantitatively their compositions and physical properties (Sloan, 1998a). That same period is also associated with a tendency to assume that clathrate hydrates are stoichiometric compounds, where the number of water molecules per guest molecule is fixed. However, it gradually became clear with the work of Villard (1895) and Schroeder (1927) that clathrate hydrates were nonstoichiometric and crystalline. The second period starting in 1934 marks a shift in gas hydrate research from a scientific novelty to a hindrance to the oil and gas industry. As such, Hammerschmidt (1934) first reported their presence in natural gas transmission lines, following which they gained industrial interest. The third period, from the mid-1960s until today, began with

the discovery of *in situ* gas hydrates in seafloor sediments along deep continental margins and in permafrost regions, as well as in extraterrestrial environments such as near the surface of Mars (Buffett, 2000). Due to their long history and untapped potential, clathrate hydrates are still studied nowadays in ways that reach back to all three landmark periods.

2.1.1   Pipeline blockage

The formation of gas hydrates in pipelines has adverse consequences, plugging transmission lines and causing costly production stoppages as long as several months (Sloan, 2003). As such, hydrate inhibition has become an important field of research with the development of thermodynamic, kinetic and antiagglomerant inhibitors (Chatti *et al.*, 2005). While thermodynamic inhibitors typically require large quantity ($\sim$ 60 %), the newly developed low dosage hydrate inhibitors only require concentrations between 0.1 and 1.0 % on a weight basis (Kelland, 2006). Thermodynamic inhibitors modify the thermodynamic conditions at which hydrates form (decrease in temperature or increase in pressure), whereas kinetic and antiagglomerant inhibitors prevent, retard or slow hydrate nucleation and growth.

2.1.2   *In situ* clathrate hydrates

The discovery of clathrate hydrates in Siberian permafrost by Makogon (1987) in 1965 paved the way to an unprecedented effort to quantify and map naturally occurring gas hydrates. Biogenic or thermogenic sources of methane, once combined with water in sediments, lead to the formation of clathrate hydrates (Kvenvolden, 1995). Even though the most recent estimates of methane hydrate deposits vary by two orders of magnitude (2.5×10^{15} - 120×10^{15} m^3 at standard temperature and pressure conditions) (Klauda and Sandler, 2005; Milkov, 2004), the quantities involved are significant compared to other fossil fuel reserves. Various projects worldwide are currently underway to assess the viability of *in situ* gas hydrate extraction, from the Messoyakha gas field in Siberia (Russia) to the Malik Production Research Program

in the Mckenzie Delta (Canada). Gas hydrates are thus viewed as a tangible alternative energy source with potentially twice as much organic carbon than current fossil fuel reserves (Suess *et al.*, 1999). At the same time, those vast and abundant gas hydrate deposits present a risk for accelerating climate change and causing geohazards. As pointed out by Kenneth *et al.* (2002), methane released from clathrate hydrates may have caused significant global warming as little as 15,000 years ago.

2.1.3 Carbon dioxide sequestration

A huge reduction of carbon dioxide emissions is required in order to stabilize the atmospheric concentrations of greenhouse gases. Marine carbon dioxide sequestration represents the largest available sink (Gentzis, 2000). Numerous studies have been and are still conducted to assess the potential and risks associated with ocean disposal of carbon dioxide. Brewer and co-workers (1999) conducted field experiments to study the fate of liquid carbon dioxide in seawater at depths where hydrate formation occurs. Holder *et al.* (1995) modeled the formation of clathrate hydrates during injection of carbon dioxide in the ocean. Harrison *et al.* (1995) studied in details the geochemical interactions resulting from carbon dioxide disposal on the seafloor. While marine sequestration is currently in the experimental stage, much controversy still subsists regarding the long-term stability of carbon dioxide hydrates in deep oceans and their impact on marine life (Harrison *et al.*, 1995). Some even suggest that sequestration in environmentally active carbon pools such as the oceans seems ill advised, trading one environmental problem for another (Lackner, 2003).

2.1.4 Transportation and storage of natural gas

Benesh (1942) was the first to suggest the use of gas hydrates to increase the load factor of gas supply systems. More conventional methods such as liquefied natural gas (LNG) or compressed natural gas (CNG) require vey cold temperatures (typically -162 ^{o}C) and elevated pressures (above 20,000 kPa) respectively (Thomas

and Dawe, 2003). On the other hand, natural gas hydrates can be transported at a temperature as high as -5 ºC under atmospheric pressure with a negligible dissociation rate (Gudmundsson *et al.*, 1994), while long-term storage is achieved at normal temperatures (0 to -10 ºC) and pressures (1,000 to 100 kPa) (Thomas and Dawe, 2003). The milder operating conditions for transportation and storage of natural gas or liquid petroleum gases (Giavarini *et al.*, 2003) in hydrate form, and its resulting easier, safer and cheaper production compensate for the smaller storage capacity. More precisely, 160, 200 and 637 m^3 of gas at standard operating temperature and pressure can be stored in gas hydrates, compressed gas and liquefied gas respectively (Thomas and Dawe, 2003). Takaoki *et al.* (2005) even reported the startup of a process development plant in Japan aimed at producing natural gas hydrate pellets for cargo transportation.

2.1.5 Separation processes

The fact that gas hydrates contain only water and the hydrate-forming substances with a composition in the hydrate crystal different than in the original mixture shows great potential for various separation technologies. Werezak (1969) investigated the possibility of using gas hydrates to concentrate temperature sensitive and/or viscous solutions. Phillips *et al.* (1991) described a process where clathrate hydrates are used to recover proteins encapsulated in reversed micellar solutions. More recently, Jean-Baptiste and Ducroux (2003) explored the potential of clathrate hydrates as a means to capture carbon dioxide from flue gas exhausted by power plants. Numerous studies were also conducted in the sixties and seventies to study the possibility of water desalination via gas hydrates. While the feasibility was demonstrated, the process never found its way in industry because it was not economically viable (Englezos, 1993).

2.1.6   Cool storage

Due to the phase change involved when gas hydrates form from an aqueous solution, gas hydrate slurries are perceived as a potential refrigerant. Their large heat of fusion (Kang *et al.*, 2001), combined with their phase change temperature above the freezing point of water (Sloan and Koh, 2007), makes them relevant in the field of air conditioning. The fact that they could be part of a distributed cool-storage system charged using off-peak electricity at night and discharged during the day further highlights their potential (Mori and Mori, 1989). As such, several studies, including those of Darbouret *et al.* (2005), are conducted to evaluate the rheological properties of clathrate hydrate slurries acting as refrigerants.

2.1.7   Hydrogen storage

Following the discovery that hydrogen can form a clathrate hydrate at elevated pressures (1.5 GPa) (Dyadin *et al.*, 1999), it was suggested that hydrogen hydrates could represent a clean, safe and affordable storage material for mobile applications (Mao *et al.*, 2007). Additional research (Florusse *et al.*, 2004) confirmed that a second guest such as tetrahydrofuran (THF) can drastically reduce by two orders of magnitude the forming pressure of hydrogen clathrates. Recent advancements have shown that the hydrogen content in THF-containing binary clathrate can be increased to 4 % (weight basis) at modest pressures by tuning their composition (Lee *et al.*, 2005). Nevertheless, the key challenge to hydrogen storage in hydrate form remains the balance between the storage capacity and the requirements for mild pressure and temperature conditions (Koh and Sloan, 2007).

2.2   Structure

Clathrate hydrates are nonstoichiometric crystalline inclusion compounds consisting of approximately 85 % water on a molecular basis. Under suitable temperature and pressure conditions, gas or volatile liquid molecules (guest) are enclosed in cav-
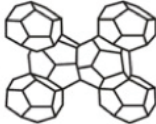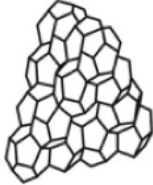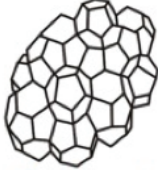
Guests	Structure	Water Cavities			
CH_4 / CO_2	sI	2 5^{12}		6 $5^{12}6^2$	
C_3H_8 / N_2	sII	16 5^{12}		8 $5^{12}6^4$	
CH_4 + C_6H_{14}	sH	3 5^{12}		2 $4^35^66^3$	1 $5^{12}6^8$

Figure 2.1: Three common hydrate unit crystal structures.

ities (host) composed of hydrogen-bounded water molecules. Weak van der Waals forces exist between the host and guest molecules. The most common structures of clathrate hydrates found in nature are both cubic structures I (sI) and II (sII) as well as hexagonal structure H (sH), as shown in Figure 2.1.

X-ray diffraction data from McMullan and Jeffrey (1965) on ethylene oxide hydrate confirmed structure I clathrates. sI hydrates contain 2 small cavities and 6 large cavities per unit cell. The 12-sided small cavity is a pentagonal dodecahedron (5^{12}) with 12 pentagonal faces, while the 14-sided large cavity is a tetrakaideca-hedron ($5^{12}6^2$) with 12 pentagonal and 2 hexagonal faces (Sloan and Koh, 2007). The cubic sI cell also contains 46 water molecules and the lattice parameter is 12 Å

(Sloan and Koh, 2007). Predominantly found in the Earth's natural environments, sI hydrates typically contain small (0.4 - 0.55 nm) guests such as methane, ethane and carbon dioxide (Sloan, 2003). While the overall cage occupancy depends on the operating conditions, Collins *et al.* (1990) reported an overall cage occupancy of 95 % for sI methane hydrate.

Claussen (1951) first suggested the polyhedral framework for type II gas hydrate. Mark and McMullan (1965) later on confirmed such a structure through X-ray diffraction of the double hydrate of tetrahydrofuran and hydrogen sulfide. sII hydrates contain sixteen 12-sided pentagonal dodecahedron (5^{12}) (also found in structure I) and eight 16-sided hexakaidecahedral cavities ($5^{12}6^4$) with 12 pentagonal and 4 hexagonal faces (Sloan and Koh, 2007). The face centered cubic sII cell contains 136 water molecules with a lattice parameter of 17.3 Å (Sloan and Koh, 2007). Contrary to sI, sII clathrates are mostly found in man-made environments with larger guests (0.6 - 0.7 nm) such as propane and nitrogen (Sloan, 2003).

Structure H was discovered more recently by Ripmeester *et al.* (1987). It consists of three 12-sided pentagonal dodecahedron (5^{12}) (found in both sI and sII), as well as 2 dodecahedron cavities ($4^35^66^3$) with 3 square, 6 pentagonal and 3 hexagonal faces and 1 icosahedron cavity ($5^{12}6^8$) with 12 pentagonal and 8 hexagonal faces (Sloan and Koh, 2007). The hexagonal sH unit cell contains 34 water molecules with lattice parameters of 12.2 and 10.1 Å (Sloan and Koh, 2007). sH hydrates occur both in natural and man-made environments but only with mixtures of small and large (0.8 - 0.9 nm) guests (Sloan, 2003) such as methane and neohexane.

As a rule of thumb, molecular size determines structure and equilibrium pressure, while the heat of dissociation (hydrate formation is an exothermic process) is a function of hydrogen bonds in the crystal, cage occupancy and is independent of guest components and mixtures of similar size components within a limited size range (Sloan and Koh, 2007). Less energy is required to dissociate structures with

multiple cavities filled, than those with only one type filled. Moreover, at very high pressure (typically in the GPa range), gas hydrates can undergo significant structural transitions, as summarized by Hirai *et al.* (2004). In particular, hydrogen, which forms structure II hydrates below 1 GPa, transforms to a filled ice II structure at around 1 GPa and a filled cubic ice Ic structure at around 2 GPa (Hirai *et al.*, 2004). Due to their high water content, gas hydrates have properties that generally resembled closely those of hexagonal ice (Ih), the most common solid form of water (Sloan and Koh, 2007). One notable exception includes a thermal conductivity 5 times less than that of ice, as measured first by Stoll and Bryan (1979) for propane hydrates. In addition, ice has been shown to deform several orders of magnitude faster than clathrate hydrates under the same applied stress (Durham *et al.*, 2003).

2.3   Phase equilibria

Following the discovery that gas hydrates can plug oil and gas transmission lines by Hammerschmidt (1934), extensive research was initiated to determine the conditions and systems for which gas hydrates can form. Efforts focused on gathering incipient gas hydrate formation data, as well as developing predictive methods for the calculation of phase equilibria. The former refers to the situation where an infinitesimal amount of the hydrate phase is present in equilibrium with other fluid phases. The most common method used was introduced by Deaton and Frost (1946) and is referred to as the isothermal pressure-search method. The hydrate-forming system is kept at constant temperature while the pressure is slowly increased and monitored for gas hydrate formation. Repeating such a procedure over a wide range of temperatures produces a partial phase diagram in the hydrate-forming region. The temperature is usually fixed and the pressure adjusted to reach both thermal and mechanical equilibrium faster than with a fixed pressure and adjustable temperature. An extensive list of gas hydrate phase equilibrium data for numerous systems is given by Sloan (2007).

With the elucidation of the various clathrate hydrate structures came the development of a statistical thermodynamics model describing the hydrate phase. The model of Van der Waals and Platteeuw (1959) represents the best example of the use of statistical thermodynamics in industry on a routine basis. For the vapor phase, any equation of state can be used. Over the years, the Peng-Robinson (1976), the Redlich-Kwong (1949) and the Trebble-Bishnoi (1987; 1988) equations of state have been used extensively. Similarly, a suitable equation of state can be used for the liquid phase, as well as an activity coefficient model. Bishnoi *et al.* (1989) first formulated and solved for the amount of gas hydrates formed from a given mixture by simultaneously solving the equilibrium and mass balance equations. The solution was based on an algorithm that solves both the phase equilibria and stability equations in a multi-component system (Gupta *et al.*, 1991).

2.4 Solubility of gases in the presence of hydrates

While the solubility of gases in water under vapor-liquid water equilibrium has been extensively studied over the years (IUPAC-NIST, various years), very few studies have been conducted on the solubility of the guest in water in the presence of gas hydrates. Due to their potential applications, most efforts have been directed toward methane-water and carbon dioxide-water systems, while other systems (*e.g.* propane-water) have been investigated more scarcely (Gaudette and Servio, 2007). Experimental measurements, as well as semi-empirical models, have been used to infer the temperature and pressure dependency of the gas solubility in water under hydrate-liquid water equilibrium.

The temperature effect on the solubility of the gas hydrate former in water is well established. The experimental work of Servio and Englezos (2001; 2002), Kim *et al.* (2003) and Yang *et al.* (2000; 2001) have all shown a positive trend, meaning that the solubility of the gas hydrate former in water increases with increasing temperature under hydrate-liquid water equilibrium, whereas the trend is reversed under

vapor-liquid water equilibrium. Zatsepina and Buffet (1997) coupled the Van der Waals and Platteeuw (1959) model with the Parrish and Prausnitz (1972) model and the Trebble-Bishnoi equation of state (1987) to show that temperature variations are more significant than pressure variations when establishing equilibrium conditions in marine sediments. While semi-empirical models have corroborated the experimental evidence of the temperature dependency of the guest solubility in water in the presence of hydrates, to the best of the author's knowledge a demonstration using fundamental principals has not been proposed yet.

Unlike temperature, much controversy exists regarding the pressure effect on the guest solubility in water under hydrate-liquid water equilibrium. The experimental measurements of Yang *et al.* (2000; 2001), Servio and Englezos (2001; 2002) and Kim *et al.* (2003) highlighted the weak pressure dependency of the guest solubility in water under hydrate-liquid water equilibrium without confirming the exact trend. Measurements performed by Seo and Lee (2002) and more recently Raman studies conducted by Lu *et al.* (2008) suggest that methane solubility in water decreases with increasing pressure under hydrate-liquid water equilibrium. Such a conclusion is in agreement with the work of Handa (1990) who showed the same trend using the model of Van der Waals and Platteeuw (1959). Interestingly, Someya *et al.* (2005) concluded that carbon dioxide solubility in water increases with increasing pressure under hydrate-liquid water equilibrium, while specifying that the pressure effect is not clear for temperatures below 4 ℃.

The data available in the literature regarding the mole fraction of the guest in the bulk liquid phase at the onset of hydrate growth and thereafter are even scarcer. Several researchers have assumed that the concentration of the guest in the bulk liquid phase drops from its turbidity value to its two-phase (Hashemi *et al.*, 2007b) or three-phase (Englezos *et al.*, 1987a; Chun and Lee, 1996) equilibrium value at the onset of hydrate growth. Assuming the former case, Hashemi *et al.* (2007b) have shown, from a modeling point of view and using the data of Clarke and Bishnoi

(2005), that the supersaturation of the bulk liquid phase (*i.e.* the concentration of the guest exceeding its equilibrium value) is null at the onset of growth, and increases over approximately the first 100 seconds of the growth stage and decreases thereafter, never exceeding 0.4 %. The work of Teng and Yamasaki (1998) is the only reference to solubility measurements performed in the hydrate-forming region in the metastable state in the absence of hydrates, as reported by Ohmura and Mori (1999).

2.5   Kinetics of formation

Experiments on the kinetics of clathrate hydrate formation typically involve a mole consumption plot, where the amount of gas consumed is plotted as a function of time. Nowadays, most kinetic setups are based on the pioneering work of Bishnoi and co-workers (1983; 1985; 1987; 1987a) to produce similar mole consumption plots. As shown in Figure 2.2, several gas reservoirs are used to maintain the pressure inside the crystallizer constant and to allow for differential pressure measurements. The bias reactor is pressurized above the crystallizer operating pressure. A differential pressure transducer is connected to the crystallizer and bias reactor (dP). The reservoir is also pressurized above the crystallizer operating pressure, while the bias reservoir is pressurized above the reservoir pressure to allow for a positive differential pressure measurement between the two. Upon a decrease in the crystallizer pressure, a control valve connecting both the gas reservoir and the crystallizer opens to let gas flow to the crystallizer, hence maintaining the desired operating pressure. Pressure measurements are recorded using a data acquisition device. Using the gas reservoir volume, temperature and pressure measurements, as well as a suitable equation of state, the pressure and time measurements can be converted to the desired mole consumption plot.

A typical mole consumption plot is displayed in Figure 2.3 for a semi-batch stirred tank crystallizer. Initially, liquid water is introduced inside the crystallizer and the
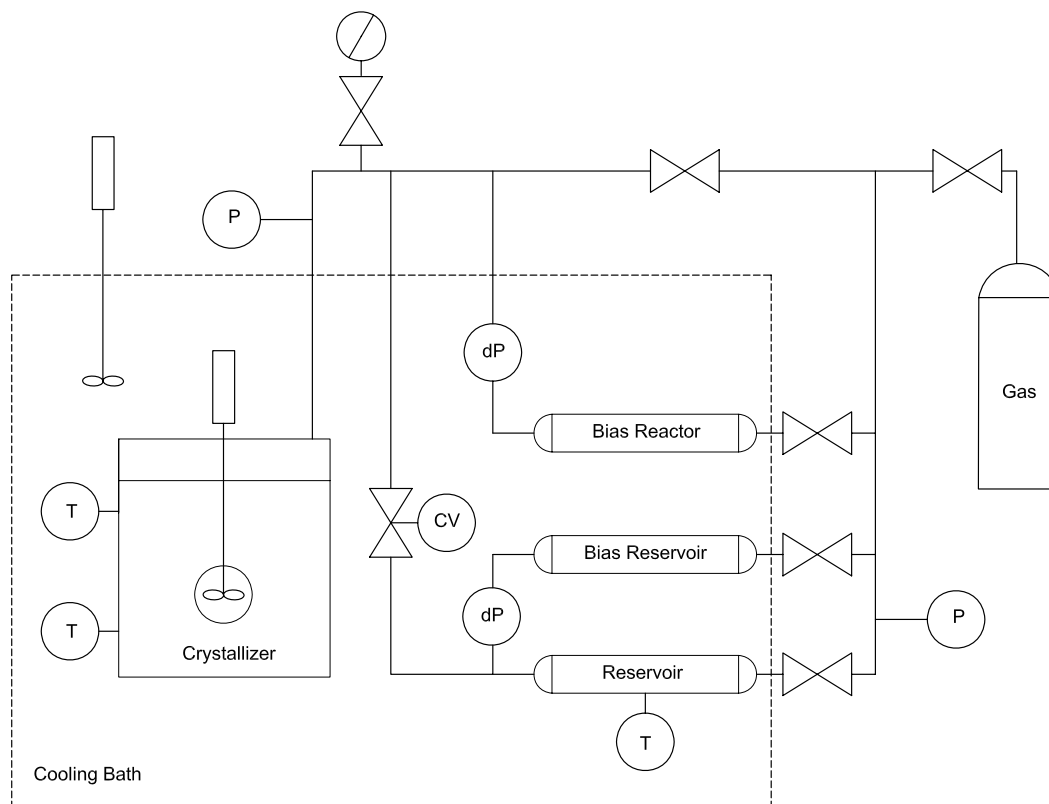
Figure 2.2: Typical setup for kinetic studies in a semi-batch stirred tank crystallizer.

system is pressurized to the desired pressure. In the case of pure-component gas hydrates, the gas used is the guest component. As it can be seen from Figure 2.3, three distinct regions can be identified during kinetic experiments. The first step is the dissolution stage. During this period, some of the gas present in the vapor phase diffuses across the vapor-liquid water interface and dissolves in the aqueous phase. The rate at which gas diffuses across the interface is a function of the interfacial area and mass transfer coefficient, both strongly depending on the agitation. Since the operating conditions are within the hydrate-forming region, the amount of gas dissolved in the aqueous phase will exceed the hypothetical two-phase vapor-liquid water equilibrium value at the given temperature and pressure conditions. Because
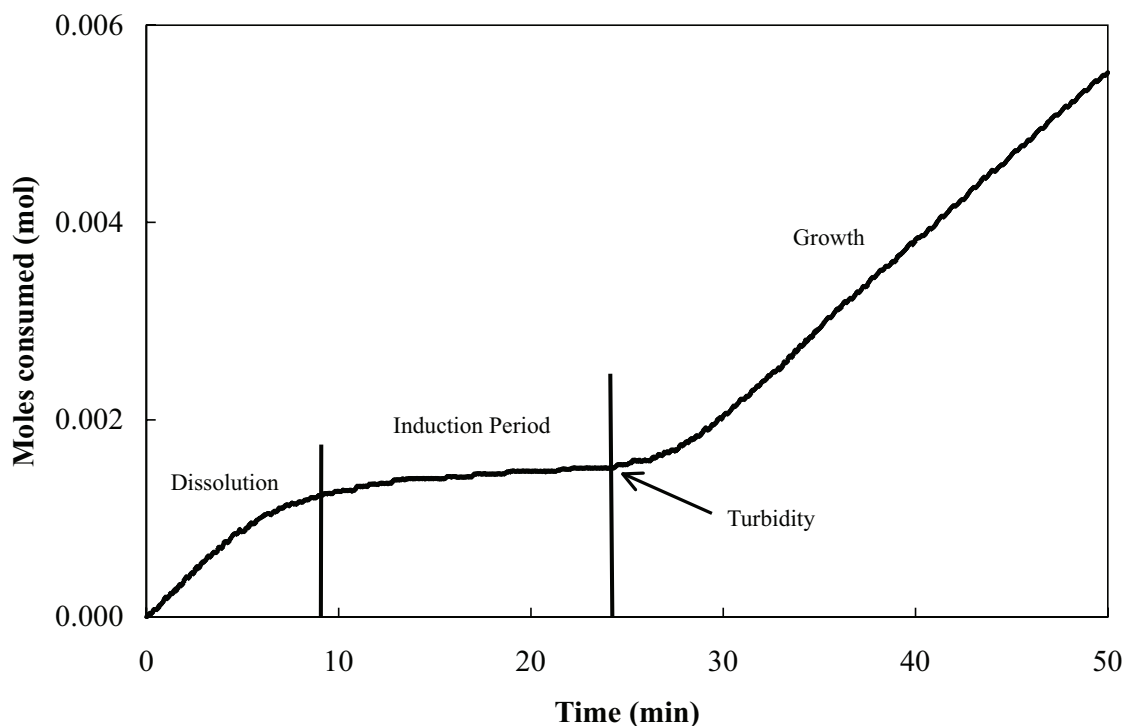
Figure 2.3: Propane gas consumption under hydrate-forming conditions at 274.2 K and 340.4 kPa.

hydrate formation is characterized by the appearance of crystals, it can be classified as a crystallization process, meaning that a state of supersaturation is essential (Mullin, 1997). At the onset of supersaturation begins the induction period, as shown in Figure 2.3. During this time, crystals form and decompose until they form a stable nucleus (nucleation) and grow to a detectable size (Mullin, 1997). Hence, the induction period is most likely dominated by the nucleation period, but also includes growth up to the point at which gas hydrates can be detected. The turbidity point marks the beginning of the growth stage, which corresponds to the last period shown in Figure 2.3. If the growth stage is left to proceed indefinitely, a decreasing gas consumption will follow, as heat and mass transfer effects will alter the rate of clathrate hydrate formation.

2.5.1   Induction period

As mentioned previously, the induction period comprises the time required for the crystals to form stable nuclei (nucleation time) and to grow to a detectable size (growth time). It is extremely difficult to isolate these steps. The estimation of the nucleation time, which depends on supersaturation, is speculative, whereas the time needed for a nucleus to be detected depends on the detection method and growth rate at this early stage (Mullin, 1997). This particular growth rate is difficult to predict since the rate of growth of a nucleus cannot be assumed to be in the same order of magnitude as that of a macrocrystal (Mullin, 1997). Nevertheless, numerous studies have been conducted to model the induction time of clathrate hydrate formation using two different approaches. The first method, or the supercooling point, represents the temperature of spontaneous freezing of a solution submitted to a constant cooling rate, such as in the work of Wilson *et al.* (2005). The other method involves holding the sample at a constant temperature and varying the driving force to measure the induction time, such as in the work of Natarajan *et al.* (1994) and Jensen *et al.* (2008). In general, the induction period is stochastic at low driving force, but less so at higher driving force (Sloan and Koh, 2007). Data and correlations regarding induction times should be used cautiously, as induction times are very scattered (particularly at low driving force under isothermal conditions), apparatus-dependent (surface area, rate of heat and mass transfer) and time-dependent (gas composition, foreign particles) (Sloan and Koh, 2007).

2.5.2   Primary nucleation

As pointed out by Mullin (1997), the condition of supersaturation or supercooling alone is necessary, but not sufficient for a system to crystallize. Before the appearance of crystals, there must exist in the solution a number of nuclei or seeds acting as centres of crystallization (Mullin, 1997). Purely homogeneous nucleation, which is rarely encountered in real world systems, occurs in the absence of impurities with a sequential formation of clusters of increasing size. Until the critical cluster size is

reached, clusters of molecules form, grow or shrink (Sloan and Koh, 2007). Once the critical cluster size is reached, spontaneous growth follows. The change in free energy of the system is due to the appearance of a new phase (ΔG_v) and the formation of a boundary between the phases (ΔG_s). Thus, the change in free energy of the system can be expressed as (Callister, 2003):

$$\Delta G = \Delta G_s + \Delta G_v = 4\pi r^2 \sigma + \frac{4}{3}\pi r^3 \Delta g_v \tag{2.1}$$

where σ is the interfacial tension and Δg_v is the free energy change of the transformation per unit volume of product formed. The maximum value in the overall excess free energy, ΔG_{crit}, corresponds to the critical nucleus size, r_c, and is obtained by maximizing equation 2.1:

$$r_c = \frac{-2\sigma}{\Delta g_v} \tag{2.2}$$

Using equation 2.1 and equation 2.2, it follows:

$$\Delta G_{crit} = \frac{4\pi\sigma r_c^2}{3} \tag{2.3}$$

With increasing supersaturation, the free energy barrier decreases to a point where nucleation can become spontaneous. In their work, Englezos *et al.* (1987a) suggested an expression for the free energy change per unit volume of product formed, as contained in equation 2.2 and based on bulk phase properties:

$$\Delta g_v = -\frac{RT}{v_H}\left(ln\frac{f^b}{f^{HLV}} + \frac{\eta_w v_w\left(P^{exp} - P^{HLV}\right)}{RT^{exp}}\right) \tag{2.4}$$

where v_H is the molar volume of the hydrate, v_w the molar volume of water and η_w the number of water molecules per gas molecule. The ratio of fugacities includes the fugacity of the gas in the bulk liquid phase, f^b, and that under three-phase equilibrium at the experimental temperature, f^{HLV}. Using equations 2.2 and 2.4, Englezos *et al.* (1987a) calculated a critical diameter for methane between 6 - 34 nm, while Nerheim *et al.* (1992) measured (light scattering), 30 seconds after the onset of

nucleation, a mean diameter above 100 nm for the methane + propane hydrate.

In practice, homogeneous nucleation is very difficult to achieve, as aqueous solutions found in laboratories can contain more than 10^6 particles per cm^3 (Mullin, 1997). Hence, heterogeneous nucleation is more likely to occur due to the presence of impurities or of a surface (fluid interface, wall). As a result, the overall free energy change associated with the formation of a critical nucleus under heterogeneous conditions, $\Delta G'_{crit}$, is less than its homogeneous counterpart (Mullin, 1997):

$$\Delta G'_{crit} = \lambda \Delta G_{crit} \tag{2.5}$$

where λ is less than unity and is a function of the contact angle between the crystalline deposit and the foreign surface. Long and Sloan (1996) collected experimental evidence that gas hydrate nucleation preferentially occurs near the vapor-liquid water interface in a quiescent system. In addition to a lower Gibbs free energy due to the presence of a surface, the vapor-liquid water interface is the location with the highest concentration of host and guest molecules. Kvamme (2000) has also proposed a unified nucleation theory where nucleation occurs on the gas side of the vapor-liquid water interface.

2.5.3 Secondary nucleation

Primary nucleation refers to a situation where no crystals are initially present. On the other hand, the presence of particles, as well as particle-particle, particle-stirrer and particle-wall collisions can induce secondary nucleation. The first studies on the kinetics of clathrate hydrate formation (Englezos *et al.*, 1987a,b) assumed that nucleation only occurs at the onset of hydrate growth (crystallization) since the excess of gas dissolved in the solution is consumed. Englezos *et al.* (1987a) also considered secondary nucleation and agglomeration but found it to be negligible due to the size of the crystals involved, based on homogeneous nucleation theory, and the time over which the experiments were conducted. More recently, Herri *et*

al. (1999b) considered the possibility of a film at the vapor-liquid water interface where primary nucleation is continuously active. In addition, they performed extensive methane hydrate turbidimetry measurements (10 μm to 150 μm) to study the possibility of secondary nucleation (true secondary nucleation, breakage, attrition) and agglomeration (Herri *et al.*, 1999a,b). Herri *et al.* (1999b) concluded that a continuously active primary nucleation and growth model was sufficient to describe the early stage of crystallization, while attrition needed to be incorporated for longer times at high stirring rates.

2.5.4   Driving force for growth

To minimize heat and mass transfer effects, numerous researchers have studied clathrate hydrate formation in semi-batch stirred tank crystallizers resulting in the definition of several driving forces using either temperature, fugacity (chemical potential) or concentration (mole fraction). Vysniauskas and Bishnoi (1983; 1985) first studied the kinetics of methane and ethane hydrate formation and concluded that the rate of formation was a function of the interfacial area, pressure, temperature and degree of supercooling. They defined the driving force for hydrate growth as the difference between the three-phase equilibrium temperature (at the experimental pressure) and the experimental (bulk) temperature (Vysniauskas and Bishnoi, 1983, 1985). In their work, Englezos *et al.* (1987a; 1987b) defined the driving force as the difference between the fugacity of the dissolved gas (experimental temperature and pressure) and that at the experimental temperature but three-phase equilibrium pressure. The driving force proposed by Skovborg and Rasmussen (1994) is based on the difference between the mole fraction of the guest at the vapor-liquid water interface and that in the bulk. Mork and Gudmundsson (2002) on the other hand used the difference between the guest concentration at the vapor-liquid interface and that at the hydrate surface, the latter evaluated at the experimental pressure and three-phase equilibrium temperature. More recently, Hashemi *et al.* (2007b) defined the driving force for hydrate growth as the difference between the guest concentration at the vapor-liquid water interface and that at the hydrate-liquid wa-

ter interface. In both cases, the concentrations are evaluated at the experimental temperature and pressure (Hashemi *et al.*, 2007b). Hashemi *et al.* (2007b) did not use three-phase equilibrium conditions because their calculations, using the data of Clarke and Bishnoi (2005), showed that the increase in temperature at the crystal surface is negligible. It should be noted that a lack of knowledge regarding the concentration of the guest in the bulk liquid phase, as described in section 2.4, has prevented researchers from adopting the more general driving force for crystallization, as defined by Karpinski (1980) to be the degree of supersaturation in solute of the bulk liquid phase.

2.5.5 Growth models

Several hydrate growth models, with conflicting perspectives, have been proposed over the years for agitated systems. Following the work of Englezos *et al.* (1987a), it is agreed that hydrate formation is composed of three steps. Both the first and second steps involve diffusion of the guest, the former from the vapor-liquid interface to the bulk liquid and the latter from the bulk liquid to the hydrate-solution interface. The final step is the reaction of water and guest molecules at the hydrate-solution interface. Some models (Englezos *et al.*, 1987a) incorporate all three steps, while others consider the first two diffusion processes (Mork and Gudmundsson, 2002) or even only the transfer at the vapor-liquid water interface (Skovborg and Rasmussen, 1994). In a recent and extensive literature review of the available hydrate growth models, Ribeiro and Lage (2008) concluded that very few models do not present severe limitations. Considering the scope of the present thesis, the four most prominent models for hydrate growth in stirred vessels are briefly discussed.

The model of Englezos-Kalogerakis-Dholabhai-Bishnoi
The model of Englezos *et al.* (1987a), which was extended to mixtures (Englezos *et al.*, 1987b), is considered a pioneering exercise in the field of hydrate kinetics. Englezos *et al.* (1987a) suggested that hydrate growth comprises two steps, namely the diffusion of gas molecules from the bulk to the crystal-liquid interface through a

laminar diffusion layer, and the subsequent reaction considered an adsorption process where the gas molecules get enclathrated. The driving force for growth was defined as the difference between the fugacity of the dissolved gas at the experimental temperature and pressure (f), and the three-phase equilibrium fugacity at the experimental temperature (f^{HLV}) (Englezos *et al.*, 1987a). The growth rate, or gas consumption, for a hydrate particle with a surface area A_p is expressed as (Englezos *et al.*, 1987a):

$$\left(\frac{dn}{dt}\right)_p = KA_p(f - f^{HLV}) \tag{2.6}$$

where K is a kinetic constant accounting for the resistances in series associated with both steps described previously, and given by:

$$\frac{1}{K} = \frac{1}{k_r} + \frac{1}{k^l_{HL}} \tag{2.7}$$

where k_r is the reaction rate constant of hydrate formation and k^l_{HL} is the mass transfer coefficient around the hydrate particle. Assuming spherical particles distributed homogeneously in the reactor, a global reaction rate, R_g, is obtained by integrating the rate per particle over all particle sizes represented by the size distribution $\varphi(r, t)$:

$$R_g = 4\pi K\mu_2(f - f^{HLV}) \tag{2.8}$$

where μ_2 is the second moment of the particle size distribution and expressed as:

$$\mu_2 = \int_0^\infty r^2\varphi(r, t)\, dr \tag{2.9}$$

At the vapor-liquid water interface, Englezos *et al.* (1987a) employed the two-film theory to include the resistance for the gas to penetrate the liquid. Assuming that hydrates can form in the film at the interface and that the rate at which gas diffuses is equal to the rate at which hydrate particles grow, the component mass balance in the film yields:

$$D\frac{d^2C}{dy^2} = 4\pi K\mu_2(f - f^{HLV}) \tag{2.10}$$

Assuming a constant concentration of water in the system (C_w^0) and adopting Henry's law to relate the gas concentration to its fugacity, equation 2.11 can be rewritten as follows (Englezos *et al.*, 1987a):

$$\frac{DC_w^0}{H}\frac{d^2(f - f^{HLV})}{dy^2} = 4\pi K\mu_2(f - f^{HLV}) \tag{2.11}$$

where H is Henry's law constant and equation 2.11 satisfies the boundary conditions $f(y = 0) = f^V$ and $f(y = y_L) = f^b$ with y_L representing the film thickness and f^V the fugacity of the gas in the vapor phase (system T and P). The rate at which gas is transported to the liquid phase where it either dissolves or forms hydrates is related to the flux at the vapor-liquid water interface. Using equation 2.11, it follows (Englezos *et al.*, 1987a):

$$\frac{dn}{dt} = -\frac{DC_w^0 A_{LV}}{H}\left(\frac{df}{dy}\right)_{y=0} = \left(\frac{DC_w^0 \zeta A_{LV}}{Hy_L}\right)\left[\frac{(f^V - f^{HLV})cosh\zeta - (f^b - f^{HLV})}{sinh\zeta}\right] \tag{2.12}$$

where D is the diffusivity of the guest in the liquid phase, A_{LV} in the vapor-liquid water interfacial area, and ζ is the Hatta number defined as:

$$\zeta = y_L\sqrt{\frac{4\pi K\mu_2 H}{DC_w^0}} \tag{2.13}$$

A component mass balance is then performed in the bulk liquid phase yielding (Englezos *et al.*, 1987a):

$$\frac{df^b}{dt} = \frac{D\zeta a_{LV}}{y_L sinh\zeta}\left[(f^V - f^{HLV}) - (f^b - f^{HLV})cosh\zeta\right] - \frac{4\pi K\mu_2 H(f^b - f^{HLV})}{C_w^0} \tag{2.14}$$

where a_{LV} in the vapor-liquid water interfacial area per unit of liquid volume.

Once the second moment of the particle size distribution contained in equation 2.13 is obtained, equations 2.12 and 2.14 can be solved simultaneously to fit the adjustable parameter k_r to the experimental gas consumption. Since Englezos *et*

al. (1987a) did not perform any size distribution measurement, they relied on a population balance to calculate μ_2. They assumed a constant, size-independent growth rate, G, as well as instantaneous primary homogeneous nucleation at the onset of growth and secondary nucleation (α_2) proportional to the second moment (Englezos *et al.*, 1987a), yielding the following ordinary differential equations:

$$\frac{d\mu_0}{dt} = \alpha_2\mu_2 \qquad \mu_0(t=0) = \mu_0^0 \tag{2.15}$$

$$\frac{d\mu_1}{dt} = G\mu_0 \qquad \mu_1(t=0) = r_c\mu_0^0 \tag{2.16}$$

$$\frac{d\mu_2}{dt} = 2G\mu_1 \qquad \mu_2(t=0) = r_c^2\mu_0^0 \tag{2.17}$$

where the critical radius (r_c) is calculated assuming homogeneous nucleation theory combining equation 2.2 with equation 2.4. The initial number of hydrate particles, μ_0^0, is calculated using the excess of gas beyond the three-phase equilibrium concentration transformed into hydrate at turbidity (Englezos *et al.*, 1987a):

$$\mu_0^0 = \frac{3MW_H(n_{tb} - \frac{C_w^0 f^{HLV}}{H})}{4\pi V_L\rho_H r_c{}^3} \tag{2.18}$$

where MW_H and ρ_H represent the molecular weight and density of the hydrate, V_L is the volume of liquid in the reactor and n_{tb} is the number of moles of gas dissolved at turbidity (Figure 2.3). The growth rate, G, which is a function of time and distance from the vapor-liquid water interface, is averaged as follows (Englezos *et al.*, 1987a):

$$G = \left(\frac{1}{L_R}\right)\left[\int_0^{y_L}\left(\frac{dr}{dt}\right)dy + \left(\frac{dr}{dt}\right)_b(L_R - y_L)\right] \tag{2.19}$$

where L_R is the height of the multiphase mixture inside the reactor and dr/dt is given by:

$$\frac{dr}{dt} = \frac{KMW_H(f - f^{HLV})}{\rho_H} \tag{2.20}$$

Sloan and Koh (2007) pointed out that the model of Englezos *et al.* (1987a) is very sensitive to the number of moles consumed at the turbidity point, which is obtained using an equation of state and has yet to be verified experimentally. Furthermore, the driving force contained in the model of Englezos *et al.* (1987a), which is based on the ideal solution assumption, includes fugacities calculated at the experimental and three-phase equilibrium pressure (system T). However, under the operating conditions (system T and P), there exists only one possible equilibrium fugacity, that is the hydrate-liquid water equilibrium fugacity. Hashemi *et al.* (2007b) demonstrated that the temperature at the surface of the crystal can be assumed to be that of the bulk.

The model of Skovborg-Rasmussen

Skovborg and Rasmussen (1994) performed a critical analysis of the model proposed by Englezos *et al.* (1987a). In particular, the inability for the model of Englezos *et al.* (1987a) to predict a decreasing gas consumption for longer times led Skovborg and Rasmussen (1994) to believe that the transport of gas from the vapor phase to the bulk liquid phase was the rate-determining step. Accordingly, they formulated that the rate of gas consumption, which can be extended to mixtures, is given by (Skovborg and Rasmussen, 1994):

$$\frac{dn}{dt} = k_{LV}^l A_{LV} C_w^0 (x^{LV} - x^b) \tag{2.21}$$

where k_{LV}^l and A_{LV} are the mass transfer coefficient in the liquid film and interfacial area at the vapor-liquid water interface and C_w^0 is the initial concentration of water in the bulk liquid phase. The driving force is composed of the difference between the guest mole fraction in water at the vapor-liquid water interface at the experimental

temperature and pressure (in equilibrium with the vapor phase) and that in the bulk liquid phase, again at the experimental temperature and pressure. The former is obtained using a suitable thermodynamic model describing vapor-liquid water equilibrium, while the latter is calculated from component mass balances in each phase. Since Skovborg and Rasmussen (1994) only revisited the data of Englezos *et al.* (1987a), the interfacial area was taken from them, whereas the mass transfer coefficient was the sole adjustable parameter in their model and was determined by minimizing the error between the experimental data of Englezos *et al.* (1987a) and their own model predictions. As pointed out by Ribeiro and Lage (2008), the model of Skovborg and Rasmussen (1994) failed to yield the same interfacial area for a given reactor under the exact same operating conditions when applied to different gases, indicating a self-consistency problem in the model.

The model of Mork-Gudmundsson

Mork and Gudmundsson (2002) studied the rate of clathrate hydrate formation in a continuously stirred tank reactor and did not observe a difference in the rate of hydrate formation at equal subcooling but different temperature. Based on such an observation, they assumed that transport processes rather than kinetic processes dominate hydrate formation (Mork and Gudmundsson, 2002). Hence, they suggested that hydrate growth was controlled by the diffusion of gas through the interfaces (vapor-liquid and hydrate-liquid), and due to a lack of knowledge regarding the concentration of the guest in the bulk liquid phase they expressed the overall rate of formation as follows (Mork and Gudmundsson, 2002):

$$\frac{dn}{dt} = \frac{C^{LV} - C^{HL}}{\frac{1}{k_{LV}^l A_{LV}} + \frac{1}{k_{HL}^l A_c}} \tag{2.22}$$

where C^{LV} is the gas concentration at the vapor-liquid interface under vapor-liquid water equilibrium (system T and P) and C^{HL} is the gas concentration at the crystal surface under hydrate-liquid water equilibrium (system P and three-phase equilibrium T). The vapor-liquid water interfacial area and the crystal-liquid interface area

are denoted by A_{LV} and A_c respectively, while k_{LV}^l and k_{HL}^l denote the vapor-liquid mass transfer coefficient and the rate constant for diffusion through the liquid film surrounding the crystal. Both concentrations were calculated using Henry's law, while the denominator in equation 2.22, which includes the resistance at both interfaces and represents the overall mass transfer coefficient, was calculated using a relationship containing the power consumption (P_g) and the superficial gas velocity (v_{sg}), yielding the following expression for the gas consumption rate (Mork and Gudmundsson, 2002):

$$\frac{dn}{dt} = a_1 \left(\frac{P_g}{V_L}\right)^{a_2} v_{sg}{}^{a_3} (C^{LV} - C^{HL}) V_L \tag{2.23}$$

where V_L is the liquid volume in the reactor and a_1, a_2 and a_3 are fitting parameters.

Application of their model (Mork and Gudmundsson, 2002) to methane and natural gas hydrates indicated that the hydrate formation rate was almost proportional to the superficial gas velocity, while a weak dependence on the stirring rate was found (Mork and Gudmundsson, 2002). Mork and Gudmundsson (2002) suggested that the simplicity of their model, compared for instance to the model of Englezos *et al.* (1987a) which incorporates population balance equations, represent a suitable engineering tool for predicting clathrate hydrate formation rate in continuously stirred tank reactors.

The model of Herri-Pic-Gruy-Cournil

Herri *et al.* (1999b) recognized the importance of mass transfer at the vapor-liquid water interface but suggested that hydrate growth models need to include population balance equations. According to their model, a stirred reactor comprises two distinct regions: the vapor-liquid water interface where continuously active primary nucleation occurs due to the high supersaturation and the liquid bulk where crystals grow but primary nucleation is also possible depending on the supersaturation (Herri *et al.*, 1999b). The model of Herri *et al.* (1999b) thus combines two differ-

ential equations, including one for the mass balance of the guest in the bulk liquid phase:

$$\frac{dC^b}{dt} = k_{LV}^l a_{LV}(C^{LV} - C^b) - \frac{4\pi G \mu_2}{v_H(1 - \alpha_H)} \tag{2.24}$$

where $k_{LV}^l a_{LV}$ is the dissolution rate at the vapor-liquid water interface obtained from solubility measurements, C^{LV} is the concentration of the guest in water in equilibrium at the vapor-liquid water interface and C^b is the concentration of the guest in the bulk liquid phase. v_H is the molar volume of the hydrate, μ_2 is the second moment, G is the crystal growth rate and α_H is the volumetric fraction of hydrate in the solution-hydrate mixture and was omitted (Ribeiro and Lage, 2008) by Herri *et al.* (1999b). Assuming that diffusion of the gas from the bulk to the surface of the particle is the rate-limiting step for crystal growth, they suggested the following relation for the growth rate (Herri *et al.*, 1999b):

$$G = k_{HL}^l(C^b - C^{HL})v_H \tag{2.25}$$

where k_{HL}^l is the mass transfer coefficient from the liquid bulk to the surface of the particle and C^{HL} is the equilibrium concentration of the dissolved gas in the presence of hydrates. The conditions at which C^{HL} should be evaluated are not clearly stated in the work of Herri *et al.* (1999b). The second differential equation included in the model of Herri *et al.* (1999b) is a population balance, only valid for the bulk liquid phase, and assumes a size-independent crystal growth rate taking into account primary and true secondary nucleation, breakage, agglomeration and attrition:

$$\frac{d\varphi}{dt} + G\frac{d\varphi}{dr} = B(r) - D(r) \tag{2.26}$$

where φ is the particle density distribution, $B(r)$ is the net birth term and $D(r)$ is the net death term. Since the model of Herri *et al.* (1999b) accounts for both the nucleation and the growth stage, the initial conditions for equations 2.25 and 2.26 assume pure water ($C^b(0) = 0$, $\varphi(r, 0) = 0$), while infinitesimal size for the nucleated crystals is assumed resulting in the following boundary condition for equation 2.26

(Herri *et al.*, 1999b):

$$G\varphi(0,t) = J_{int} + J_b \tag{2.27}$$

where J_{int} and J_b denote the nucleation rate at the vapor-liquid water interface and that in the bulk liquid phase. The former was assumed to be a function of the gas concentration profile in the stagnant film at the vapor-liquid water interface, while the latter was assumed to be a function of the bulk supersaturation and position-independent (Herri *et al.*, 1999b).

Herri *et al.* (1999b) did not perform direct comparisons between their model and the experimental mole consumption. They were interested in determining the importance of primary and true secondary nucleation, as well as breakage, agglomeration and attrition. Their methane hydrate turbidimetry measurements, for particle sizes between 10 and 150 μm, showed that a primary nucleation and growth model was sufficient to describe the early stage of crystallization, whereas attrition needed to be included for longer times at high stirring rates (600 rpm) (Herri *et al.*, 1999b). The model of Herri *et al.* (1999b), in comparison to the other models described previously, is the only one to consider both the nucleation and the growth stage. The assumption of continuously active primary nucleation represents another departure from previous models and is a more general case, since the experimental data of Clarke and Bishnoi (2005) showed that the assumption of instantaneous nucleation is suitable under low supersaturation (driving force) conditions only. They defined the supersaturation as $[(f^V - f^{HLV})/f^{HLV}]$ (Clarke and Bishnoi, 2005), which is based on the driving force of Englezos *et al.* (1987a). Such conditions where shown to prevail for a supersaturation of 14 % or lower (Clarke and Bishnoi, 2005).

2.5.6   Reaction rate constant

Multiple studies have been performed to measure the intrinsic kinetics of clathrate hydrate formation using the models discussed in section 2.5.5. Englezos *et al.* (1987a; 1987b) measured the reaction rate constant of methane and ethane hy-

drate formation, as well as their mixtures, using their model. Their studies did not involve any size distribution measurement and was based on a population balance incorporating homogeneous nucleation theory and a constant number of hydrate particles (Englezos *et al.*, 1987a,b). They reported a value for the reaction rate constant in the order of 10^{-6} mol/(m² s MPa) for methane, with values decreasing from 274 to 276 K and increasing from 276 to 282 K (Englezos *et al.*, 1987a). Monfort and Nzihou (1993) followed with particle size distributions measurements (5.6 - 564 μm) to study the kinetics of cyclopropane hydrate formation. Malegaonkar *et al.* (1997) studied the kinetics of carbon dioxide and methane hydrate formation using a modified version of the model of Englezos *et al.* (1987a) to account for a minor inconsistency in the particle size used in the derivation, as well as the high solubility of carbon dioxide in water. Their approach was the same as the one used by Englezos *et al.* (1987a; 1987b), that is based on a population balance incorporating homogeneous nucleation theory and a constant number of hydrate particles. They obtained a reaction rate constant in the order of 10^{-5} mol/(m² s MPa) and 10^{-4} mol/(m² s MPa) for methane and carbon dioxide respectively (Malegaonkar *et al.*, 1997). As in the case of Englezos *et al.* (1987a), they reported a minimum value for the reaction rate constant at a temperature of 276 K (Malegaonkar *et al.*, 1997). Chun and Lee (1996) also used the model of Englezos *et al.* (1987a) to study the kinetics of carbon dioxide hydrate formation. Their values for the reaction rate constant of carbon dioxide hydrate formation were two orders of magnitude smaller than those of Malegaonkar *et al.* (1997) (Chun and Lee, 1996). Clarke and Bishnoi (2005) used the model of Englezos *et al.* (1987a) and particle size distribution measurements for chord lengths greater than 0.5 μm to study the kinetics of carbon dioxide hydrate formation. Their values for the reaction rate constant were one order of magnitude greater than those of Malegaonkar *et al.* (1997), while they reported a decreasing reaction rate constant from 274.15 to 277.15 K and an increasing one from 277.15 to 279.6 K (Clarke and Bishnoi, 2005). More recently, Hashemi *et al.* (2007b) modified the model of Englezos *et al.* (1987a) with a concentration driving force and revisited the data of Clarke and Bishnoi (2005). Hashemi *et al.*

(2007b) concluded that the second moment measured experimentally by Clarke and Bishnoi (2005) was three orders of magnitude smaller than that determined from a population balance using homogeneous nucleation theory and a constant number of hydrate particles. Hashemi *et al.* (2007b) also mentioned that due to inaccurate surface area measurements, a true reaction rate constant has yet to be determined.

In their studies, Vysniauskas and Bishnoi (1983; 1985) reported a negative activation energy for hydrate growth. They included both the temperature dependence of the reaction rate constant and that of the concentration of water and methane or ethane monomers at the interface, which they could not measure, in an Arrhenius expression (Vysniauskas and Bishnoi, 1983, 1985). Bollovaram *et al.* (2000), in their sII single crystal growth studies, suggested that the kinetic constant (a parameter combining the reaction rate constant, degree of subcooling and average heat transfer coefficient) follows an Arrhenius-type relationship, increasing with the degree of subcooling. Freer *et al.* (2001), in their methane film growth kinetic experiments, assumed an Arrhenius-type expression for the reaction rate constant of clathrate hydrate formation, yielding an activation energy for methane hydrate growth of 171 kJ/mol. As a comparison, Mullin (1997) reported a value of 40 - 60 kJ/mol for surface integration processes and of 10 - 20 kJ/mol for diffusion processes.

Chapter 3

Propane Clathrate Formation

3.1   Preface

As pointed out in Chapter 2, the most prominent hydrate growth models available in the literature are believed to contain limitations mostly because of a lack of technology at the time. Moreover, there are considerable discrepancies in the values reported for the reaction rate constant of hydrate formation among different authors using variations of the same model. Recognizing hydrate growth as a crystallization process, a new model for hydrate growth was developed. The approach used was that of the standard engineering expression, where the rate equals a driving force over a resistance. Pure-component propane hydrate was first studied to determine its reaction rate constant of formation due to the pressure rating (500 kPa) of the standard flow-through cell part of the particle size analyzer employed.

3.2 Reaction rate constant of propane hydrate formation

Sébastien Bergeron, Phillip Servio
Department of Chemical Engineering, McGill University, Canada

3.2.1 Abstract

Experimental data on the rate of formation of propane hydrates were obtained using a particle size analyzer capable of detecting particles with diameters as small as 0.6 nanometers, while operating in a closed loop system. Experiments were carried out at temperatures around 274 K and pressures between 314 and 340 kPa in a semi-batch stirred tank crystallizer. The experimental data were analyzed using a newly developed kinetic model based on crystallization theory and as a result, the actual reaction rate constant of propane hydrate formation was successfully determined. An average value of $(2.0\pm0.2) \times 10^{-7}$ m/s is reported at 274.2 K, while it was found that the dissolution rate of propane at the vapor-liquid water interface was enhanced by a factor of four during the growth stage, compared to the value obtained during typical solubility experiments.

3.2.2 Introduction

Gas hydrates are crystalline solids that form when a gas or a volatile liquid molecule suitable for hydrate formation is enclosed in a network consisting of water molecules linked together through hydrogen bonding. The presence of the hydrate-forming gas molecule stabilizes the water lattice through physical bonding via weak van der Waals forces. Up to now, three common hydrate structures have been reported in the literature, including structure I (sI), structure II (sII) and structure H (sH) (Sloan and Koh, 2007). In particular, carbon dioxide and methane form structure I hydrate, while propane and neohexane (in the presence of methane) form structure II and structure H hydrate respectively. Considerable research is being conducted

on gas hydrates due to their potential applications, including methane hydrates as an alternate energy source (Chatti *et al.*, 2005), storage and transportation of natural gas hydrates (Chatti *et al.*, 2005) or liquefied pretroleum gases (Giavarini *et al.*, 2003) and carbon dioxide sequestration (Chatti *et al.*, 2005). Such promising new technologies are reasons why kinetics studies should be further investigated. In particular, accurate determination of the reaction rate constant of hydrate formation is required for proper reactor design, as it is the only parameter affecting any reactor throughput and conversion that remains constant upon scale-up, while both heat transfer and mass transfer effects will vary. Figure 3.1 shows the three-phase equilibrium line for the propane-water system using the experimental data of Deaton and Frost (1946), where hydrate, liquid water and vapor are at equilibrium. Above the three-phase line, hydrate-liquid water is present, while below the line, vapor-liquid water is present. A typical mole consumption plot for a hydrate kinetic experiment is shown in Figure 3.2. The first stage is the dissolution stage where gas dissolves into the bulk liquid phase up to its equilibrium value, at the experimental temperature and pressure. Any further dissolution leads to a supersaturated solution where hydrate nuclei can form and decompose until they reach a critical nuclei diameter and grow to a detectable size. This subsequent step is called the induction period. Once the turbidity point is reached, that is when the mole consumption deviates from its constant value reached at the end of the induction period, the growth stage is initiated.

Various studies have been conducted to determine the reaction rate constant of gas hydrate formation. Englezos *et al.* (1987a; 1987b) performed experiments using methane and ethane hydrates without any particle size distribution measurement. They used an average growth based on a population balance and assumed homogeneous nucleation. Malegaonkar *et al.* (1997) repeated the same procedure (no particle size distribution measurement) and assumptions made previously by Englezos *et al.* (1987a), but for methane and carbon dioxide hydrates. More recently, Clarke and Bishnoi have performed experiments to determine the intrinsic reac-
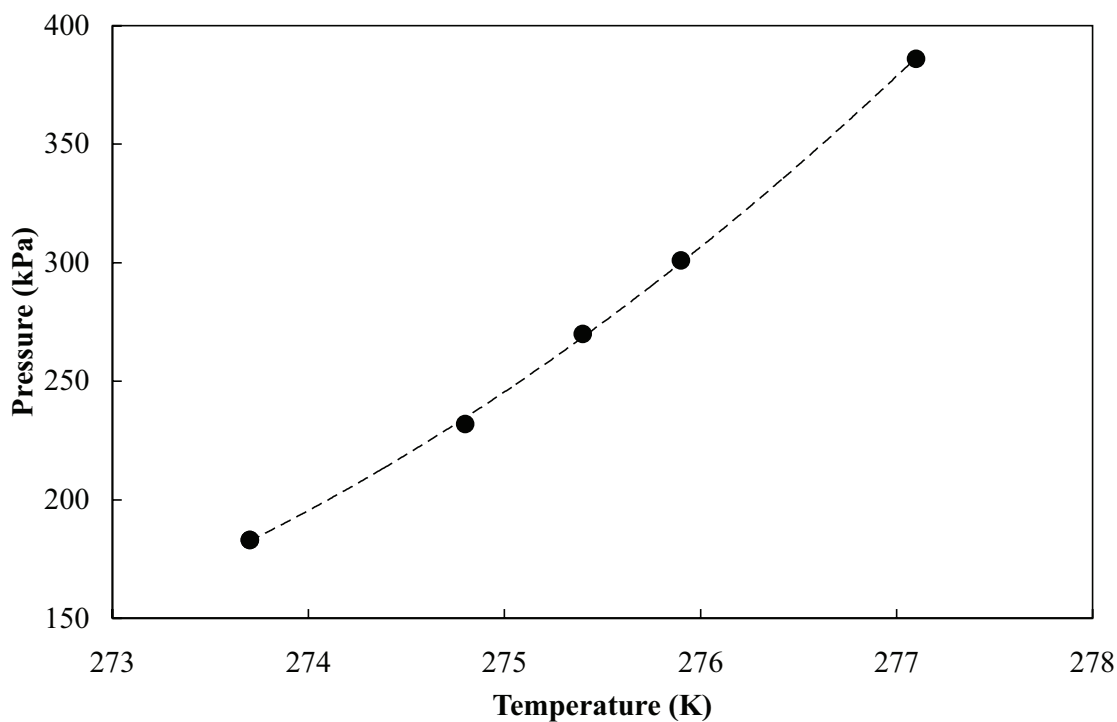
Figure 3.1: Propane-water three-phase hydrate-liquid water-vapor equilibrium line using the experimental data of Deaton and Frost (1946).

tion rate constant (formation and dissociation) for various hydrate systems (2000a; 2000b; 2001b; 2001a; 2004; 2005). Throughout their work, they used *ex situ* and *in situ* particle size analyzers to obtain the particle size distribution of both carbon dioxide and ethane gas hydrates, as well as mixtures of methane and ethane hydrates. The apparatus used allowed them to measure particles with chord lengths as small as 0.5 μm (Clarke and Bishnoi, 2005). Due to instrument limitations, they had to extrapolate their particle size distributions for chord lengths smaller than 0.5 μm. Recently, Hashemi *et al.* (2007b) have highlighted some points that need to be addressed concerning the determination of the intrinsic reaction rate constant of hydrate formation. The current work proposes a newly developed kinetic model based on the work of Englezos *et al.* (1987a; 1987b), as well as a novel experimental setup to accurately measure the true reaction rate constant of propane hydrate
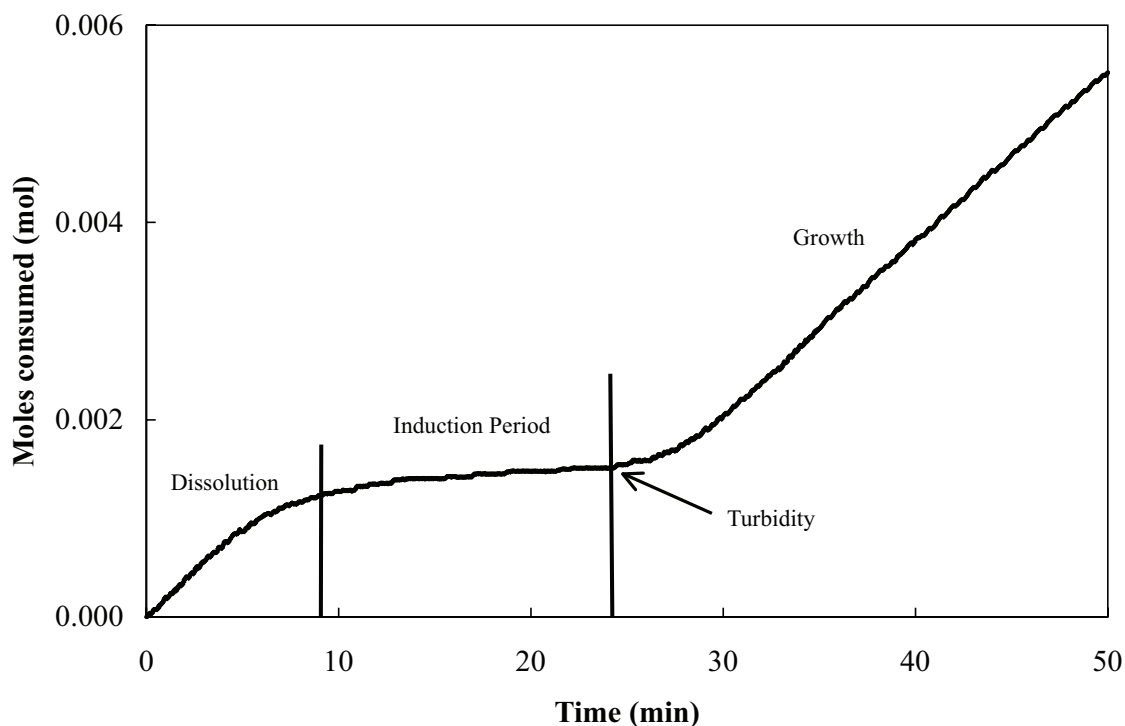
Figure 3.2: Propane mole consumption at 274.2 K and 340.4 kPa.

formation. This work can be readily expanded to other hydrate systems, including methane and carbon dioxide gas hydrates.

3.2.3 Experimental apparatus

As shown in Figure 3.3, the current experimental setup consists of an isothermal/isobaric semi-batch stirred tank crystallizer, a gas supply reservoir for hydrate formation and a Zetasizer Nano ZS particle size analyzer (Malvern Instruments). Hydrates are formed in the 600 cm^3 internal volume stainless steel crystallizer (12,000 kPa pressure rating). A PPI DYNA/MAG MM-006 mixer (0 - 2,500 rpm) has been mounted on top of the crystallizer to ensure sufficient mixing. Gas is supplied from the stainless steel reservoir (internal volume of 300 cm^3) using a Baumann 51000 Series Low Flow control valve. Both the crystallizer and the reservoir
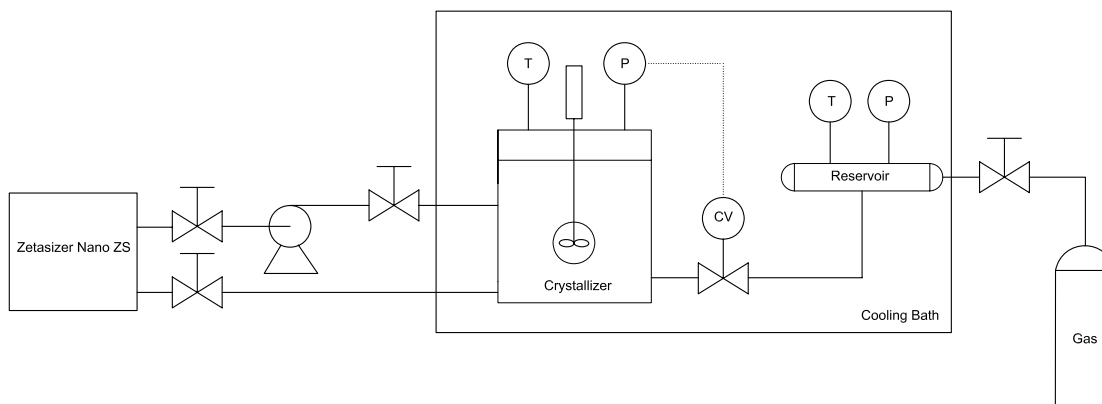
Figure 3.3: Simplified schematic of the experimental setup.

are submerged in a cooling bath controlled via a Thermo NESLAB RTE Series re-
frigerated bath. The liquid phase is continuously circulated through a flow cell with
a 500 kPa pressure rating (Hellma) in the Zetasizer Nano ZS particle size analyzer
by means of a LabAlliance Model 1500 dual piston pump. The Zetasizer Nano ZS
particle size analyzer is capable of detecting particles with diameters ranging from
0.6 nanometers to 6 micrometers, with a maximum uncertainty between 10 and
15 % on the size obtained from the intensity distribution. In addition, it has an in-
ternal cooling system to maintain the proper operating temperature inside the cell.
Temperature and pressure measurements are performed using standard resistance
temperature devices (± 0.3 ^{o}C) and Rosemount 3051S Series pressure transducers
with a reference accuracy of ± 0.04 % of the span. The readouts are then recorded
and displayed using the National Instruments NI-DAQ7 data acquisition device and
the LabVIEW software. The LabVIEW interface was written to calculate the num-
ber of moles of gas in the hydrate phase at any time during the experiment using
the Trebble-Bishnoi equation of state (1987), the gas reservoir temperature and
pressure measurements, as well as the gas reservoir volume, with an uncertainty of
$\pm 2 \times 10^{-4}$ mol.

3.2.4 Experimental procedure

Prior to any experiment, the crystallizer is cleaned using HPLC grade water and purged several times using the selected gas (propane with instrument grade 99.5 % purity). A syringe is used to introduce 180 ml of HPLC grade water and the dual piston pump is started. Once thermal equilibrium has been reached, the crystallizer is pressurized above the three-phase equilibrium pressure at the experimental temperature (Figure 3.1). Once the temperature in the reservoir and in the crystallizer has stabilized, both the data acquisition program and the crystallizer stirrer are started. Figure 3.2 shows a typical mole consumption plot for a kinetic experiment using propane. When the mole consumption deviates from its turbidity value (onset of growth), a particle size distribution measurement is performed in order to determine the critical nuclei diameter. Accordingly, the dual piston pump is shut off and the particle size analyzer is isolated by means of manual valves and a measurement is performed. Once the measurement is completed, the manual valves are reopened and the dual piston pump is restarted. Various particle size distribution measurements are performed at regular time intervals to properly describe the growth stage of hydrate formation.

3.2.5 Theory

3.2.5.1 Kinetic model

The newly developed kinetic model was derived using crystallization theory and is based on the Englezos model (1987a; 1987b). The overall resistance to hydrate growth is represented by:

$$R = \frac{1}{A_p} \left(\frac{1}{k_{HL}^l} + \frac{1}{k_r} \right) + \frac{1}{K_{OL}} \tag{3.1}$$

where A_p is the total solid surface area (hydrate particles), k_{HL}^l is the mass transfer coefficient in the diffusion layer around the hydrate particle, k_r is the reaction rate constant and K_{OL} is the vapor-liquid water interfacial conductance. From a scaling

analysis (Deen, 1998), it follows that the resistance on the gas side of the vapor-liquid water interface is negligible compared to that on the liquid side. Moreover, the Sherwood number for solid particles in an agitated vessel is given by (Perry and Green, 1997):

$$Sh = \frac{k_{HL}^l L}{D} = 2 + 0.6 Re^{1/2} Sc^{1/3} \tag{3.2}$$

where D is the diffusivity of the gas hydrate former in water, Re is the Reynolds number and Sc is the Schmidt number. Using the correlation of Wilke and Chang (1955) with the parameters of Hayduk and Laudie (1974), the diffusion coefficient of the gas hydrate former in water can be estimated. It follows that the diffusivity (D) is in the order of 1×10^{-10} m^2/s at temperatures around the freezing point of water. Assuming a stagnant film ($Sh = 2$) and a diameter of 6 μm (largest detectable diameter by the Zetasizer Nano ZS), in other words the smallest possible mass transfer coefficient, it follows that k_{HL}^l is in the order of 1×10^{-5} m/s. On the other hand, Hashemi et $al.$ (2007b), who revisited the work of Clarke and Bishnoi (2005) showed that k_r for carbon dioxide hydrate (sI) formation is in the order of 1×10^{-8} m/s. Therefore, it is reasonable to assume that $1/k_{HL}^l$ is negligible compared to $1/k_r$.

Using equation 3.1 and the driving force proposed in the work of Hashemi et $al.$ (2007b), the number of moles consumed for hydrate growth is given by:

$$\frac{dn}{dt} = \frac{C_w^0 \left(x^{LV} - x^{HL} \right)}{\frac{1}{A_p k_r} + \frac{1}{k_{LV}^l A_{LV}}} \tag{3.3}$$

where C_w^0 is the initial concentration of water in the bulk liquid phase (assumed constant), x^{LV} is the gas hydrate former solubility in the liquid phase under hypothetical vapor-liquid water equilibrium (T^{exp}, P^{exp}) and x^{HL} is the gas hydrate former solubility in the liquid phase under hydrate-liquid water equilibrium (T^{exp}, P^{exp}). The interfacial area at the vapor-liquid water interface is denoted by A_{LV}. Expressing the total solid surface area as a function of the second moment of the particle

size distribution and assuming spherical particles, equation 3.3 becomes:

$$\frac{dn}{dt} = \frac{C_w^0 \left(x^{LV} - x^{HL} \right)}{\frac{1}{\pi \mu_2 V_L k_r} + \frac{1}{k_{LV}^l A_{LV}}} \tag{3.4}$$

where V_L is the volume of liquid in the crystallizer and the second moment of the particle size distribution is defined as (Kane *et al.*, 1974):

$$\mu_2(t) = \int_0^\infty L^2 \varphi(L, t) \, dL \tag{3.5}$$

where L is the hydrate diameter, t is the time and φ is the particle density distribution. Assuming no breakage, no agglomeration and no secondary nucleation, the initial number of particles is assumed constant and is given by:

$$\mu_0^0 = \frac{6 MW_H \left(n_{tb} - n^{HL} \right)}{\eta \pi V_L \rho_H L_c^3} \tag{3.6}$$

where n_{tb} is the number of moles of gas hydrate former dissolved at turbidity, *i.e.* at the onset of growth, n^{HL} is the number of moles of gas hydrate former dissolved under hydrate-liquid water equilibrium and η is the number of gas molecules per hydrate molecule. Both MW_H and ρ_H denote the molecular weight and the density of the hydrate particle respectively. The critical nuclei diameter (L_c) is determined by taking the mean diameter from the particle size distribution obtained at the onset of growth, which accounts for both homogeneous and heterogeneous nucleation. In order to calculate the particle density distribution, the cumulative oversize particle distribution (γ) is first obtained using equation 3.6 and the various particle size distributions (obtained experimentally from the Zetasizer Nano ZS) by fitting a lognormal function. Then, the particle density distribution is calculated as follows:

$$\varphi = -\frac{d\gamma}{dL} \tag{3.7}$$

after which the second moment is calculated using equation 3.5. Rearranging equation 3.4, the reaction rate constant can be determined:

$$\frac{dn}{dt} = \frac{V_L \rho_w}{MW_w} \frac{\left(x^{LV} - x^{HL} \right)}{\frac{1}{\pi \mu_2 k_r} + \frac{1}{k_{LV}^l a_{LV}}}$$

(3.8)

where ρ_w is the density of water at T^{exp}, MW_w is the molecular weight of water and $k_{LV}^l a_{LV}$ is the dissolution rate in the liquid film at the vapor-liquid water interface.

3.2.5.2 Population balance

The reaction rate constant can also be derived from a semitheoretical approach using the newly developed kinetic model and a population balance. In particular, assuming that there is no breakage, no agglomeration, no secondary nucleation and a size-independent growth, the population balance for a batch crystallizer yields (Kane *et al.*, 1974):

$$\frac{d\varphi}{dt} + \frac{d\left(G\varphi \right)}{dL} = 0$$

(3.9)

where G is the growth rate. Using the mean diameter obtained for each particle size distribution measurement performed, an expression for the growth rate can be obtained using the following:

$$G = \frac{dL}{dt}$$

(3.10)

Equation 3.9 can then be transformed into a set of differential equations and performing the moment transformations (Kane *et al.*, 1974):

$$\frac{d\mu_j}{dt} = jG\mu_{j-1}$$

(3.11)

where μ_j is the jth moment of the particle size distribution. Hence, solving equation 3.11:

$$\mu_0 = \mu_0^0$$

(3.12)

$$\mu_1 = \mu_0^0 Gt + \mu_1^0 \tag{3.13}$$

$$\mu_2 = \mu_0^0 G^2 t^2 + 2\mu_1^0 Gt + \mu_2^0 \tag{3.14}$$

where μ_0, μ_1 and μ_2 are the zeroth, first and second moments respectively. Incorporating equation 3.14 into equation 3.4:

$$\frac{dn}{dt} = \frac{C_w^0 \left(x^{LV} - x^{HL}\right)}{\frac{1}{\pi\left(\mu_0^0 G^2 t^2 + 2\mu_1^0 Gt + \mu_2^0\right)V_L k_r} + \frac{1}{k_{LV}^l A_{LV}}} \tag{3.15}$$

The initial number of particles per unit of liquid volume (μ_0^0) is given by equation 3.6, while μ_1^0 and μ_2^0 are given by:

$$\mu_1^0 = L_c \mu_0^0 \tag{3.16}$$

$$\mu_2^0 = L_c^{\,2} \mu_0^0 \tag{3.17}$$

It follows that equation 3.15 can be rewritten as:

$$\frac{dn}{dt} = \frac{V_L C_w^0 \left(x^{LV} - x^{HL}\right)}{\frac{1}{\pi\left(\mu_0^0 G^2 t^2 + 2L_c \mu_0^0 Gt + L_c^{\,2} \mu_0^0\right)k_r} + \frac{1}{k_{LV}^l a_{LV}}} \tag{3.18}$$

3.2.5.3 Dissolution rate

Solubility experiments were conducted to determine the dissolution rate in the liquid film at the vapor-liquid water interface, as required in equation 3.8 and equation 3.18. Neglecting the resistance on the gas side of the vapor-liquid water interface (section 3.2.5.1) and assuming that the total number of moles is constant and equal to the initial number of moles of water in the liquid phase, the rate at which gas is

dissolving can be expressed as:

$$\frac{dx}{dt} = k^l_{LV} a_{LV} \left(x^{LV} - x \right) \tag{3.19}$$

where x is the mole fraction of the gas hydrate former in the liquid phase at a given time t.

3.2.6 Results and discussion

Solubility experiments were first performed to determine the dissolution rate in the liquid film at the vapor-liquid water interface. These experiments were performed at the same temperature as the kinetic experiments, but at slightly lower pressures to ensure that the system was under vapor-liquid water equilibrium. The crystallizer stirrer was also set to the same speed as for the kinetic experiments, *i.e.* 750 rpm. All variables contained in equation 3.19 were obtained experimentally from the solubility experiments, except for the dissolution rate which was calculated by minimizing the residuals between the experimental data and the model predictions. Experiments conducted at 274.2 K and 248.8 kPa yielded a dissolution rate of 2.21×10^{-3} 1/s with an average absolute relative error of 5.8 %.

Kinetic experiments were performed to determine the reaction rate constant of sII propane hydrate formation. Experiments were conducted at 274.2 K and pressures between 314 and 340 kPa. Since propane can only occupy the larger cavities of structure II hydrates due to its size (Sloan, 1998b), full occupancy of the larger cavities was assumed when calculating the initial number of particles. Moreover, the initial number of particles is assumed to remain constant throughout the entire experiment and thus, secondary nucleation, breakage and agglomeration are assumed negligible. To foster such a hypothesis, the mean count rate, which is an indication of the number of photons detected per second, was monitored on a continuous basis using the Zetasizer Nano ZS with an uncertainty of ±0.1 kcps. Since the current setup analyses only a very small sample of the liquid phase, it
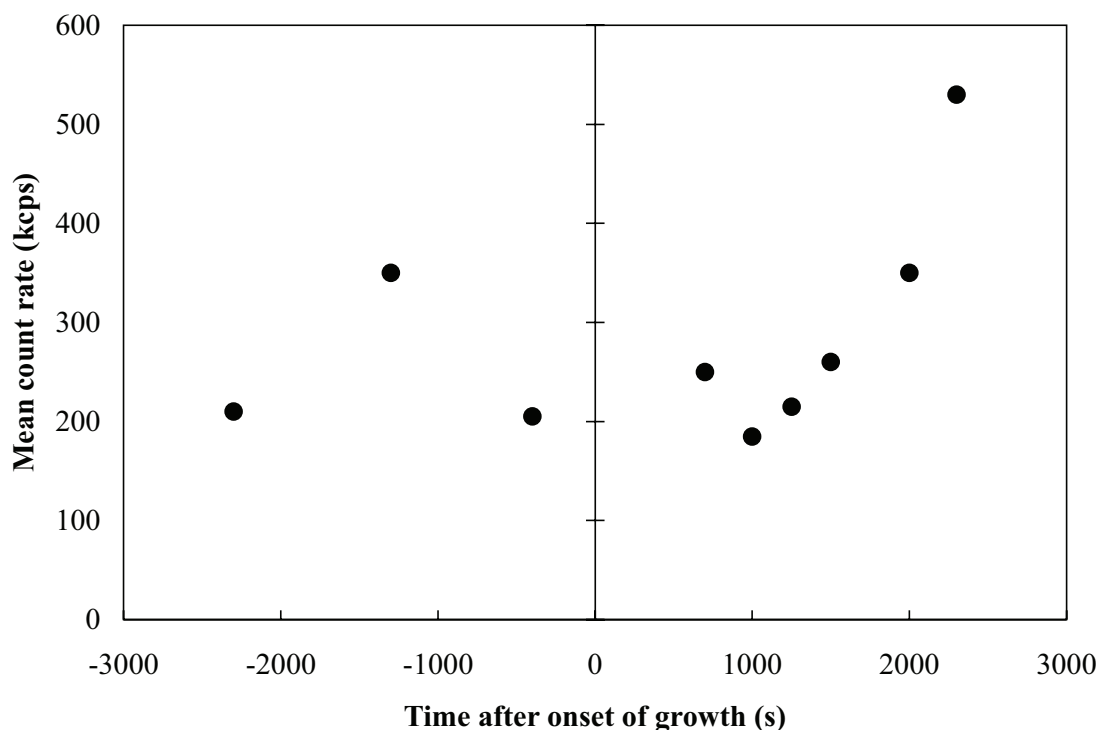
Figure 3.4: Mean count rate at 274.1 K and 314.8 kPa.

is expected that the mean count rate will fluctuate through time. Nevertheless, a relatively constant mean count rate (order of magnitude) implies that the number of particles remains constant, while a steadily increasing or decreasing count rate indicates an aggregating or sedimenting sample respectively. As seen in Figure 3.4, the order of magnitude of the mean count remains relatively constant throughout the experiment, which validates the assumptions made when calculating the number of particles. Furthermore, particle size distribution measurements performed at the onset of growth revealed a mean diameter of 118 nm at 274.2 K and 340.4 kPa.

To calculate the reaction rate constant, equation 3.8 was integrated and compared to the experimental mole consumption. Due to a lack of available models for the propane-water system, x^{LV} was calculated using the fugacity of pure propane in the
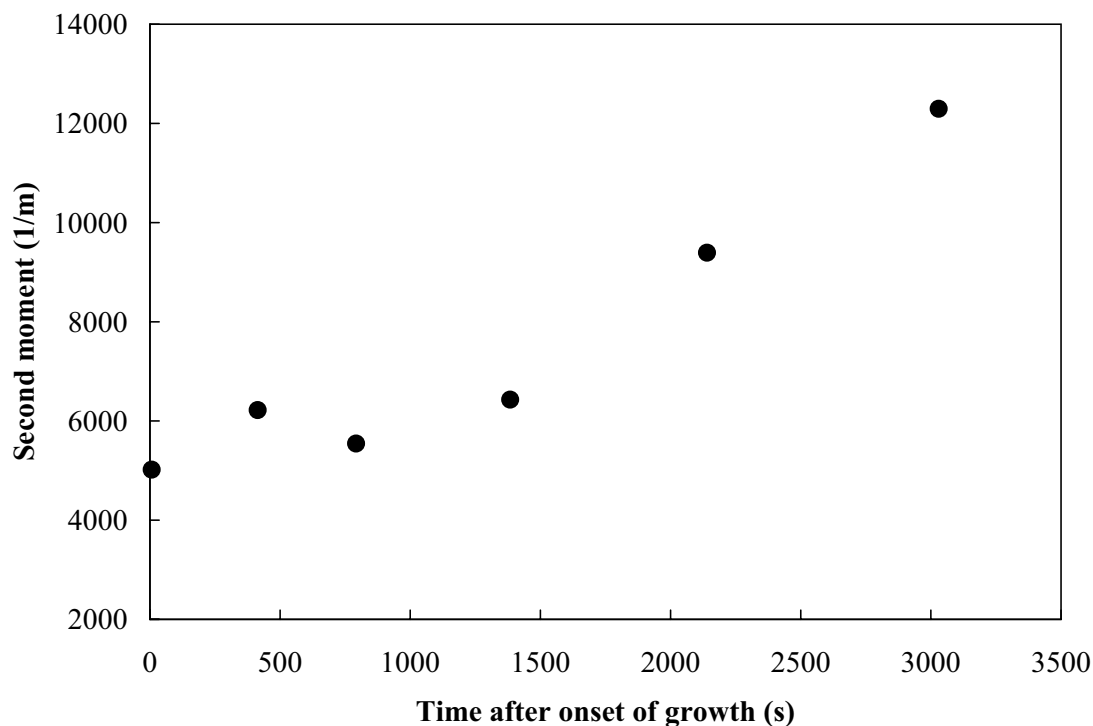
Figure 3.5: Second moment of the particle size distribution at 274.2 K and 340.4 kPa.

vapor phase at the experimental temperature and pressure, based on the Trebble-Bishnoi equation of state (1987), as well as using a hypothetical Henry's law constant from the correlation of Chapoy *et al.* (2004b). As for x^{HL}, it was obtained from the solubility experiments of Gaudette and Servio (2007). The second moment, which increases with time, was obtained experimentally (section 3.2.5.1) and is displayed in Figure 3.5.

The reaction rate constant was regressed using the Gauss-Newton method with Levenberg-Marquardt's modification. Using the dissolution rate obtained experimentally (2.21×10^{-3} 1/s) yielded a reaction rate constant that could vary by ten orders of magnitude without having a significant impact, while no fit was possible
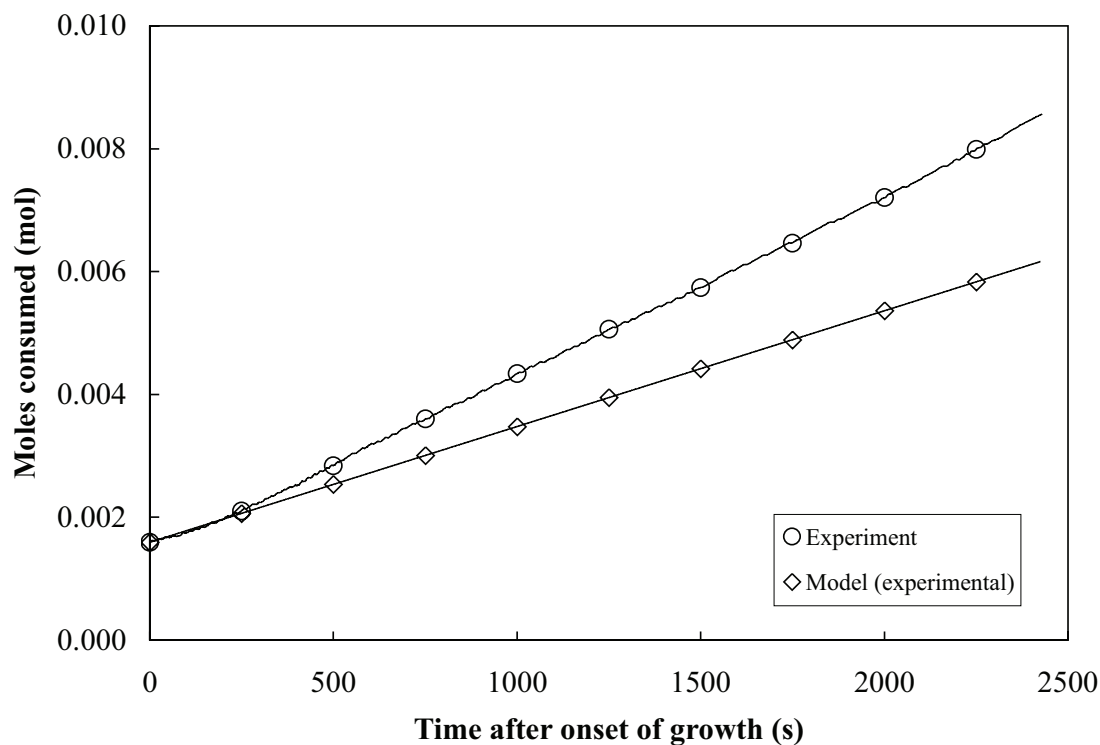
Figure 3.6: Model predictions at 274.2 K and 340.4 kPa using the dissolution rate from solubility experiments.

with the experimental data, as shown in Figure 3.6 (k_r set to 1×10^3 m/s). It was evident that the value obtained from the solubility experiments was underestimated and thus, the resistance at the vapor-liquid water interface was overestimated. It is hypothesized that hydrate crystals present in the bulk solution alter the dissolution rate at the vapor-liquid water interface. Indeed, hydrate crystals are likely to either create turbulence at the interface, reducing the effective boundary layer thickness and increasing the mass transfer coefficient in a similar way as that reported for other systems by Kluytmans *et al.* (2003), or increase the effective interfacial area. It follows that the dissolution rate for hydrate growth will be significantly larger than that determined from solubility experiments. Hence, both the reaction rate constant and the dissolution rate were determined using equation 3.8. It is believed
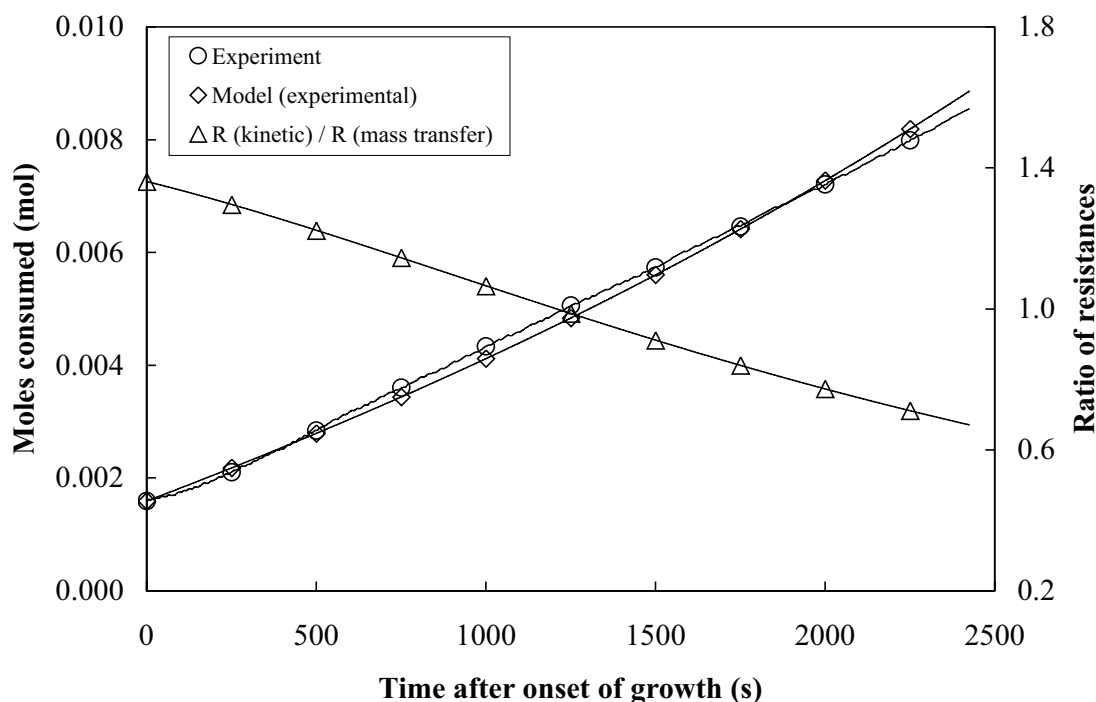
Figure 3.7: Model predictions with experimental reaction rate constant at 274.2 K and 340.4 kPa.

that initially, the resistance to hydrate growth will be mostly due to kinetics, the hydrate crystals being relatively small and requiring very little gas to grow. However, as the hydrate particles continue to expand, they require more and more gas to grow further, up to a point where the resistance due to mass transfer overcomes that due to kinetics. The Gauss-Newton method with Levenberg-Marquardt's modification was used to regress the reaction rate constant and the dissolution rate, the former over the parabolic portion of the mole consumption plot (first 600 seconds), the latter over the linear portion. Using such an approach, the kinetic experiments conducted at 274.2 K yielded an average reaction rate constant of $(2.0 \pm 0.2) \times 10^{-7}$ m/s and a dissolution rate four times larger than the one determined from solubility experiments. Figure 3.7 shows the comparison between the mole consumption obtained experimentally at 274.2 K and 340.4 kPa and the kinetic model, with an
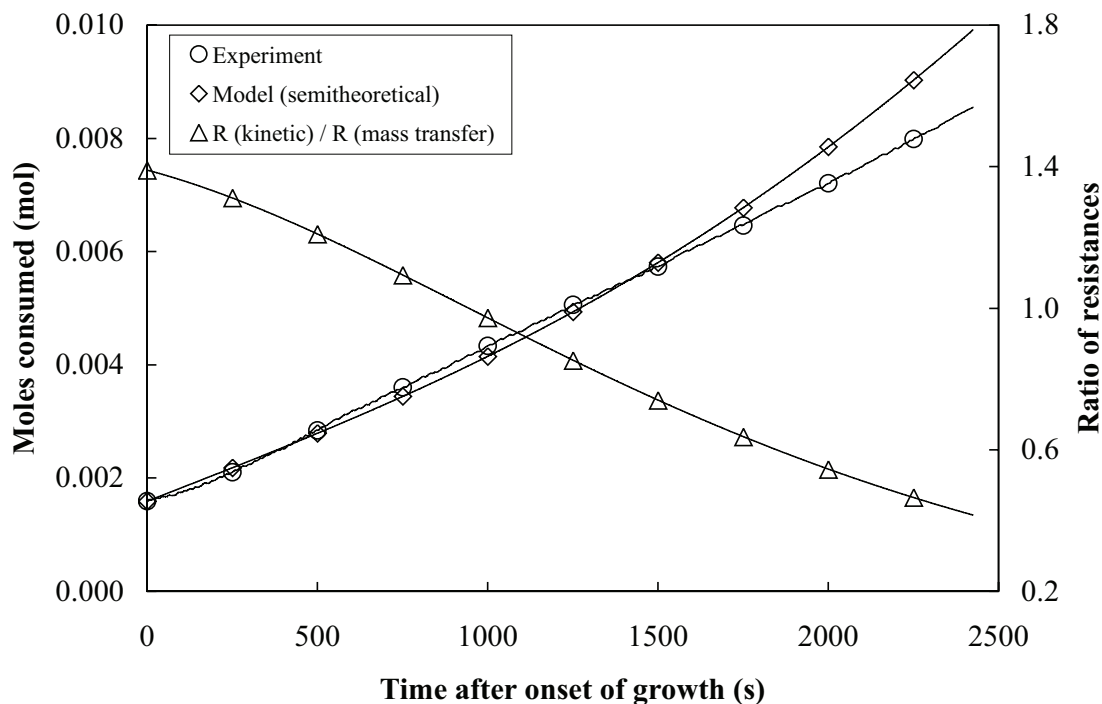
Figure 3.8: Model predictions with semitheoretical reaction rate constant at 274.2 K and 340.4 kPa.

AARE between the model and the experimental data of 2.9 %. The ratio of the kinetic resistance to the mass transfer resistance at the vapor-liquid water interface was also included. It can be seen that the magnitude of the kinetic resistance gradually decreases as time progresses, the system becoming more and more mass transfer limited. A sensitivity analysis was also performed to assess the variability of the reaction rate constant. An increase in the dissolution rate of 20 %, 30 % and 50 % yielded a decrease in the reaction rate constant of 3.9 %, 5.3 % and 7.5 % respectively. Similarly, a decrease in the dissolution rate of 20 %, 30 % and 50 % resulted in an increase in the reaction rate constant of 6.5 %, 11.7 % and 32.2 % respectively.

Due to inaccurate hydrate surface area measurements (Hashemi *et al.*, 2007b), researchers have not been able so far to relate the reaction rate constant obtained

experimentally to the one obtained from a population balance. Consequently, the reaction rate constant was also calculated using equation 3.18 and compared to the value obtained using equation 3.8. The same procedure was used as in the case of equation 3.8, except for the second moment which was calculated using a population balance and an average growth rate (section 3.2.5.2). For comparison purposes, the dissolution rate was assumed to be the same as the one determined using equation 3.8, while the reaction rate constant was regressed using the Gauss-Newton method with Levenberg-Marquardt's modification, yielding an average reaction rate constant of $(1.9 \pm 0.1) \times 10^{-7}$ m/s at 274.2 K. Again, Figure 3.8 shows the comparison between the mole consumption obtained experimentally at 274.2 K and 340.4 kPa and the kinetic model, with an AARE between the model and the experimental data of 5.0 %.

3.2.7   Conclusion

The reaction rate constant of sII propane hydrate formation was successfully determined at 274.2 K with a value of $(2.0 \pm 0.2) \times 10^{-7}$ m/s using a novel experimental setup and a newly developed kinetic model. The reaction rate constant obtained experimentally is in good agreement with that predicted by a population balance, *i.e.* $(1.9 \pm 0.1) \times 10^{-7}$ m/s.

3.2.8   Acknowledgements

Notation

Please refer to Chapter 9.

References

Please refer to the general bibliography found at the end of the thesis document.

Addendum

The analysis presented previously (Chapter 3) regarding the mean count rate was found to be incomplete following additional work and further analysis well after the article was published. The mean count rate needs to be converted into a derived count rate, which is normalized for the cell position and the attenuation used, when comparing measurements. In addition, the derived count rate is a function of both the number of particles and their size. A comprehensive technique based on the comparison of the derived count and the cumulative relative scattering was subsequently developed to accurately determine whether or not the number of hydrate particles remains constant (Chapters 5 and 6). It was shown that for both pure-component carbon dioxide and methane hydrate formation experiments, the number of hydrate particles remained constant over the time interval of interest of the growth stage. These findings highlight the fact that even though the reasoning behind the assumption of a constant number of particles for the propane hydrate formation experiments (Chapter 3) is incomplete, the end outcome, that is the assumption of a constant number of hydrate particles, remains probable and does not affect the reported values for the reaction rate constant of propane hydrate formation.

Chapter 4

Guest Mole Fraction in Bulk Liquid Phase

4.1 Preface

The experimental work detailed in Chapter 3 highlighted the fact that the dissolution rate at the vapor-liquid water interface ($k^l_{LV} a_{LV}$) is altered, compared to the value obtained from solubility experiments (under vapor-liquid water equilibrium conditions rather than hydrate-forming conditions) due to the presence of hydrate particles during growth. While propane is poorly soluble in water ($x \sim 10^{-4}$), methane and carbon dioxide are ten and a houndred times more soluble in water respectively. As a result, accurate mole fraction measurements of the guest (carbon dioxide and methane) in the bulk liquid phase at the onset of hydrate growth and thereafter could be performed to assess the effect of temperature, pressure and time on the guest concentration. An alternate formulation of the kinetic model introduced in Chapter 3 was developed, incorporating the guest mole fraction in the bulk liquid phase as part of the driving force, thus eliminating the need for the dissolution at the vapor-liquid water interface.

4.2 CO_2 and CH_4 mole fraction measurements during hydrate growth in a semi-batch stirred tank reactor and its significance to kinetic modeling

Sébastien Bergeron, Phillip Servio
Department of Chemical Engineering, McGill University, Canada

4.2.1 Abstract

A new experimental technique has been developed to measure the mole fraction of the gas hydrate former in the bulk liquid phase at the onset of hydrate growth and thereafter in a semi-batch stirred tank reactor. The mole fraction of carbon dioxide and methane in the bulk liquid phase was obtained for the first 11 and 13 minutes of the growth stage, for the carbon dioxide-water and methane-water systems respectively. Experiments were conducted at temperatures ranging from 275.3 to 281.4 K and at pressures ranging from 2,017 to 4,000 kPa for the carbon dioxide-water system, while temperatures ranging from 275.1 to 279.1 K and pressures ranging from 3,858 to 6,992 kPa were investigated for the methane-water system. The mole fraction of carbon dioxide in the bulk liquid phase was found to be constant during the growth period, varying on average by 0.6 % and 0.3 % at 275.4 K and 279.5 K. Similarly, the mole fraction of methane in the bulk liquid phase was found to remain constant during the growth stage, varying on average by 2.0 %, 0.8 % and 0.2 % at 275.1 K, 277.1 K and 279.1 K respectively. The mole fraction of the guest in the bulk liquid phase was also found to increase with pressure and decrease with temperature, while remaining greater than its hydrate-liquid water equilibrium value. As a result, an alternate formulation of a hydrate growth model is proposed.

4.2.2 Introduction

Gas hydrates, or clathrate hydrates, are nonstoichiometric crystalline compounds in which a gas or a volatile liquid molecule suitable for hydrate formation is enclosed in a network consisting of water molecules linked together through hydrogen bonding. The presence of the gas molecule stabilizes the water lattice via weak van der Waals forces. Three naturally occurring hydrate structures have been reported in the literature, including structure I (sI), structure II (sII) and structure H (sH) (Sloan, 1998b). In particular, carbon dioxide and methane form structure I hydrate, while propane and neohexane (in the presence of methane) form structure II and structure H hydrate respectively. Considerable research is being conducted on gas hydrates due to their potential applications, including naturally occurring methane hydrates as an alternate energy source (Chatti *et al.*, 2005), storage and transportation of natural gas or liquefied petroleum gases in hydrate form (Chatti *et al.*, 2005; Giavarini *et al.*, 2003), as well as carbon dioxide sequestration as a means to mitigate the global warming effect (Chatti *et al.*, 2005). Such promising new technologies are reasons why kinetic studies should be further investigated. In particular, an accurate value for the reaction rate constant of hydrate formation is required for proper reactor design aimed at large-scale hydrate production. The reaction rate constant is the sole parameter affecting any reactor throughput and conversion that remains constant upon scale-up, as both heat and mass transfer effects will change. Recently, Ribeiro and Lage (2008) performed an extensive literature review of the existing hydrate growth kinetic models. Some of the most well-known models include the pioneering work of Englezos *et al.* (1987a; 1987b), as well as the model of Skovborg and Rasmussen (1994). The former can be used to determine the reaction rate constant of hydrate formation, while the latter limits hydrate growth to a mass transfer problem, without any reaction rate constant. More recently, Hashemi *et al.* (2007b) have proposed a new driving force for hydrate growth. Their driving force is based on the concentration of the guest in water under hypothetical vapor-liquid water equilibrium, at the experimental temperature and experimental pressure, and that under hydrate-liquid water equilibrium, again at the experimental temperature

and experimental pressure (Hashemi *et al.*, 2007b). Following this, Bergeron and Servio (2008b) have incorporated this new driving force into a modified version of the model of Englezos *et al.* (1987a), resulting in a new kinetic model for hydrate growth aimed at determining the reaction rate constant of hydrate formation. Nevertheless, all these models need to account for the dissolution rate at the vapor-liquid water interface, which its determination has been shown to be controversial. In their work, Bergeron and Servio (2008b) hypothesized that the dissolution rate at the vapor-liquid water interface was enhanced, compared to the value obtained from solubility experiments, due to the presence of hydrate particles during growth. Kluytmans *et al.* (2003) also concluded that the presence of particles in a system could readily increase the dissolution rate at the vapor-liquid water interface by creating turbulence and reducing the effective boundary layer thickness, which would increase the mass transfer coefficient. Even though several authors have measured the solubility of carbon dioxide (Someya *et al.*, 2005; Servio and Englezos, 2001; Yang *et al.*, 2000) and methane (Servio and Englezos, 2002; Kim *et al.*, 2003; Yang *et al.*, 2001; Lu *et al.*, 2008; Seo and Lee, 2002) in the liquid phase under hydrate-liquid water equilibrium, to the best of our knowledge, there is no experimental data regarding the mole fraction of the gas hydrate former in the bulk liquid phase at the onset of hydrate growth and thereafter. The work of Teng and Yamasaki (1998) is the only reference to solubility measurements approximating the solubility of carbon dioxide in the metastable absence of hydrates, as reported by Ohmura and Mori (1999). In addition, Hashemi *et al.* (2007b) have shown from a modeling point of view and using the work of Clarke and Bishnoi (2005), that the bulk concentration of the gas hydrate former does not change significantly with time after the onset of growth. In their analysis, they assumed that at the onset of growth the concentration of carbon dioxide in the bulk liquid phase dropped from its turbidity value to its equilibrium value (Hashemi *et al.*, 2007b). To assess these issues from an experimental point of view and to eliminate the need to rely on uncertain values for the dissolution rate at the vapor-liquid water interface, an alternate formulation of the model of Bergeron and Servio (2008b) is suggested, based on experimental

measurements of the mole fraction of carbon dioxide and methane in the bulk liquid phase at the onset of hydrate growth and thereafter.

4.2.3 Experimental apparatus

As shown in Figure 4.1, the current experimental setup consists of an isothermal/isobaric semi-batch stirred tank crystallizer, a gas supply reservoir for hydrate formation and a digital gasometer (Chandler Engineering) to measure the volume of gas expanded from the liquid sample bomb. Hydrates are formed in the 600 cm^3 internal volume stainless steel (316) crystallizer with a 12,000 kPa pressure rating. A PPI DYNA/MAG MM-006 mixer (0 - 2,500 rpm) has been mounted on top of
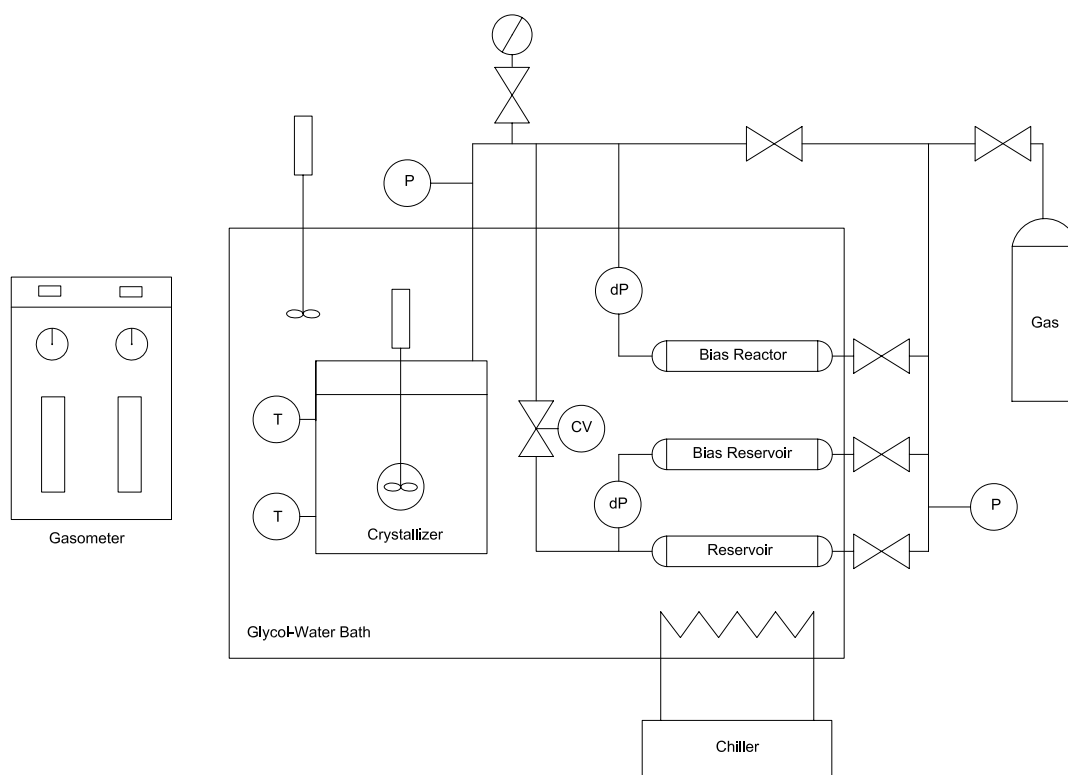
Figure 4.1: Simplified schematic of the experimental setup.

the crystallizer to ensure sufficient mixing. Gas is supplied from the stainless steel reservoir (internal volume of 1,000 cm^3) using a Baumann 51000 Series Low Flow control valve. Both the crystallizer and the reservoir are submerged in a cooling bath composed of 10 % glycol and water mixture controlled via a Thermo NESLAB RTE Series refrigerated bath. Temperature and pressure measurements are performed using standard resistance temperature devices (±0.3 ^{o}C) and Rosemount 3051S Series pressure transducers with a reference accuracy of ±0.04 % of the span. The readouts are then recorded and displayed using the National Instruments NI-DAQ 7 data acquisition device and the LabVIEW software. The LabVIEW interface was written to calculate the number of moles consumed at any time during the experiment using the Trebble-Bishnoi equation of state (1987), the gas reservoir pressure and temperature measurements, as well as the gas reservoir volume. The standard uncertainties were estimated to be $u_T = 0.3$ K, $u_P = 5.6$ kPa, $u_{gasometer} = 1$ ml and $u_{bomb} = 0.2$ ml, for temperature, pressure, gasometer and the sample bomb respectively.

4.2.4 Experimental procedure

Prior to any experiment, the crystallizer is cleaned using HPLC grade water and purged several times using the selected gas (carbon dioxide with Coleman instrument grade 99.99 % purity or methane with grade 4.0 99.99 % purity). A syringe is used to introduce 180 ml of HPLC grade water in the crystallizer. Once thermal equilibrium has been reached, the crystallizer is pressurized above the three-phase equilibrium pressure at the experimental temperature. Once the temperature in the reservoir and in the crystallizer has stabilized, both the data acquisition program and the crystallizer stirrer are started. The crystallizer stirrer is set to 750 rpm to minimize both heat and mass transfer effects. The onset of hydrate growth is identified by a sudden increase in the crystallizer liquid phase temperature, following which the crystallizer stirrer is stopped to halt hydrate growth and a measurement is performed. An evacuated sample bomb of approximately 10 cm^3 is used to collect a sample from the crystallizer bulk liquid phase. The sample bomb is evacuated

prior to any experiment and weighed before and after the sample has been collected to determine its exact mass. Finally, a 500 nm high-pressure stainless steel filter (Norman Filter Company) is used inline to remove any hydrate particle from the sampling line.

4.2.5 Theory

4.2.5.1 Mole fraction in the bulk liquid phase

An analytic flash technique similar to the one used by Gaudette and Servio (2007) was employed to calculate the mole fraction of carbon dioxide and methane in the bulk liquid phase at the onset of hydrate growth and thereafter. Through the use of the digital gasometer, the content of the sample bomb is brought to room temperature and atmospheric pressure. As the sample bomb reaches room temperature and atmospheric pressure, some of the gas dissolved in the liquid phase gradually evolves from the sample bomb into a floating piston where its volume and temperature are recorded. The number of moles of gas that expanded inside the gasometer is given by:

$$n^{gm} = \left(P^{atm} - P^V_{H_2O}\right) \frac{V^{gm}}{Z^V R T^{atm}} \tag{4.1}$$

where P^{atm} and T^{atm} are the atmospheric pressure and room temperature, $P^V_{H_2O}$ is the vapor pressure of water at room temperature, V^{gm} is the volume displaced in the gasometer, Z^V is the compressibility factor of the vapor phase at room temperature and atmospheric pressure, obtained using the model of Hashemi *et al.* (2006), and R is the universal gas constant. The mole fraction of the gas hydrate former in water at room temperature and atmospheric pressure $\left(x^{LV}\right)$ is obtained from the model of Hashemi *et al.* (2006). Since the sample bomb is weighed before and after the sample has been collected, the number of moles of water contained in the sample $\left(n^b_{H_2O}\right)$ is known. It follows that the mole fraction of the gas hydrate former in the

bulk liquid phase is given by:

$$x^b = \frac{\frac{x^{LV} n^b_{H_2O}}{1-x^{LV}} + n^{gm}}{\frac{x^{LV} n^b_{H_2O}}{1-x^{LV}} + n^{gm} + n^b_{H_2O}} \quad (4.2)$$

Based on the procedure described above and using a coverage factor of $k' = 2$ (Chirico *et al.*, 2003), while assuming the corresponding standard uncertainties given previously have a normal distribution (Chirico *et al.*, 2003), the expanded uncertainty, U_x, on the mole fraction of carbon dioxide and methane in the bulk liquid phase was estimated to vary between 6.5×10^{-4} and 8.8×10^{-4}, and between 1.2×10^{-4} and 1.3×10^{-4} respectively, depending on the experimental conditions.

4.2.5.2 Kinetic model

Incorporating the driving force of Hashemi *et al.* (2007b), Bergeron and Servio (2008b) have proposed a new kinetic model for hydrate formation based on the model of Englezos *et al.* (1987a). According to their model, the number of moles consumed for hydrate growth is given by (Bergeron and Servio, 2008b):

$$\frac{dn}{dt} = \frac{V_L \rho_w}{MW_w} \frac{\left(x^{LV} - x^{HL}\right)}{\frac{1}{\pi \mu_2(t) k_r} + \frac{1}{k^l_{LV} a_{LV}}} \quad (4.3)$$

where V_L is the volume of liquid in the crystallizer, ρ_w is the density of water at the experimental temperature, MW_w is the molecular weight of water, x^{LV} is the gas hydrate former solubility in the liquid phase under hypothetical vapor-liquid water equilibrium (T^{exp}, P^{exp}) and x^{HL} is the gas hydrate former solubility in the liquid phase under hydrate-liquid water equilibrium (T^{exp}, P^{exp}). Also, μ_2 is the second moment of the particle size distribution, k_r is the reaction rate constant and $k^l_{LV} a_{LV}$ is the dissolution rate in the liquid film at the vapor-liquid water interface.

Based on the driving force used in equation 4.3, that is the difference in the guest

solubility in water under vapor-liquid water and hydrate-liquid water equilibrium, the resistance to hydrate growth is composed of two terms. The first resistance is due to kinetics and is represented by $1/(\pi\mu_2 k_r)$. The other resistance is due to the gas dissolving into the liquid phase at the vapor-liquid water interface and is represented by $1/(k_{LV}^l a_{LV})$. If one was able to measure the mole fraction of the gas hydrate former in the bulk liquid phase during hydrate growth, one could eliminate the resistance at the vapor-liquid water interface and rewrite equation 4.3. Such an approach corresponds to the standard engineering expression where the rate is equal to the ratio of the driving force over the resistance. Since the driving force for hydrate growth would no longer include the vapor-liquid water interface, the corresponding resistance would only include the one due to hydrate kinetics. Incorporating the mole fraction of the gas hydrate former in the bulk liquid phase, equation 4.3 becomes:

$$\frac{dn}{dt} = \frac{V_L \rho_w}{MW_w} \frac{\left(x^b - x^{HL}\right)}{\frac{1}{\pi\mu_2(t)k_r}} \tag{4.4}$$

where x^b is the mole fraction of the guest in the bulk liquid phase at the experimental temperature and experimental pressure. Equation 4.4 thus represents another form of the model proposed by Bergeron and Servio (2008b) that can be used to calculate the reaction rate constant of hydrate formation. Once the mole fraction of the gas hydrate former in the bulk liquid phase is known, the reaction rate constant for hydrate formation can be determined from particle size distributions measurements.

Another important parameter in hydrate kinetics is the initial number of hydrate particles at the onset of growth. So far, researchers have assumed that the mole fraction of the gas hydrate former in the bulk liquid phase drops from its turbidity value to its two-phase (Hashemi *et al.*, 2007b; Bergeron and Servio, 2008b) or three-phase (Englezos *et al.*, 1987a; Chun and Lee, 1996) equilibrium value at the onset of growth. Consequently, the initial number of hydrate particles is given by:

$$\mu_0^0 = \frac{6MW_H\left(n_{tb} - n^{eq}\right)}{\eta\pi V_L \rho_H L_c^3} \tag{4.5}$$

where n_{tb} is the number of moles of gas hydrate former dissolved at turbidity, n^{eq} is the number of moles of gas hydrate former dissolved in water under hydrate-liquid water or hydrate-liquid water-vapor equilibrium, and η is the number of moles of gas per mole of hydrate. Both MW_H and ρ_H denote the molecular weight and the density of the hydrate particle respectively, while L_c is the critical nuclei diameter for hydrate formation.

The underlying assumption of equation 4.5 is that the mole fraction of the guest in the liquid phase drops from its turbidity value to its equilibrium value at the onset of growth. To eliminate such an assumption, equation 4.5 can be rewritten as follows:

$$\mu_0^0 = \frac{6MW_H \left(n_{tb} - n^b\right)}{\eta \pi V_L \rho_H L_c^3} \tag{4.6}$$

where n^b is the number of moles of gas hydrate former dissolved in the bulk liquid phase a the onset of growth and is determined from measurements performed at that precise moment.

4.2.6 Results and discussion

To verify the accuracy of the measurements using the current apparatus and experimental procedure, two measurements were performed under vapor-liquid water equilibrium and compared to data available in the literature, for both the carbon dioxide-water and methane-water systems. For the carbon dioxide-water system, measurements at 274.7 K and 1,208 kPa, as well as 278.6 K and 2,998 kPa, yielded a carbon dioxide mole fraction in the liquid phase of 1.25×10^{-2} and 2.27×10^{-2} respectively. As a comparison, Chapoy *et al.* (2004a) reported a value of 1.420×10^{-2} at 274.83 K and 1,201 kPa, while Servio and Englezos (2001) reported a value of 2.220×10^{-2} at 278.55 K and 3,000 kPa. For the methane-water system, measurements at 274.4 K and 2,560 kPa, as well as 278.5 K and 3,509 kPa, yielded a mole fraction of methane in the liquid phase of 1.09×10^{-3} and 1.24×10^{-3} respectively. Again, Lekvam and Bishnoi (1997) reported a value of 9.78×10^{-4} at 274.29 K and

2,515 kPa, while Servio and Englezos (2002) reported a value of 1.190×10^{-3} at 278.65 K and 3,500 kPa.

Carbon dioxide-water system

Measurements at the onset of hydrate growth were performed for various experimental conditions, with temperatures ranging from 275.3 to 281.4 K and pressures ranging from 2,017 to 4,000 kPa. Figure 4.2 below shows the various data points,
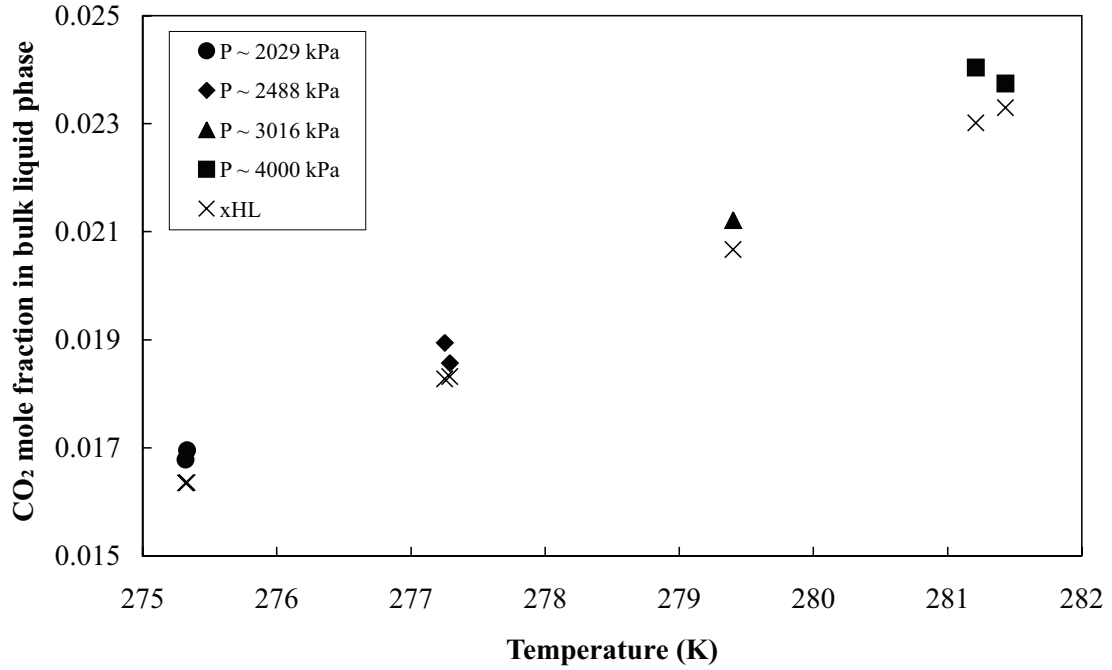
Figure 4.2: Mole fraction of carbon dioxide in the bulk liquid phase at the onset of hydrate growth compared to its solubility under hydrate-liquid water equilibrium using the model of Hashemi *et al.* (2006).

while the exact values can be found in Table 4.1. To study the supersaturation of the bulk liquid phase once hydrates formed, the solubility of carbon dioxide in water under hydrate-liquid water equilibrium (T^{exp}, P^{exp}), as predicted by the model of Hashemi *et al.* (2006), was included in Figure 4.2. It can be seen that the bulk liquid phase remains supersaturated at the onset of hydrate growth. Consequently,

Table 4.1: Mole fraction of carbon dioxide in the bulk liquid phase at the onset of hydrate growth and thereafter.

Temperature (K)	Pressure (kPa)	Time (s)	x^b ($\times 10^{-2}$)	U_x ($\times 10^{-2}$)
275.3	2,017	0	1.68	0.07
275.3	2,041	0	1.70	0.07
275.6	2,028	200	1.68	0.07
275.5	2,030	535	1.66	0.07
277.3	2,482	0	1.90	0.07
277.3	2,494	0	1.86	0.07
279.4	3,016	0	2.12	0.08
279.6	3,006	369	2.10	0.08
279.5	3,007	645	2.11	0.08
281.4	4,000	0	2.38	0.09
281.2	4,000	0	2.40	0.09

equation 4.6 should be used in replacement of equation 4.5 when calculating the initial number of hydrate particles.

In addition, measurements were performed through the growth stage to determine whether or not the mole fraction of carbon dioxide in the bulk liquid phase remains constant. These measurements were conducted at temperatures of 275.4 K and 279.5 K and at pressures of 2,029 kPa and 3,010 kPa respectively. It is clear from Figure 4.3 that the mole fraction of carbon dioxide in the bulk liquid phase does not vary significantly with time once in the growth stage, as the mole fraction varied on average by 0.6 % and 0.3 % at 275.4 K and 279.5 K respectively.

Measurements performed previously were done to reflect typical conditions used for carbon dioxide kinetic experiments, which includes a high stirring rate (750 rpm) to minimize both heat and mass transfer effects. Nevertheless, the effect of stirring rate on the mole fraction of carbon dioxide in the bulk liquid phase was also studied. Unfortunately, any stirring rate greater than 750 rpm compromised the integrity of the crystallizer stirrer due to some persistent wobbling. On the other hand, a stir-
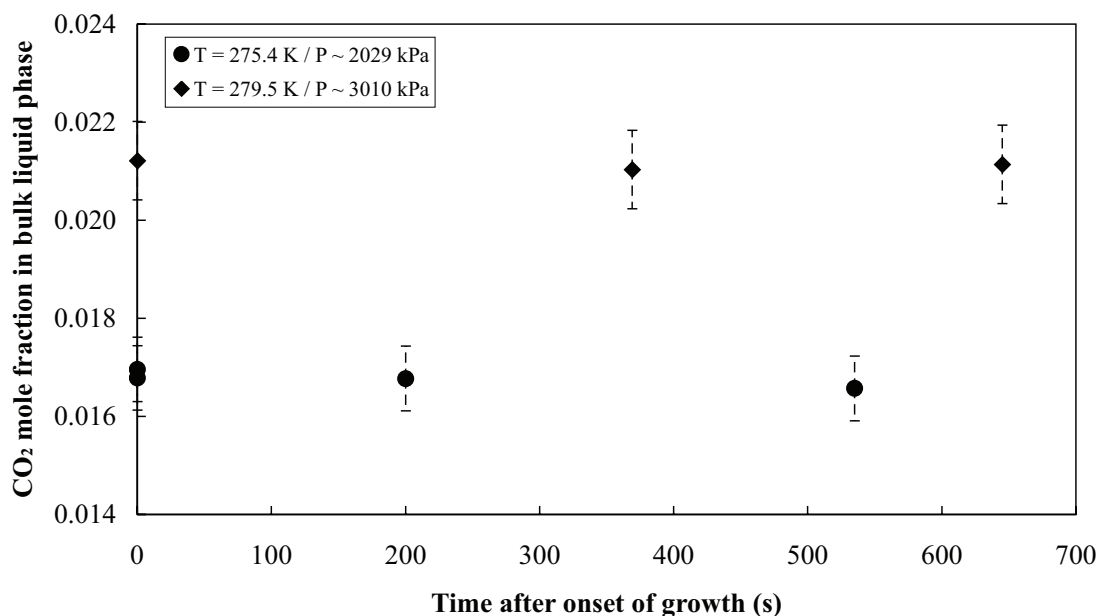
Figure 4.3: Mole fraction of carbon dioxide in the bulk liquid phase during hydrate growth.

ring rate of 500 rpm or less caused the bulk liquid phase to be quasi-stagnant. Visual inspection revealed the formation of a thin hydrate layer at the vapor-liquid water interface, while no such film would form at 750 rpm. A measurement performed at 500 rpm ($T = 295.3$ K and $P = 2,016$ kPa) revealed a mole fraction in the bulk liquid phase 2.8 % smaller than that at 750 rpm ($T = 295.3$ K and $P = 2,017$ kPa). Since the measurement at 500 rpm included a hydrate layer at the interface, while no film was present at 750 rpm, it is precarious to conclude that the difference in mole fraction is significant. Nevertheless, it can be concluded that under similar hydrodynamic, heat and mass transfer conditions, the mole fraction of carbon dioxide in the bulk liquid phase at the onset of hydrate growth and thereafter does not change significantly with time.

Methane-water system

Measurements at the onset of hydrate growth were performed for various experimental conditions with temperatures ranging from 275.1 to 279.1 K and pressures ranging from 3,858 to 6,992 kPa. The stirring rate was set to 750 rpm for the same reasons as mentioned previously. Figure 4.4 shows the various data points, while the exact values can be found in Table 4.2. It can be seen that the mole fraction of methane in the bulk liquid phase at the onset of hydrate growth is a function of both temperature and pressure.
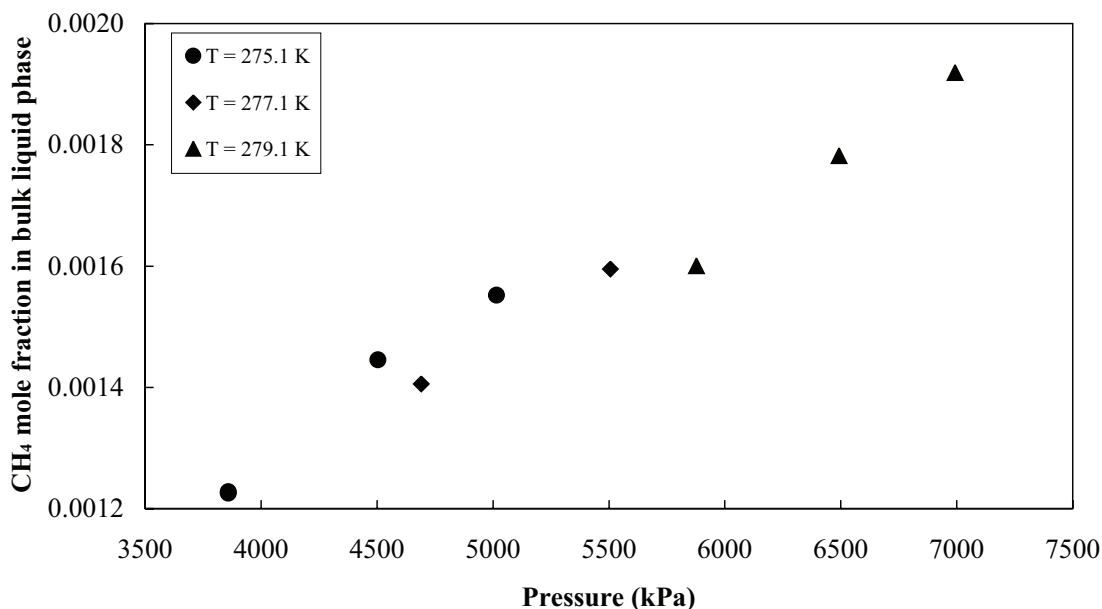
Figure 4.4: Mole fraction of methane in the bulk liquid phase at the onset of hydrate growth.

While various authors (Someya *et al.*, 2005; Servio and Englezos, 2002; Seo and Lee, 2002; Gaudette and Servio, 2007; Handa, 1990) have reported that the solubility of the gas hydrate former in water under hydrate-liquid water equilibrium is not a strong function of pressure, the present work shows that the mole fraction of methane in the bulk liquid phase at the onset of hydrate growth behaves quite differently, increasing significantly with pressure. It is well documented in the lit-

Table 4.2: Mole fraction of methane in the bulk liquid phase at the onset of hydrate growth and thereafter

Temperature (K)	Pressure (kPa)	Time (s)	x^b $(\times 10^{-3})$	U_x $(\times 10^{-3})$
275.1	5,015	0	1.55	0.13
275.2	4,503	0	1.45	0.13
275.2	3,858	0	1.23	0.12
275.1	3,858	0	1.23	0.12
275.1	3,863	332	1.28	0.12
275.1	3,863	687	1.27	0.12
277.0	5,506	0	1.60	0.13
277.1	4,690	0	1.41	0.13
277.1	4,674	770	1.38	0.12
279.1	6,992	0	1.92	0.13
279.1	6,491	0	1.78	0.13
279.1	5,876	0	1.60	0.13
279.1	5,876	400	1.61	0.12

erature (Servio and Englezos, 2002; Kim *et al.*, 2003; Yang *et al.*, 2001; Lu *et al.*, 2008; Seo and Lee, 2002; Hashemi *et al.*, 2006; Bergeron *et al.*, 2007) that the mole fraction of methane in water, under hydrate-liquid water equilibrium, increases with increasing temperature. Interestingly, the current work suggests that the mole fraction of methane in the bulk liquid phase at the onset of hydrate growth follows an opposite behavior, decreasing with increasing temperature.

Additional measurements were performed during hydrate growth for temperatures between 275.1 and 279.1 K and pressures between 3,858 and 5,876 kPa in order to determine whether or not the mole fraction of methane in the bulk liquid phase remains constant, as in the case of carbon dioxide. Figure 4.5 shows the various measurements as a function of time. It can be seen that the mole fraction of methane in the bulk liquid phase does not vary significantly during the growth stage, varying on average by 2.0 %, 0.8 % and 0.2 % at 275.1 K, 277.1 K and 279.1 K respectively, which is in agreement with the findings for the carbon dioxide-water system. Hence, it can be concluded that under similar hydrodynamic, heat and mass transfer con-
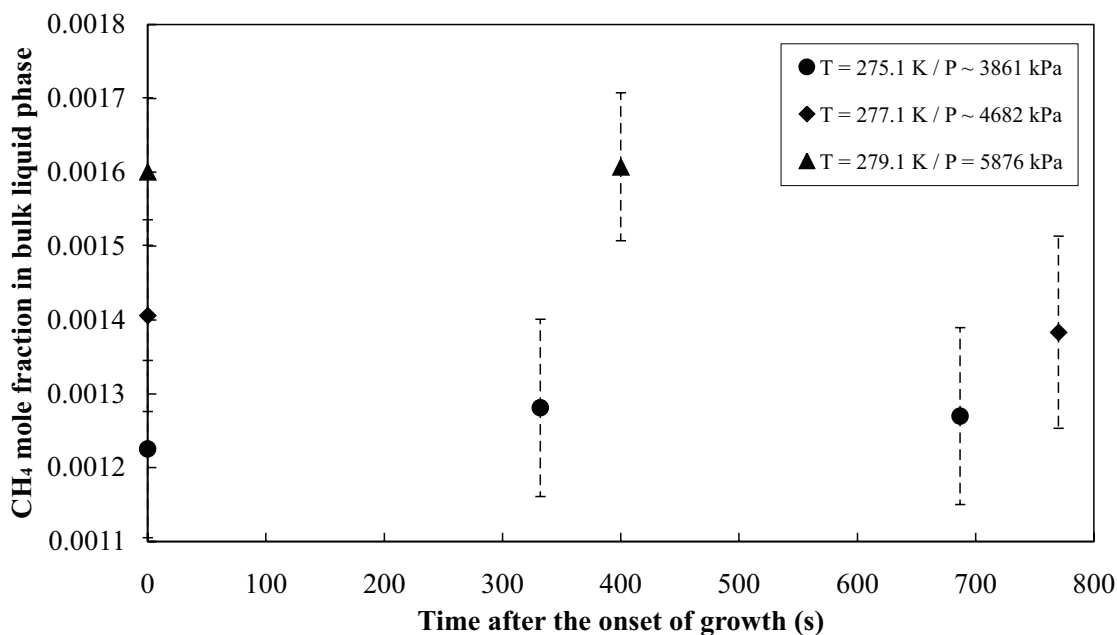
Figure 4.5: Mole fraction of methane in the bulk liquid phase during hydrate growth.

ditions, the mole fraction of the gas hydrate former in the bulk liquid phase at the onset of hydrate growth and thereafter does not change significantly with time. It should be noted that the values reported in this work, for both methane and carbon dioxide, are specific to the geometry of the reactor and the conditions that the experiments were performed at. In other words, these are not equilibrium values and the significance in the results lies in the fact that if you operate a semi-batch crystallizer, at a constant temperature and pressure, the mole fraction will remain constant at the onset of hydrate growth and thereafter.

4.2.7   Conclusion

New experimental data regarding the mole fraction of both carbon dioxide and methane in the bulk liquid phase at the onset of hydrate growth in a semi-batch stirred tank reactor were obtained for various operating conditions. As a result, a

new driving force for hydrate growth was proposed. The new driving force substantially simplifies existing hydrate growth models aimed at determining the reaction rate constant of hydrate formation and eliminates the need to account for the resistance at the vapor-liquid water interface. Moreover, it was shown that under similar hydrodynamic, heat and mass transfer conditions, the mole fraction of the gas hydrate former in the bulk liquid phase does not vary significantly with time during the growth stage. It was also shown that the mole fraction of the guest in the bulk liquid phase at the onset of hydrate growth increases with pressure and decreases with temperature.

4.2.8   Acknowledgements

Notation

Please refer to Chapter 9.

References

Please refer to the general bibliography found at the end of the thesis document.

Chapter 5

Carbon Dioxide Clathrate Formation

5.1 Preface

The design of a custom flow-through cell by Hellma with a pressure rating of 6,000 kPa allowed for the study of the carbon dioxide-water system and its relatively high hydrate-liquid water-vapor equilibrium pressures. Furthermore, the availability of carbon dioxide mole fraction measurements in the bulk liquid phase during hydrate growth for various operating conditions, as presented in Chapter 4, enabled the use of the alternate formulation of the kinetic model, thus circumventing the issues associated with the dissolution rate at the vapor-liquid water interface (Chapter 3). The intrinsic kinetics of structure I carbon dioxide hydrate were also investigated for comparison with those of structure II propane hydrate determined previously (Chapter 3). New insights regarding the supersaturation of the bulk liquid phase during hydrate growth, as provided by the experimental measurements highlighted in Chapter 4, as well as the elaboration of a new technique based on the scattering of hydrate particles, enabled a considerable refinement in the calculation of the number of hydrate particles and its evolution during the growth stage.

5.2   Reaction rate constant of CO_2 hydrate formation and verification of old premises pertaining to hydrate growth kinetics

Sébastien Bergeron, Phillip Servio

Department of Chemical Engineering, McGill University, Canada

5.2.1   Abstract

Experimental data on the rate of carbon dioxide hydrate formation in a semi-batch stirred tank reactor were obtained using a particle size analyzer capable of detecting particles as small as 0.6 nanometers in a closed-loop system. Experiments were carried out at temperatures between 275.3 and 279.4 K and pressures ranging from 2,014 to 3,047 kPa. The reaction rate constant of CO_2 hydrate formation was determined using a newly developed kinetic model independent of the dissolution rate at the vapor-liquid water interface. The average reaction rate constant determined experimentally was found to increase with temperature following an Arrhenius-type relationship, from 1.8×10^{-8} m/s to 1.8×10^{-7} m/s, over the 4-degree range investigated. Similarly, the reaction rate constant calculated from a population balance varied from 1.4×10^{-8} m/s to 1.7×10^{-7} m/s over the same temperature interval. The initial number of hydrate particles was calculated using the mole fraction of the gas hydrate former in the bulk liquid phase at the onset of hydrate growth rather than the equilibrium solubility. The cumulative relative scattering was also compared to the derived count rate to determine whether or not the number of hydrate particles remained constant during the hydrate growth experiment.

5.2.2   Introduction

Clathrate hydrates are nonstoichiometric crystalline compounds in which a gas or a volatile liquid molecule suitable for hydrate formation is enclosed in a network

consisting of water molecules linked together through hydrogen bonding. The presence of the gas molecule stabilizes the water lattice via weak van der Waals forces. Three different structures can be found naturally and have been reported in the literature, including structure I (sI), structure II (sII) and structure H (sH) hydrate (Sloan and Koh, 2007). In particular, structure I hydrates contain 2 small cavities and 6 large cavities per unit cell, as well as 46 water molecules (Sloan and Koh, 2007). Assuming full occupancy, it follows that there are 5.75 moles of water per mole of gas hydrate former. As an example, both carbon dioxide and methane form structure I hydrate, while propane forms structure II. Structure H needs two components and water and an example of this is neohexane in the presence of methane. A great deal of research is being conducted on gas hydrates due to their potential applications. Naturally occurring methane hydrates are seen as an alternate energy source (Chatti *et al.*, 2005). Furthermore, it has been suggested that storage and transportation of natural gas (Chatti *et al.*, 2005) or liquefied petroleum gases (Giavarini *et al.*, 2003) could be carried out in hydrate form over more conventional methods such as liquefied natural gas or compressed natural gas. Carbon dioxide sequestration is also looked upon as a means to mitigate the global warming effect (Chatti *et al.*, 2005). Moreover, hydrogen storage in hydrate form is currently studied for mobile applications (Mao *et al.*, 2007). Such promising new technologies are reasons why kinetic studies should be further investigated. In particular, an accurate value for the reaction rate constant of hydrate formation is required for proper reactor design aimed at large-scale hydrate production, such as three-phase slurry reactors (Hashemi *et al.*, 2007a). The reaction rate constant is the sole parameter affecting any reactor throughput and conversion that remains constant upon scale-up, as both heat and mass transfer effects will change.

Numerous studies have been performed to determine the reaction rate constant of hydrate formation in semi-batch stirred tank reactors. Vysniauskas and Bishnoi (1983; 1985) first studied the kinetics of methane and ethane hydrate formation and concluded that the rate of formation was a function of the interfacial area,

pressure, temperature and degree of supercooling. Englezos *et al.* (1987a; 1987b) followed with their pioneering work, in which they proposed a kinetic model for hydrate formation based on crystallization and two-film theory, with one adjustable parameter, *i.e.* the reaction rate constant. They studied the kinetics of methane and ethane hydrate formation, as well as their mixtures. Later on, Monfort and Nzihou (1993) used a laser granulometer capable of detecting particles with sizes between 5.6 - 564 μm, as well as the model of Englezos *et al.* (1987a), to study the kinetics of cyclopropane hydrate formation. Skovborg and Rasmussen (1994) have suggested that hydrate growth is mass transfer limited, where the transport of the gas molecules from the gas phase to the liquid water phase is the rate-determining step. Using the model of Englezos *et al.* (1987a), Chun and Lee (1996) studied the kinetics of carbon dioxide hydrate formation, yielding a reaction rate constant in the order of 10^{-6} mol/(m^2 s MPa). Malegaonkar *et al.* (1997) also studied the kinetics of carbon dioxide hydrate formation. They used a corrected version of the model of Englezos *et al.* (1987a) to account for a minor inconsistency, as well as a correction for the high solubility of carbon dioxide in water, and concluded that the reaction rate constant of carbon dioxide hydrate formation was in the order of 10^{-4} mol/(m^2 s MPa) (Malegaonkar *et al.*, 1997). Mork and Gudmundsson (2002) followed a similar approach to that of Skovborg and Rusmussen (1994), introducing a model for hydrate formation based solely on mass transfer. Clarke and Bishnoi (2005) studied the kinetics of carbon dioxide hydrate formation using an *in situ* particle size analyzer, capable of detecting particles with chord lengths greater than 0.5 μm, and the model of Englezos *et al.* (1987a) Their results yielded a reaction rate constant in the order of 10^{-3} mol/(m^2 s MPa). More recently, Hashemi *et al.* (2007b) concluded that hydrate kinetic models should be based on a concentration driving force. Using their new driving force and the model of Englezos *et al.* (1987a), they revisited the work of Clarke and Bishnoi (2005) and obtained a reaction rate constant of carbon dioxide hydrate formation in the order of either 10^{-5} m/s or 10^{-8} m/s using the surface area measured experimentally by Clarke and Bishnoi (2005) and the one determined from a population balance respectively.

Based on their results, they concluded that a true reaction rate constant of hydrate formation has yet to be determined due to inaccurate surface area measurements (Hashemi *et al.*, 2007b). Bergeron and Servio (2008b) used the driving force proposed by Hashemi *et al.* (2007b) and developed a new kinetic model for hydrate growth. Using such a model and a particle size analyzer capable of detecting particles with a diameter as small as 0.6 nm, they studied the kinetics of propane hydrate formation and obtained a reaction rate constant in the order of 10^{-7} m/s (Bergeron and Servio, 2008b). Nevertheless, due to some ambiguity regarding the actual value of the dissolution rate at the vapor-liquid water interface for a system containing particles (Bergeron and Servio, 2008b; Kluytmans *et al.*, 2003), Bergeron and Servio (2009) introduced an alternate formulation of their model with a driving force based on the difference between the mole fraction of the gas hydrate former in the bulk liquid phase and that under hydrate-liquid water equilibrium. They also reported mole fraction measurements of the gas hydrate former in the bulk liquid phase during hydrate growth. Their results showed that the concentration of the guest remains constant in the bulk liquid phase during hydrate growth and can be used to better estimate the initial number of hydrate particles (Bergeron and Servio, 2009). The current work uses the model of Bergeron and Servio (2009) to determine the reaction rate constant of carbon dioxide hydrate formation.

5.2.3 Experimental apparatus

As shown in Figure 5.1, the current experimental setup consists of an isothermal/isobaric semi-batch stirred tank crystallizer, a gas supply reservoir for hydrate formation and a Zetasizer Nano ZS particle size analyzer (Malvern Instruments). The Zetasizer Nano ZS particle size analyzer can detect particles with diameters between 0.6 and 6,000 nm with a maximum uncertainty of 10 to 15 % on the size obtained from the intensity distribution. Due to the use of Mie theory to convert the intensity distribution into a number distribution, spherical particles are assumed. In addition, the Zetasizer Nano ZS contains an internal cooling device to maintain the desired operating temperature inside the cell. Hydrates are formed in
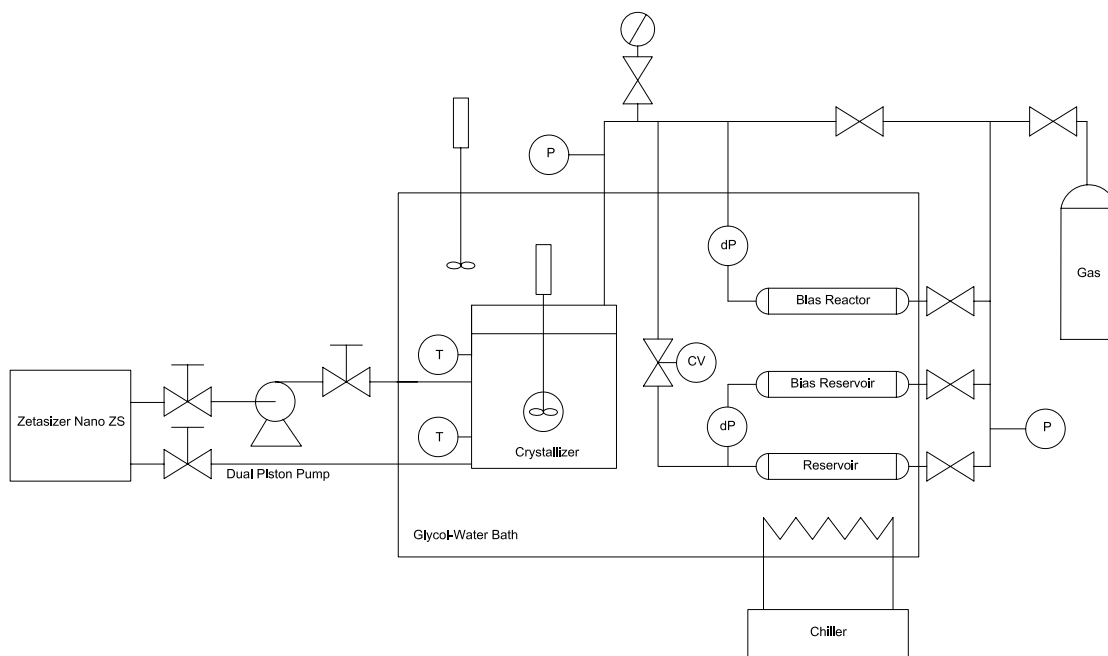
Figure 5.1: Simplified schematic of the experimental setup.

the 600 cm^3 internal volume stainless steel crystallizer (12,000 kPa pressure rating). A PPI DYNA/MAG MM-006 mixer (0 - 2,500 rpm) has been mounted on top of the crystallizer to ensure sufficient mixing. Gas is supplied from the stainless steel reservoir (internal volume of 1,000 cm^3) using a Baumann 51000 Series Low Flow control valve. Part of the crystallizer liquid phase is continuously circulated from the crystallizer to the particle size analyzer using a LabAlliance Model 1500 dual piston pump and a custom flow-through cell (6,000 kPa pressure rating, Hellma). Both the crystallizer and the reservoir are submerged in a cooling bath composed of 10 % glycol and water mixture controlled via a Thermo NESLAB RTE Series refrigerated bath. Temperature and pressure measurements are performed using standard resistance temperature devices (±0.3 ºC) and Rosemount 3051S Series pressure transducers with a reference accuracy of ±0.04 % of the span. The read-outs are then recorded and displayed using the National Instruments NI-DAQ 7 data

acquisition device and the LabVIEW software. The LabVIEW interface was written to calculate the number of moles consumed at any time during the experiment using the Trebble-Bishnoi equation of state (1987), the gas reservoir pressure and temperature measurements, as well as the gas reservoir volume. The standard error propagation technique led to an uncertainty of 3×10^{-3} mol on the experimental mole consumption.

5.2.4   Experimental procedure

Prior to any experiment, the crystallizer is cleaned using HPLC grade water and purged several times using the selected gas (carbon dioxide with Coleman instrument grade 99.99 % purity). A syringe is used to introduce 180 ml of HPLC grade water in the crystallizer. Once thermal equilibrium has been reached, the crystallizer is pressurized above the hydrate-liquid water-vapor equilibrium pressure at the experimental temperature but below the hydrate-liquid carbon dioxide-vapor equilibrium pressure (Figure 5.2). The dual piston pump is then started. Once the temperature in the reservoir and in the crystallizer has stabilized, both the data acquisition program and the crystallizer stirrer are started. The crystallizer stirrer is set to 750 rpm to minimize both heat and mass transfer effects and to reproduce the conditions in the work of Bergeron and Servio (2009). The onset of hydrate growth is identified by a sudden increase in the crystallizer liquid phase temperature, following which several particle size distribution measurements are performed at different times to proper describe the growth stage of hydrate formation.

5.2.5   Theory

5.2.5.1   Kinetic model

Bergeron and Servio (2009) have proposed an alternate formulation of their kinetic model that is independent of the dissolution rate at the vapor-liquid water interface. According to their model, the rate at which gas is consumed for hydrate growth is
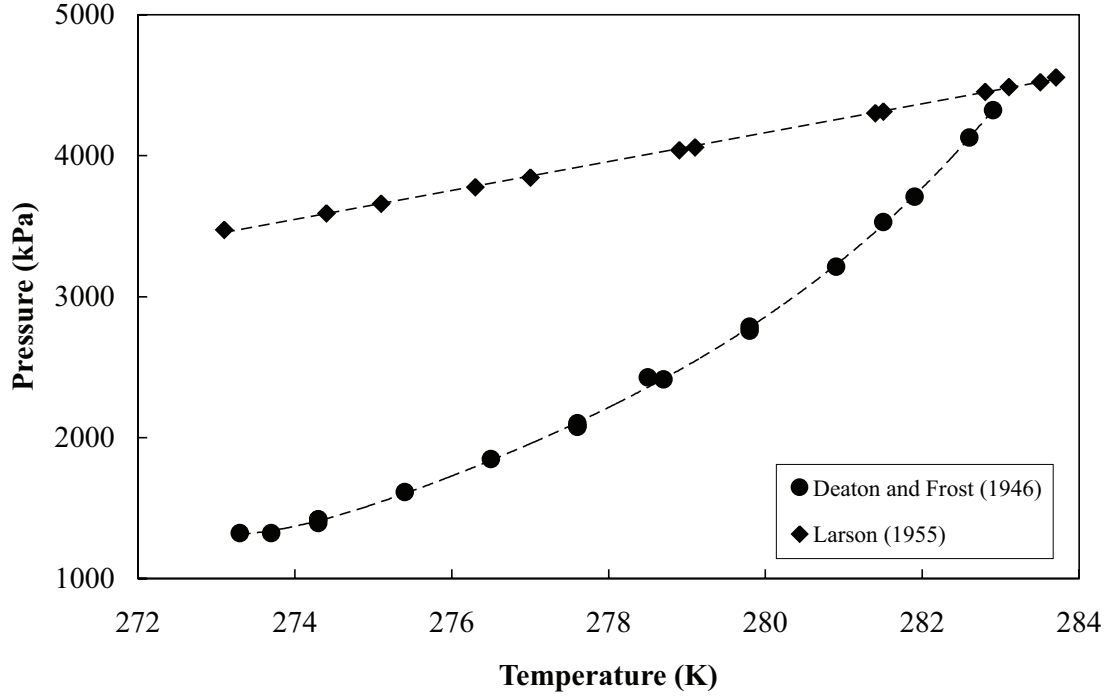
Figure 5.2: Carbon dioxide-water phase diagram using the experimental data of Deaton and Frost (1946) and Larson (Sloan, 1998b).

given by (Bergeron and Servio, 2009):

$$\frac{dn}{dt} = \frac{V_L \rho_w}{MW_w} \frac{\left(x^b - x^{HL}\right)}{\pi \mu_2(t) k_r} \tag{5.1}$$

where V_L, ρ_w and MW_w is the volume of liquid water, the density of water and the molecular weight of water respectively. In addition, x^b is the mole fraction of the gas hydrate former in the bulk liquid phase at the experimental temperature and experimental pressure, while x^{HL} is the solubility in water of the gas hydrate former under hydrate-liquid water equilibrium at the experimental temperature and experimental pressure. In their work, Bergeron and Servio (2009) concluded that the mole fraction of the guest in the bulk liquid phase remains constant during hydrate growth. μ_2 is the second moment of the particle size distribution and k_r

is the reaction rate constant of hydrate formation. Note that a detailed derivation of equation 5.1 and its parameters can be found elsewhere (Bergeron and Servio, 2008b, 2009).

As mentioned previously, the model of Bergeron and Servio (2009) was proposed due to the difficulty in measuring an accurate value for the dissolution rate at the vapor-liquid water interface. In previous kinetic studies (Englezos *et al.*, 1987a; Chun and Lee, 1996; Malegaonkar *et al.*, 1997; Clarke and Bishnoi, 2005), researchers used the value obtained from solubility experiments where the dissolution rate was measured in a system under vapor-liquid water equilibrium conditions. Hence, no hydrate particles were present and it seemed legitimate to assume that both the vapor-liquid water interfacial area and the mass transfer coefficient at the interface remained constant. However, in their recent study, Bergeron and Servio (2008b) suggested that due to the presence of hydrate particles during hydrate growth experiments, either the vapor-liquid water interfacial area, or the mass transfer coefficient at the interface, or both, could differ from the values measured through typical solubility experiments. These conclusions were also based on the work of Kluytmans *et al.* (2003) performed with systems containing carbon particles. Since the driving force used in equation 5.1 is based on the mole fraction of the gas hydrate former in the bulk liquid phase, the model is independent of the dissolution rate and removes any ambiguity regarding such an issue.

The optical properties required by the particle size analyzer, namely the refractive index and the absorption of carbon dioxide hydrates, were obtained from the work of Bonnefoy *et al.* (2005) and Warren (1984) respectively. In the latter case, since only an order of magnitude estimate was required, carbon dioxide hydrates were assumed to have absorption values similar to that of ice Ih (hexagonal ice), which is the most common solid form of water (Sloan and Koh, 2007). Such an assumption is based on the fact that hydrates are comprised of roughly 85 % water on a molecular basis. Furthermore, x^b is obtained from the work of Bergeron and

Servio (2009), while x^{HL} is obtained from the model of Hashemi *et al.* (2006). As for μ_2, it can be obtained either experimentally, using the particle size analyzer, or from a semitheoretical approach using a population balance. In the latter case, assuming a constant volume, a size-independent growth and a constant number of particles, the population balance yields (Kane *et al.*, 1974):

$$\frac{d\varphi}{dt} + \frac{d(G\varphi)}{dL} = 0 \tag{5.2}$$

where G is the growth rate and L the hydrate diameter. Using the mean diameter obtained for each particle size distribution measurement performed, an expression for the growth rate can be obtained using the following:

$$G = \frac{dL}{dt} \tag{5.3}$$

Equation 5.2 can then be transformed into a set of differential equations and performing the moment transformations (Kane *et al.*, 1974) leads to:

$$\mu_0 = \mu_0^0 \tag{5.4}$$

$$\mu_1 = \mu_0^0 Gt + \mu_1^0 \tag{5.5}$$

$$\mu_2 = \mu_0^0 G^2 t^2 + 2\mu_1^0 Gt + \mu_2^0 \tag{5.6}$$

where μ_0, μ_1 and μ_2 are the zeroth, first and second moments respectively. The initial number of particles is discussed in the subsequent section, while μ_1^0 and μ_2^0 are given by:

$$\mu_1^0 = L_c \mu_0^0 \tag{5.7}$$

$$\mu_2^0 = L_c{}^2 \mu_0^0 \tag{5.8}$$

where L_c is the critical nuclei diameter and is obtained by performing a size distribution measurement at the onset of hydrate growth. Incorporating equations 5.6, 5.7 and 5.8 into equation 5.1 allows for the determination of the reaction rate constant using a population balance:

$$\frac{dn}{dt} = \frac{V_L \rho_w}{MW_w} \frac{\left(x^b - x^{HL}\right)}{\pi \left(\mu_0^0 G^2 t^2 + 2 L_c \mu_0^0 G t + L_c^2 \mu_0^0\right) k_r} \tag{5.9}$$

5.2.5.2 Number of hydrate particles

Bergeron and Servio (2009) also suggested that the initial number of hydrate particles should be calculated using the number of moles of the gas hydrate former in the bulk liquid phase at the onset of hydrate growth. Accordingly, the initial number of hydrate particles is given by (Bergeron and Servio, 2009):

$$\mu_0^0 = \frac{6 MW_w \left(n_{tb} - n^b\right)}{\eta \pi V_L \rho_w L_c^3} \tag{5.10}$$

where MW_w and ρ_w is the molecular weight and density of the hydrate respectively. The number of moles of gas dissolved at turbidity is given by n_{tb}, while η is the number of moles of gas per mole of hydrate. Note that full occupancy of both the small and large cavities was assumed in the calculations.

There is some controversy regarding the assumption that the number of hydrate particles remains constant during the growth stage. Englezos *et al.* (1987a) considered secondary nucleation but concluded that it was negligible since hydrate crystals are very small. Herri *et al.* (1999a; 1999b) studied the role of primary nucleation, true secondary nucleation, breakage, attrition and agglomeration on methane hydrate crystallization. Their turbidimetry measurements allowed for the detection of particles with sizes between 10 and 150 μm. They concluded that a simplified model of continuously active primary nucleation and growth was sufficient to explain the early stage of crystallization and the effect of the stirring rate on the initial mean diameter and the initial number of particles (Herri *et al.*, 1999b). They also sug-

gested that attrition could explain the behavior of crystallization for longer times at high stirring rates (Herri *et al.*, 1999b). The authors of the present work are skeptical regarding the possibility of true secondary nucleation due to the intense mixing (750 rpm) occurring in the current semi-batch stirred tank reactor. For true secondary nucleation to proceed, local supersaturation of the gas hydrate former in the bulk liquid phase would have to persist long enough for new nuclei to form. On the other hand, we believe it is more likely that existing hydrate particles will consume any excess in gas.

In their extensive literature review of existing hydrate growth models, Ribeiro and Lage (2008) concluded that future models should account for the particle size distribution, including particle agglomeration and breakage. In an attempt to determine if particle breakage, agglomeration and/or attrition play a significant role, a new technique was developed to assess whether or not the number of hydrate particles remains constant during hydrate growth. First, the Zetasizer Nano ZS particle size analyzer provides the derived count rate for each size distribution measurement performed. Such a count rate, which is normalized for the cell position and the attenuation used, represents the number of photons detected by the particle size analyzer. The software package used with the Zetasizer Nano ZS particle size analyzer also includes a utility that uses Mie theory to predict the relative scattering per particle for a given set of optical properties. Hence, for the size range detectable by the Zetasizer Nano ZS, namely from 0.6 to 6,000 nm, the relative scattering distribution can be obtained. For certain size range, *e.g.* from approximately 1 to 240 nm, Mie theory predicts an increasing relative scattering per particle. However, for other size range, *e.g.* from approximately 240 to 340 nm, Mie theory predicts a decreasing relative scattering per particle. It follows that depending on the size range the hydrate particles are in, the relative scattering per particle will either increase or decrease from one measurement to the other. Using the various size distributions obtained experimentally, the cumulative relative scattering is calculated for each measurement. Hence, comparing the trend of the cumulative relative

scattering to the derived count rate can shed light on the number of particles. In the event that both the derived count rate and the cumulative relative scattering follow the same trend over time, it can be assumed that the number of particles remains constant. Even though it is impossible to confirm with certainty such an assumption, a significant change in the number of hydrate particles would lead to opposite trends for the derived count rate and the cumulative relative scattering.

5.2.6 Results and discussion

Several experiments were performed over a 4-degree interval to determine the reaction rate constant of carbon dioxide hydrate formation. As mentioned previously,
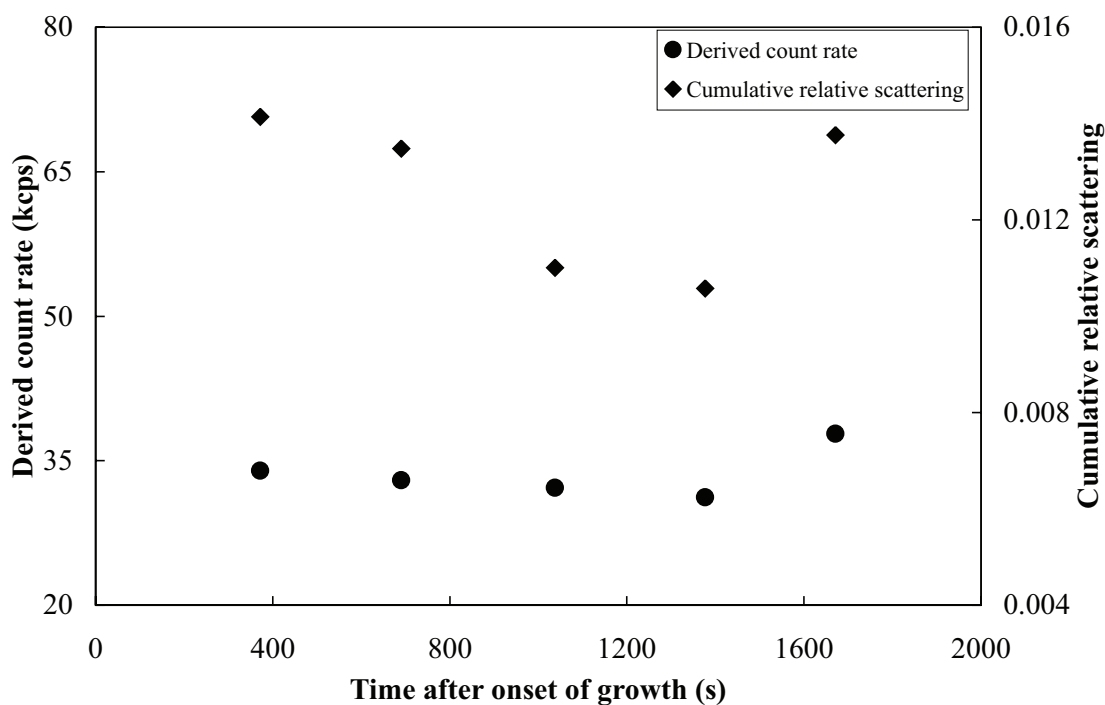
Figure 5.3: Comparison of the derived count rate and the cumulative relative scattering at 279.2 K and 3,047 kPa.

the reaction rate constant was determined using both equations 5.1 and 5.9, to com-

pare the experimental value to the semitheoretical one (population balance). For each experiment, the derived count rate was compared to the cumulative relative scattering to determine if the number of hydrate particles remains constant during the growth stage. Figure 5.3 shows such a comparison at 279.2 K and 3,047 kPa. It can be seen that over the entire duration of the experiment, both the derived count rate and the cumulative relative scattering follow the same trend, fostering the hypothesis that the number of hydrate particles remains constant. Figure 5.4 shows the second moment obtained experimentally using the particle size analyzer at 279.2 K and 3,047 kPa. As expected, hydrate particles grow with time, resulting
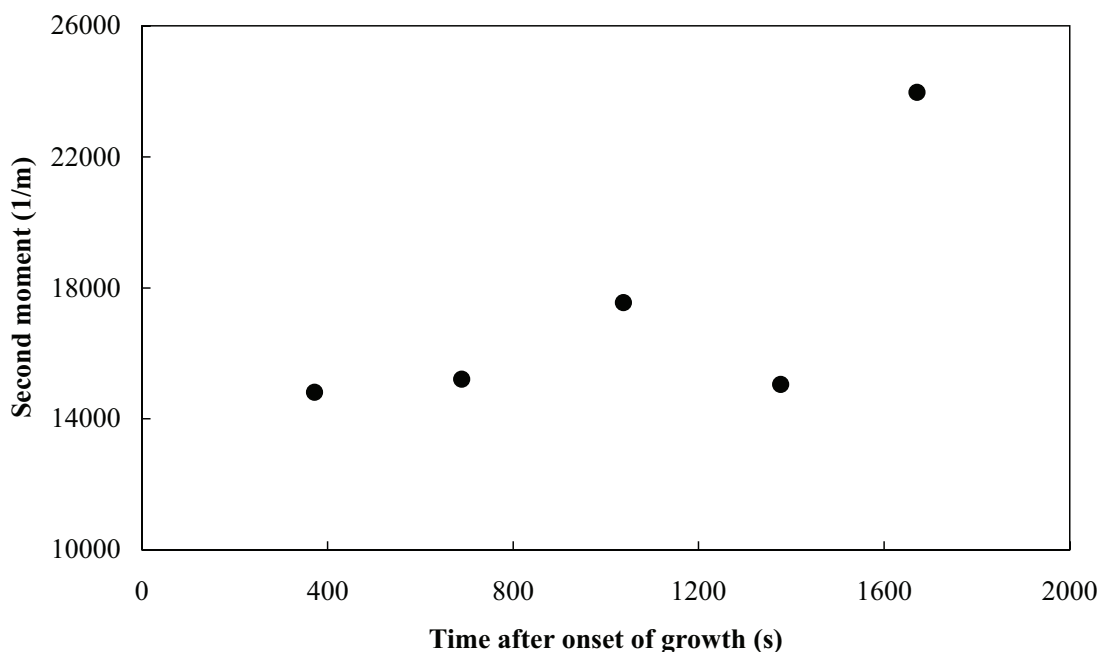
Figure 5.4: Experimental second moment of the particle size distribution at 279.2 K and 3,047 kPa.

in an increase in the total surface area and thus, an increase in the second moment. Both equations 5.1 and 5.9 were integrated and compared to the experimental mole consumption. The reaction rate constant was regressed using the Gauss-Newton method with Levenberg-Marquardt's modification. Figure 5.5 shows the compari-
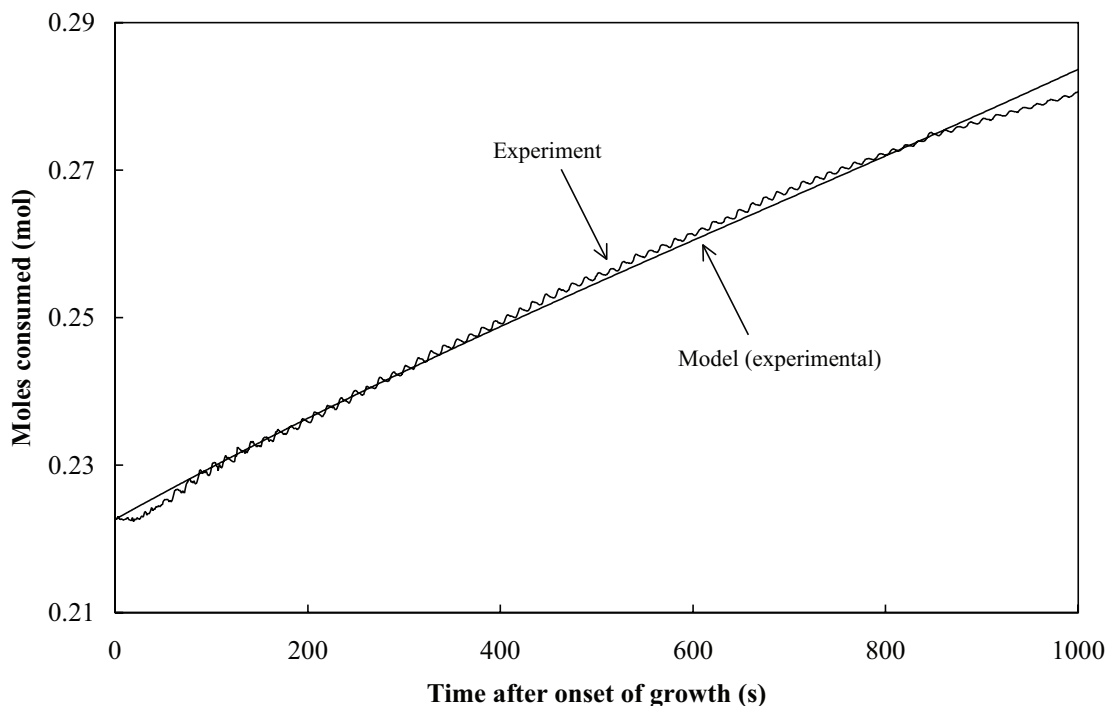
Figure 5.5: Comparison between the experimental mole consumption and the model predictions at 279.2 K and 3,047 kPa.

son between the experimental mole consumption and the model predictions at 279.2 K and 3,047 kPa. For those conditions, a reaction rate constant of 1.62×10^{-7} m/s was obtained experimentally, while a value of 1.44×10^{-7} m/s was obtained using a population balance. Clearly, a very good agreement exists between the experimental data and the model, with an average absolute relative error of 0.3 % for the experimental reaction rate constant and of 0.7 % for the semitheoretical one.

Table 5.1: Average reaction rate constant of CO_2 hydrate formation ($\times 10^{-8}$ m/s)

Average temperature (K)	Experimental k_r	Semitheoretical k_r
275.5	1.8 $\pm$0.3	1.4 $\pm$0.2
277.5	4.5 $\pm$1.0	4.1 $\pm$0.4
279.3	18.0 $\pm$2.0	17.0 $\pm$2.0
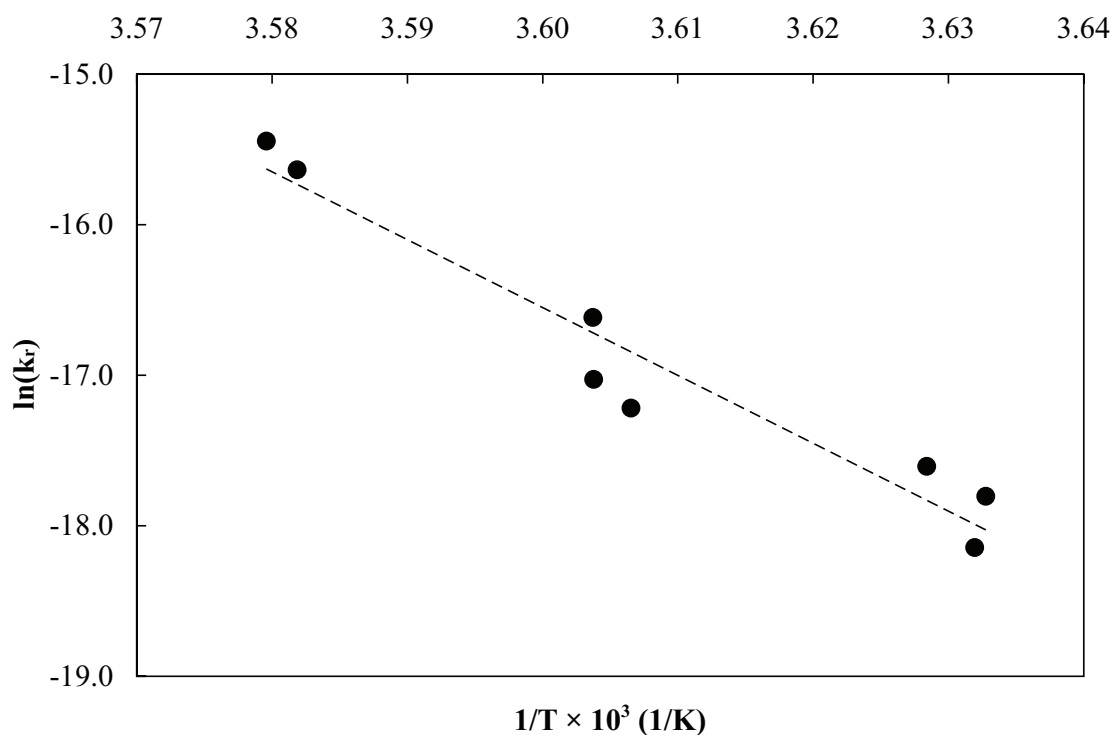
Figure 5.6: Reaction rate constant of CO_2 hydrate formation over a 4-degree interval.

Table 5.1 lists the average reaction rate constant obtained for various temperatures based on replicates. As it can be seen from Figure 5.6, the reaction rate constant increases with temperature and follows an Arrhenius-type relationship. To the best of our knowledge, we are the first to report such a trend for the reaction rate constant of any hydrate former, based on experimental measurements. Indeed, some researchers (Englezos *et al.*, 1987a; Malegaonkar *et al.*, 1997; Clarke and Bishnoi, 2005) have reported a minimum value for the reaction rate constant of several hydrate formers around 277 K, while Englezos *et al.* (1987a) highlighted that such a trend coincides with the highest density of water. The authors are skeptical regarding such an implication since no such trend was observed in the current study. Moreover, the change in water density is not significant over the temperature inter-

val investigated. Finally, all the studies reporting such a minimum in the reaction rate constant incorporated the model of Englezos *et al.* (1987a) and two-film theory, while the current study is the first to use a different approach.

Since previous studies for the reaction rate constant of carbon dioxide hydrate formation were based on a fugacity driving force (Chun and Lee, 1996; Malegaonkar *et al.*, 1997; Clarke and Bishnoi, 2005), the current values can only be compared to the work of Hashemi *et al.* (2007b), who revisited the work of Clarke and Bishnoi (2005) using a concentration driving force and the model of Englezos *et al.* (1987a). The values reported in the present work for the reaction rate constant of CO_2 hydrate formation at 277.5 K, namely 4.5 $\times 10^{-8}$ m/s and 4.1 $\times 10^{-8}$ m/s depending on the method used, are in relative agreement with the value reported by Hashemi *et al.* (2007b) using a population balance at 277.15 K, *i.e.* 1.20 $\times 10^{-8}$ m/s.

5.2.7   Conclusion

The reaction rate constant of carbon dioxide hydrate formation was successfully determined over a 4-degree interval. The reaction rate constant determined experimentally was found to increase with temperature following an Arrhenius-type relationship, from 1.8 $\times 10^{-8}$ m/s to 1.8 $\times 10^{-7}$ m/s, over the 4-degree range investigated. Similarly, the reaction rate constant calculated from a population balance varied from 1.4 $\times 10^{-8}$ m/s to 1.7 $\times 10^{-7}$ m/s over the same temperature interval.

5.2.8   Acknowledgements

Notation

Please refer to Chapter 9.

References

Please refer to the general bibliography found at the end of the thesis document.

Chapter 6

Methane Clathrate Formation

6.1 Preface

The results obtained for the intrinsic kinetics of propane (Chapter 3) and carbon dioxide (Chapter 5) hydrate formation indicated faster intrinsic kinetics for structure II propane hydrate than for structure I carbon dioxide hydrate. To foster such a claim, additional kinetic experiments were performed to determine the reaction rate constant of methane clathrate formation (structure I). As detailed in Chapter 5, only the temperature dependency of the reaction rate constant of carbon dioxide hydrate formation, found to follow an Arrhenius-type relationship, was investigated due to the appearance of a liquid carbon dioxide phase for pressures as low as 3,600 kPa ($T \sim 275$ K). Since no such limitations exist for the methane-water system, both the temperature and pressure dependency of the reaction rate constant were investigated. An energy balance at the onset of methane hydrate growth was also included to further support the calculation of the number of hydrate particles.

6.2 Reaction rate constant of methane clathrate formation

Sébastien Bergeron, Juan G. Beltrán, Phillip Servio
Department of Chemical Engineering, McGill University, Canada

6.2.1 Abstract

Particle size distribution measurements were performed during the growth stage of methane hydrate formation in a semi-batch stirred tank crystallizer. Experiments were carried out at temperatures between 275.1 and 279.2 K and pressures ranging from 3,873 to 5,593 kPa. The reaction rate constant of methane hydrate formation was determined using the model of Bergeron and Servio (AIChE J. 54(2008)2964). The experimental reaction rate constant was found to increase with temperature, following an Arrhenius-type relationship, from 8.3 $\times 10^{-8}$ m/s to 6.15 $\times 10^{-7}$ m/s over the 4-degree range investigated, resulting in an activation energy of 323 kJ/mol. An increase in pressure of approximately 600 kPa did not have any effect on the reaction rate constant. Population balances, based on the measured critical nuclei diameter and that predicted by homogeneous nucleation theory, were also used for comparison purposes. The initial number of hydrate particles was calculated using the mole fraction of methane in the bulk liquid phase and compared to that predicted by an energy balance.

6.2.2 Introduction

Clathrate hydrates are nonstoichiometric compounds that form when small molecules come in contact with water at relatively low temperatures and high pressures. The host molecules (water) are linked together through hydrogen bonding, while weak van der Waals forces exist between the host and guest molecules. The most common hydrate structures found in nature are structure I (sI), structure II (sII) and structure H (sH) (Sloan and Koh, 2007). Methane forms structure I hydrate with 46

water molecules forming two small cavities and six large cavities per unit cell (Sloan and Koh, 2007). Hydrates are studied for various reasons, including the possibility to store and transport liquefied petroleum gases or natural gas in hydrate form (Giavarini *et al.*, 2003; Thomas and Dawe, 2003). Carbon dioxide sequestration in hydrate form is also looked upon as a means to mitigate the global warming effect (Chatti *et al.*, 2005). Considering such applications, large-scale hydrate production is of prime interest. The reaction rate constant of hydrate formation is the sole parameter affecting any reactor conversion and throughput, such as a three-phase slurry reactor (Hashemi *et al.*, 2007a), that remains constant upon scale-up, as both heat and mass transfer effects will change. Consequently, an accurate value for the reaction rate constant of hydrate formation is required for proper reactor design aimed at large-scale hydrate production. Simarly, the study of hydrate growth *in situ* represents another reason why intrinsic kinetic experiments, and the subsequent determination of the reaction rate constant, are of prime interest.

Numerous studies have been performed to study the intrinsic kinetics of hydrate formation in semi-batch stirred tank crystallizers. Vysniauskas and Bishnoi (1983; 1985) studied the kinetics of methane and ethane hydrate formation and assumed an Arrhenius-type function for the temperature dependence of the reaction rate constant. Englezos *et al.* (1987a; 1987b) work followed with pioneering studies on the kinetics of methane and ethane hydrate formation, as well as their mixtures. The model of Englezos *et al.* (1987a) was based on crystallization and two-film theory, using the reaction rate constant as the sole adjustable parameter. They reported a value in the order of 10^{-6} mol/(m^2 s MPa) for the reaction rate constant of methane hydrate formation (Englezos *et al.*, 1987a). The reaction rate constant was also found to decrease from 274 to 276 K, while increasing from 276 to 282 K (Englezos *et al.*, 1987a). Monfort and Nzihou (1993) followed with particle size distribution measurements to study the kinetics of cyclopropane hydrate formation. Using a laser granulometer, they could detect particles between 5.6 and 564 μm (Monfort and Nzihou, 1993). Malegaonkar *et al.* (1997) used a modified version

of the model of Englezos *et al.* (1987a) to account for a minor inconsistency and studied the kinetics of carbon dioxide and methane hydrate formation. They reported a value for the reaction rate constant of methane hydrate formation in the order of 10^{-5} mol/(m^2 s MPa) (Malegaonkar *et al.*, 1997). As it was the case with Englezos *et al.* (1987a), the reaction rate constant was found to decrease from 274 to 276 K and to increase from 276 to 282 K. Herri *et al.* (1999a; 1999b) studied the role of primary nucleation, secondary nucleation (breakage, attrition, true secondary nucleation) and agglomeration on methane hydrate crystallization. Their turbidimetry measurements allowed for the detection of particles with sizes between 10 and 150 μm (Herri *et al.*, 1999b). Chun and Lee (1996), using the model of Englezos *et al.* (1987a), determined the reaction rate constant of carbon dioxide hydrate formation. Clarke and Bishnoi (2005), using the model of Englezos *et al.* (1987a) and particle size distribution measurements for chord lengths greater than 0.5 μm, reported a value for the reaction constant of carbon dioxide hydrate formation one and three orders of magnitude greater than that determined by Malegaonkar *et al.* (1997) and Chun and Lee (1996) respectively. Clarke and Bishnoi measured a reaction rate constant decreasing from 274.15 to 277.15 K, while increasing from 277.15 to 279.65 K (2005). Hashemi *et al.* (2007b) modified the model of Englezos *et al.* (1987a) using concentrations as the driving force and revisited the work of Clarke and Bishnoi (2005). They concluded that the second moment measured experimentally by Clarke and Bishnoi (2005) was three orders of magnitude smaller than that determined from a population balance using homogeneous nucleation theory and a constant number of hydrate particles (Hashemi *et al.*, 2007b). In their literature review, Ribeiro and Lage (2008) concluded that any future hydrate growth model should include particle size distribution measurements and account for particle agglomeration and breakage. Bergeron and Servio (2008b) developed a new hydrate growth model using the driving force of Hashemi *et al.* (2007b) and determined the reaction rate constant of propane hydrate formation with a particle size analyzer capable of detecting particles in the nanometer range. They reported a value in the order of 10^{-7} m/s at 274.2 K (Bergeron and Servio, 2008b). More recently,

Bergeron and Servio (2009) measured the mole fraction of both carbon dioxide and methane in the bulk liquid phase at the onset of hydrate growth and thereafter. Their results showed that the mole fraction of the gas hydrate former in the bulk liquid phase increases with pressure, decreases with temperature and remains constant during at least the first 13 minutes of the growth stage (Bergeron and Servio, 2009). Based on these results, they proposed an alternate formulation to their existing model independent of the dissolution rate at the vapor-liquid water interface (Bergeron and Servio, 2009). They successfully measured the reaction rate constant of carbon dioxide hydrate formation (Bergeron and Servio, 2008a), and concluded that the reaction rate constant of CO_2 hydrate formation follows an Arrhenius-type relationship. In addition, they collected experimental evidence to support the claim that the number of hydrate particles remained constant over the early stage of the growth period.

There is some controversy regarding the rate-limiting step for hydrate growth in a semi-batch stirred tank crystallizer. While some consider the hydrate intrinsic kinetics to be the limiting step (Englezos *et al.*, 1987a; Malegaonkar *et al.*, 1997; Chun and Lee, 1996; Clarke and Bishnoi, 2005; Bergeron and Servio, 2008b), others like Skovborg and Rasmussen (1994) and Mork and Gudmundsson (2002) have proposed models that neglect the reaction rate constant, and are solely based on mass transfer considerations. The most recent model of Bergeron and Servio (2009) circumvents this ambiguity for it relies on experimental measurements of the mole fraction of the gas hydrate former in the bulk liquid phase to accurately predict hydrate growth regardless of the rate-limiting step. It can be expected that a change in the interfacial area or in the mass transfer coefficient at the vapor-liquid water interface will alter the rate at which gas is transported to the liquid phase. As a result, the concentration of the gas hydrate former in the bulk liquid phase will reach a value to equate the rate at which gas is consumed for hydrate growth to the rate at which it is replenished in the liquid phase. Since the model of Bergeron and Servio (2009) uses the mole fraction of the gas hydrate former in bulk liquid

phase, it can account for such changes and can be used to accurately measure the intrinsic kinetics of hydrate formation. From a more general point of view, the debate over the rate-limiting step for hydrate growth in a stirred tank crystallizer is of little importance when considering that other types of reactors, such as three-phase slurry reactors (Hashemi *et al.*, 2007a), require an accurate value of the reaction rate constant for proper design. Hence, the current work uses a similar approach to that of Bergeron and Servio (2008a) to determine the reaction rate constant of methane hydrate formation.

6.2.3   Experimental apparatus

The current experimental setup displayed in Figure 6.1 consists of an isothermal/isobaric semi-batch stirred tank crystallizer, a 1,000 cm^3 gas supply reservoir for hydrate formation and a Zetasizer Nano ZS particle size analyzer (Malvern Instruments). The Zetasizer Nano ZS can detect particles between 0.6 and 6,000 nm in diameter (sample-dependent), with a maximum uncertainty of 10 to 15 % on the size obtained from the intensity distribution. Spherical particles are assumed when converting the intensity distribution to a number distribution through the use of Mie theory. The particle size analyzer also contains an internal cooling device to maintain the desired operating temperature inside the custom flow-through cell where the measurements are performed. The quartz flow-through cell was custom designed by Hellma with an internal volume of approximately 100 μl, a 8.5 mm centre height and a 6,000 kPa pressure rating. Hydrates are formed in the 600 cm^3 internal volume stainless steel crystallizer (7.62 cm internal diameter, 12,000 kPa pressure rating). A PPI DYNA/MAG MM-006 mixer (0 - 2,500 rpm) with a 3.175 cm four-blade paddle has been mounted on top of the crystallizer to ensure sufficient mixing. The four-blade paddle is located approximately halfway in the liquid phase. Gas is supplied from the stainless steel reservoir using a Baumann 51000 Series Low Flow control valve. A sample of the crystallizer liquid phase is continuously circulated to the particle size analyzer using a LabAlliance Model 1500 dual piston pump. Both the crystallizer and the reservoir are submerged in a cooling bath com-
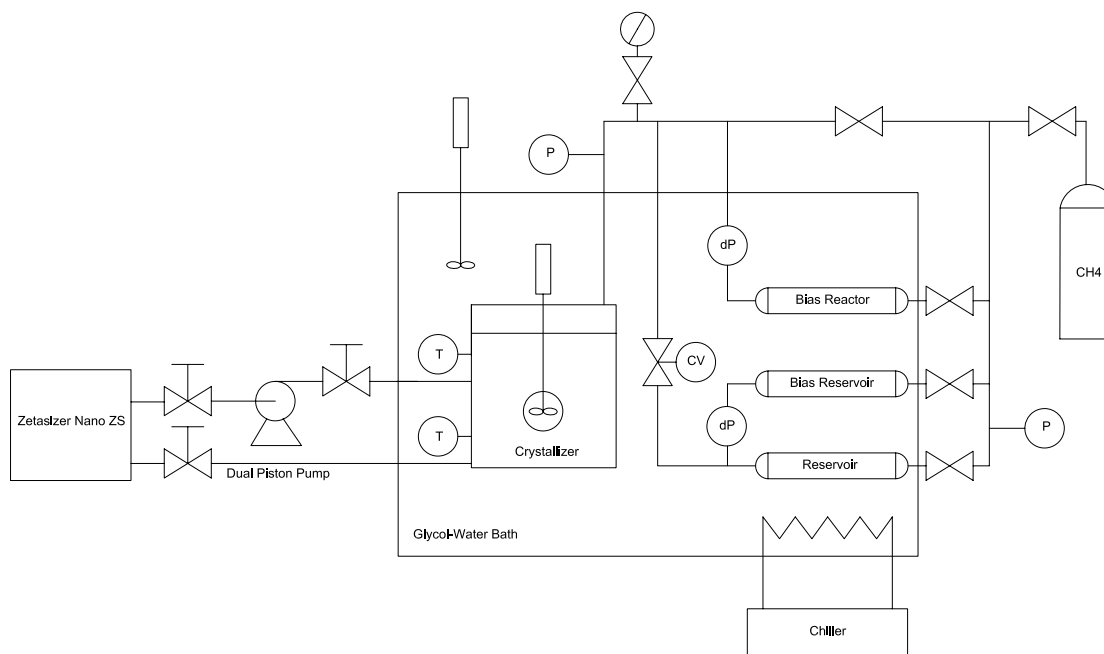
Figure 6.1: Simplified schematic of the experimental setup.

posed of a 10 % glycol and water mixture controlled via a Thermo NESLAB RTE Series refrigerated bath. Temperature and pressure measurements are performed using standard resistance temperature devices ($\pm 0.3\ ^oC$) and Rosemount 3051S Series pressure transducers with a reference accuracy of ± 0.04 % of the span. The readouts are then recorded and displayed using the National Instruments NI-DAQ 7 data acquisition device and the LabVIEW software. The LabVIEW interface was written to calculate the number of moles consumed at any time during the experiment using the Trebble-Bishnoi equation of state (1987), the gas reservoir pressure and temperature measurements, as well as the gas reservoir volume.

6.2.4 Experimental procedure

Prior to any experiment, the crystallizer is cleaned using HPLC grade water and purged several times using methane gas (grade 4.0 99.99 % purity). A syringe is

used to introduce 180 ml of HPLC grade water in the crystallizer. Once thermal equilibrium has been reached, the crystallizer is pressurized above the hydrate-liquid water-vapor equilibrium pressure at the experimental temperature and the dual piston pump is started. Once the temperature in the reservoir and in the crystallizer has stabilized, both the data acquisition program and the crystallizer stirrer are started. The crystallizer stirrer is set to 750 rpm to minimize resistance to both heat and mass transfer, and to reproduce the conditions used in the work of Bergeron and Servio (2009). The onset of hydrate growth is identified by a sudden increase in the crystallizer liquid phase temperature, following which several particle size distribution measurements are performed at different times to properly describe the growth stage of hydrate formation.

6.2.5 Theory

6.2.5.1 Kinetic model

The model used in the current work is that of Bergeron and Servio (2009), where the rate at which gas is consumed for hydrate growth is given by:

$$\frac{dn}{dt} = \frac{V_L \rho_w}{MW_w} \frac{(x^b - x^{HL})}{\frac{1}{\pi \mu_2(t) k_r}} \tag{6.1}$$

where MW_w is the molecular weight of water, ρ_w is the density of water at the experimental temperature and V_L is volume of water contained in the crystallizer. The resistance to hydrate growth comprises the second moment of the particle size distribution (μ_2) and the reaction rate constant (k_r). Even though there is an additional resistance to hydrate growth, namely a diffusion layer around the hydrate particles where the gas molecules need to diffuse, Bergeron and Servio (2008b) have shown that such a resistance is negligible compared to the kinetic resistance for the system at hand. The driving force for hydrate growth is defined as (x^b - x^{HL}). The mole fraction of the gas hydrate former in the bulk liquid phase (x^b), at the experimental temperature and pressure, is obtained from the

experimental measurements of Bergeron and Servio (2009), while its solubility under hydrate-liquid water equilibrium (x^{HL}), again at the experimental temperature and pressure, is calculated using the model of Hashemi *et al.* (2006). The equilibrium solubility is evaluated at the experimental temperature and pressure because under these constant conditions, the methane-water mixture strives towards this value in accordance with the Gibbs phase rule.

6.2.5.2 Number of hydrate particles

There is some disagreement regarding the assumption that the number of hydrate particles remains constant during the growth stage. Englezos *et al.* (1987a) considered secondary nucleation but concluded that it was negligible since hydrate crystals are very small, as predicted by homogeneous nucleation theory. They suggested that if hydrate growth was left to proceed for extended periods of time, agglomeration and breakage, due to particle-particle, particle-stirrer and particle-wall collisions, could become significant (Englezos *et al.*, 1987a). Herri *et al.* (1999b) concluded that a simplified model of continuously active primary nucleation and growth was sufficient to explain the early stage of crystallization and the effect of the stirring rate on the initial mean diameter and the initial number of particles. They also suggested that attrition could explain the behavior of crystallization for longer times at high stirring rates, while true secondary nucleation could not play a significant role in the crystallization of methane hydrate (Herri *et al.*, 1999b). The apparatus used by Herri *et al.* (1999b) allowed them to measure particles with a minimum size of 10 μm, which could explain why they reported a rapid increase in the number of particles initially, as the growing particles gradually enter the size range detectable by the apparatus. Bergeron and Servio (2008a) studied the kinetics of carbon dioxide hydrate formation using the same particle size analyzer as in the present work (capable of detecting particles in the nanometer range) and concluded that the number of hydrate particles remains constant during the early stage of crystallization. Their conclusion highlights the fact that the time interval over which the kinetic studies are performed is another key aspect in determining if the number of hydrate

particles remains constant. Agglomeration, breakage and attrition are more likely to occur as particles reach considerable sizes. Since the reaction rate constant of hydrate formation is an intrinsic parameter independent of time, the experiments are conducted over approximately the first 15 minutes of the growth stage, as the particles remain in the nanometer range.

The following technique was used to confirm whether or not the number of hydrate particles remains constant during the growth stage. For each size distribution measurement, a derived count rate is obtained, which is a measure of the number of photons detected and is normalized for the cell position and attenuation used. The software package used with the particle size analyzer uses Mie theory to predict the relative scattering per particle for a given set of optical properties. The relative scattering per particle can be obtained for the size range detectable by the apparatus, namely from 0.6 to 6,000 nm. Mie theory predicts an increasing relative scattering per particle from approximately 1 to 240 nm, yet it predicts a decreasing relative scattering per particle from approximately 240 to 340 nm. It follows that depending on the size range the hydrate particles are in, the cumulative relative scattering will either increase or decrease from one measurement to the other. Comparing the trend of the cumulative relative scattering to that of the derived count rate with respect to time can shed light on the number of particles. In the event that both the derived count rate and the cumulative relative scattering follow the same trend over time, it can be assumed that the number of particles remains constant, while a significant change in the number of hydrate particles would lead to opposite trends.

The number of particles per unit of liquid volume (μ_0^0) is calculated at the onset of hydrate growth using the method proposed by Bergeron and Servio (2009):

$$\mu_0^0 = \frac{6MW_H(n_{tb} - n^b)}{\eta \pi V_L \rho_H L_c{}^3} \tag{6.2}$$

where MW_H is the molecular weight of the hydrate, ρ_H is the density of the hydrate and η is the number of moles of gas per mole of hydrate. Full occupancy

is assumed when calculating the variables mentioned previously. The volume of liquid in the crystallizer is denoted by V_L and L_c is the critical nuclei diameter for hydrate formation. The latter is either measured experimentally using the particle size analyzer at the onset of hydrate growth, or calculated assuming homogeneous nucleation theory (details are given in section 6.2.5.4). The number of moles of gas entering the hydrate phase (n_{tb} - n^b) is the difference between the number of moles of methane dissolved at turbidity and that in the bulk liquid phase, based on the experimental measurements of Bergeron and Servio (2009).

One of the most recurrent critiques of the various hydrate growth models is their sensitivity with regards to the number of moles consumed at turbidity for the determination of the number of hydrate particles (Sloan and Koh, 2007). Using the number of moles in the bulk liquid phase in equation 6.2, rather than the two (Hashemi *et al.*, 2007b; Bergeron and Servio, 2008b) or three-phase (Englezos *et al.*, 1987a; Malegaonkar *et al.*, 1997; Chun and Lee, 1996) equilibrium value, yields a better estimate for the number of hydrate particles. Furthermore, to test the veracity of the value obtained for the number of moles dissolved at turbidity using the experimental mole consumption, an energy balance is also performed at the onset of hydrate growth to relate the increase in temperature (hydrate formation is an exothermic process) to the number of moles of methane that entered the hydrate phase. Assuming full occupancy, the number of moles of methane dissolved at turbidity is given by:

$$n_{tb} = \frac{m_w C p_w \Delta T}{\Delta H_{form}} + n^b \tag{6.3}$$

where m_w is the mass of water in the crystallizer, Cp_w is the heat capacity of water, ΔH_{form} is the heat of methane hydrate formation taken from the work of Kang *et al.* (2001) and ΔT is the change in temperature measured at the onset of hydrate growth in the liquid phase of the crystallizer. The number of moles of methane in the bulk liquid phase (n^b) is obtained from the experimental measurements of Bergeron and Servio (2009). Equation 6.3 can be used to compare the number of moles of methane dissolved at turbidity obtained from the experimental mole

consumption to that predicted by an energy balance.

6.2.5.3 Optical and physical properties of the water-hydrate solution

The Zetasizer Nano ZS, which operates at a wavelength of 633 nm, requires the refractive index and the absorption value for the particles to be measured. The refractive index of methane hydrates was taken from the work of Bonnefoy *et al.* (2005). As for the absorption value, only an order of magnitude estimate is required and hence, methane hydrates were assumed to have a value comparable to that of ice Ih (hexagonal ice), which is the most common solid form of water (Sloan and Koh, 2007), and taken from the work of Warren (1984). Such an assumption is based on the fact that hydrates are comprised of roughly 85 % water on a molecular basis. The viscosity of the solution was assumed to be that of water at the experimental temperature. To ensure that the smallest size detectable by the Zetasizer Nano ZS (0.6 nm and sample-dependent) was valid for a hydrate-water solution, the scattering efficiency of methane hydrates was calculated with the input parameters of 633 nm wavelength and 173° for the detector, the methane hydrates optical properties given above and the MiePlot software. A scattering efficiency in the order of 10^{-11} was obtained for a hypothetical particle radius of 1 nm, while values in the order of 10^{-7} and 10^{-4} were obtained for a hypothetical particle radius of 10 and a 100 nm respectively. As per the manufacturer specifications, scattering efficiencies of 10^{-12} or greater are appropriate for size measurements with the Zetasizer Nano ZS, while values as small as 10^{-13} - 10^{-14} can be suitable for highly concentrated samples and long measurement times.

6.2.5.4 Experimental, semitheoretical and theoretical approaches

Equation 6.1 requires a value for the critical nuclei diameter of hydrate formation (L_c), as well as the second moment of the particle size distribution (μ_2). For comparison purposes, three different approaches are used to obtain the reaction rate constant and are described below.

Experimental method

Equation 6.1 is used as is, with both the critical nuclei diameter and the second moment obtained experimentally from measurements performed with the particle size analyzer at the onset of hydrate growth and thereafter.

Semitheoretical method

As in the case of the experimental approach, the critical nuclei diameter is measured experimentally at the onset of hydrate growth. The second moment, on the other hand, is obtained from a population balance. Assuming a constant volume, a size-independent growth, a constant number of particles and performing the moment transformations, the population balance yields for the second moment (Kane *et al.*, 1974):

$$\mu_2(t) = \mu_0^0 G^2 t^2 + 2L_c \mu_0^0 G t + L_c^2 \mu_0^0 \tag{6.4}$$

where μ_0^0, L_c, t and G are the initial number of particles per unit of liquid volume, the critical nuclei diameter, the time and the growth rate respectively. A more detailed derivation of equation 6.4 can be found elsewhere (Bergeron and Servio, 2008b). Assuming full occupancy, the time derivative of the radius of a spherical hydrate particle is given by:

$$\frac{dr}{dt} = \frac{dn}{dt} \frac{MW_H}{\rho_H} \frac{1}{A_p} \tag{6.5}$$

where A_p is the total surface area of the hydrate particle. Since the surface area is a function of the second moment of the particle size distribution, equation 6.5 can be combined with equation 6.1, leading to:

$$G = \frac{d(2r)}{dt} = 2\frac{\rho_w}{MW_w} \frac{MW_H}{\rho_H \eta} k_r (x^b - x^{HL}) \tag{6.6}$$

It follows that the growth rate, based on equation 6.6, is a constant for a given temperature and pressure. Combining equations 6.1, 6.4 and 6.6 and using the critical nuclei diameter measured experimentally, the reaction rate constant can be

obtained from a semitheoretical approach.

Theoretical method

Equation 6.1 combined with equations 6.4 and 6.6 can be used to determine the reaction rate constant from a theoretical approach. The only difference from the semitheoretical method is to assume homogeneous nucleation theory when determining the critical nuclei diameter. As such, the change in free energy of the system is due to the appearance of a new phase and the formation of a boundary between the phases. Thus, the change in free energy of the system can be expressed as (Callister, 2003):

$$\Delta G = \Delta G_s + \Delta G_v = A_p \sigma + \Delta g_v V_p \tag{6.7}$$

where ΔG_s is the change in free energy due to the formation of a boundary, ΔG_v is the change in free energy due to the appearance of a new phase (hydrate), σ is the surface energy for the hydrate-water system and Δg_v is the change in free energy per unit volume of product formed (hydrate). Equation 6.7 goes through a maximum at the critical nuclei diameter, which implies the following:

$$L_c = -\frac{4\sigma}{\Delta g_v} \tag{6.8}$$

Assuming an ideal solution (Tester and Modell, 1997) and full occupancy, the change in free energy of the liquid phase per unit volume of product formed (hydrate) is given by:

$$v_H \Delta g_v = RT^{exp} \left[ln \left(\frac{x^{HL}}{x_{tb}} \right) + \eta_w ln \left(\frac{1 - x^{HL}}{1 - x_{tb}} \right) \right] \tag{6.9}$$

where v_H is the molar volume of the hydrate, R is the universal gas constant and η_w is the number of moles of water per mole of hydrate. Both x^{HL} and x_{tb} are the mole fraction of methane in water under hydrate-liquid water equilibrium, at the experimental temperature and pressure, and the mole fraction of methane in water at turbidity. The critical nuclei diameter can be calculated combining equations 6.8 and 6.9, following which the reaction rate constant can be regressed using equations

6.1, 6.4 and 6.6.

6.2.5.5 Uncertainty on the second moment

A reasonable estimate of the uncertainty on the second moment determined experimentally was obtained using the error propagation technique. To yield a meaningful estimate, the uncertainty on the second moment was calculated as follows:

$$w_{\mu_2(t)} = w_{\mu_0^0} L^2 \tag{6.10}$$

where $w_{\mu_0^0}$ is the uncertainty on the initial number of hydrate particles per unit of liquid volume and L is the mean diameter obtained from the particle size distribution measurement at a given time. From equation 6.2, the uncertainty on the initial number of hydrate particles is given by:

$$w_{\mu_0^0} = \left[\left(\frac{\partial \mu_0^0}{\partial V_L} w_{V_L} \right)^2 + \left(\frac{\partial \mu_0^0}{\partial L_c} w_{L_c} \right)^2 + \left(\frac{\partial \mu_0^0}{\partial (n_{tb} - n^b)} w_{n_{tb} - n^b} \right)^2 \right]^{1/2} \tag{6.11}$$

where the uncertainty on the liquid volume in the crystallizer (w_{V_L}) was estimated as ± 1 ml. The uncertainty on the critical nuclei diameter (w_{L_c}) was based on measurements of a polydisperse sample (± 16.2 %), as detailed in the following section. The uncertainty on the difference between the number of moles dissolved at turbidity obtained from the experimental mole consumption and that predicted by equation 6.3 was taken as $w_{n_{tb} - n^b}$, with a value of ± 13.9 % (see the following section).

6.2.6 Results and discussion

Preliminary experiments were performed to test the accuracy of the Zetasizer Nano ZS and to study the effect, if any, of flowing part of the liquid phase from the crystallizer to the particle size analyzer by means of the dual piston pump. A polydisperse particle standard (soda lime glass) from Whitehouse Scientific with nominal sizes

between 0.1 and 1 μm was circulated and particle size distribution measurements were performed with the flow-through cell. The average error between the measured sizes and those reported on the certificate of analysis was of 16.2 %. In addition, an average error of 5.8 % was calculated between the sizes measured in the experimental setup using the flow-through cell and those obtained from a single measurement using a standard cuvet.

Several experiments were performed over a 4-degree interval to determine the reaction rate constant of methane clathrate formation. The effect of pressure on the reaction rate constant was also investigated at 275.1 and 277.1 K. This could not be done at 279.1 K due to the maximum pressure rating of the flow-through cell (6,000 kPa). For all three approaches (experimental, semitheoretical and theoretical), the model was integrated and compared to the experimental mole consumption. The reaction rate constant was regressed using the Gauss-Newton method with Levenberg-Marquardt's modification. For each experiment, the trend for the derived count rate, which is a function of the sample concentration and particle size, was compared to that for the cumulative relative scattering (size-dependent only) to determine whether or not the number of hydrate particles remained constant for the duration of the growth period investigated. Figure 6.2 shows such a comparison at 278.9 K and 5,559 kPa. For the first two measurements, the derived count rate and the cumulative relative scattering trends seem to be in close agreement. The third data point however shows a different trend, with the derived count rate sharply increasing while the cumulative relative scattering decreases. This particular data point could represent an outlier when considering the lower than expected second moment for that particular measurement, as seen in Figure 6.3 (third data point). The fourth measurement (Figure 6.2) on the other hand reveals a good agreement between the derived count rate and cumulative relative scattering trends. For the final measurement, even though both the derived count rate and the cumulative relative scattering increase, the increase in the derived count rate is considerably less than in the cumulative relative scattering, which could indicate a decrease in
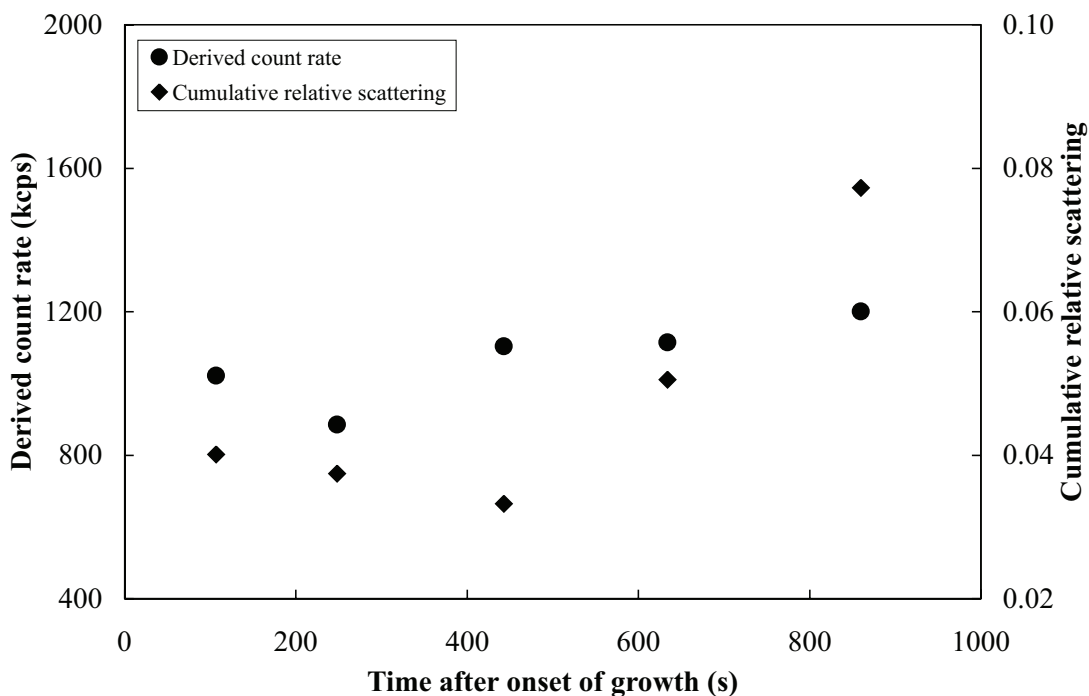
Figure 6.2: Comparison of the derived count rate and the cumulative relative scattering at 278.9 K and 5,559 kPa.

the sample concentration. As mentioned previously, hydrate kinetic experiments are performed over a relatively small time interval to minimize agglomeration and breakage due to particle-particle, particle-wall and particle-stirrer collisions. The derived count rate and cumulative relative scattering analysis presented here highlights such a fact, as the assumption of a constant number of hydrate particles appears less plausible after 800 seconds.

The second moment obtained from the particle size analyzer is also displayed in Figure 6.3, with error bars calculated using equations 6.10 and 6.11. The number of moles of methane dissolved at turbidity obtained from the experimental mole consumption was also compared to the value obtained from an energy balance, as predicted by equation 6.3. As such, a typical increase in the liquid phase temper-
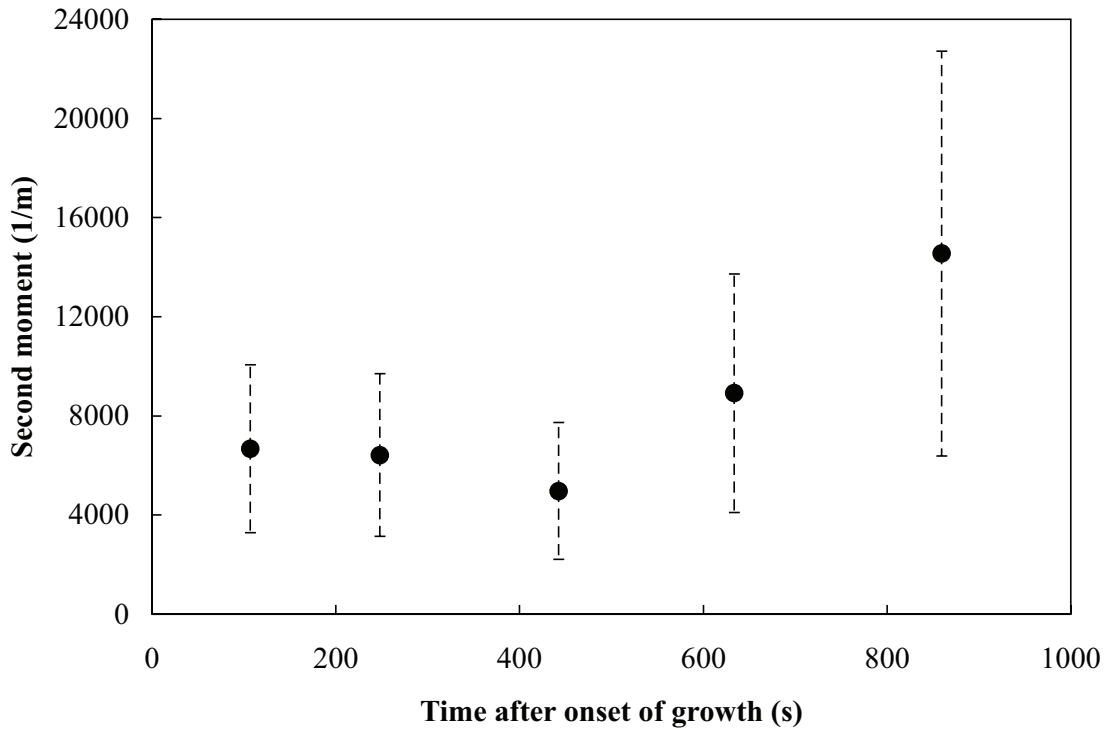
Figure 6.3: Experimental second moment of the particle size distribution at 278.9 K and 5,559 kPa.

ature at the onset of hydrate growth is shown in Figure 6.4 for a temperature of 275.1 K and a pressure of 4,458 kPa. The percent error between the number of moles dissolved at turbidity obtained from the experimental mole consumption and that predicted by equation 6.3 differed on average by 11.9 %, 13.4 % and 12.0 % at 275.1 K, 277.1 K and 279.1 K respectively. Figure 6.5 shows the model predictions compared to the experimental mole consumption at 279.2 K and 5,519 kPa, with an average absolute relative error of 1.2 % for the experimental approach and 4.7 % for both the semitheoretical and theoretical ones.

Table 6.1 lists the average reaction rate constant of methane hydrate formation over the 4-degree range investigated and based on replicates for all three approaches.
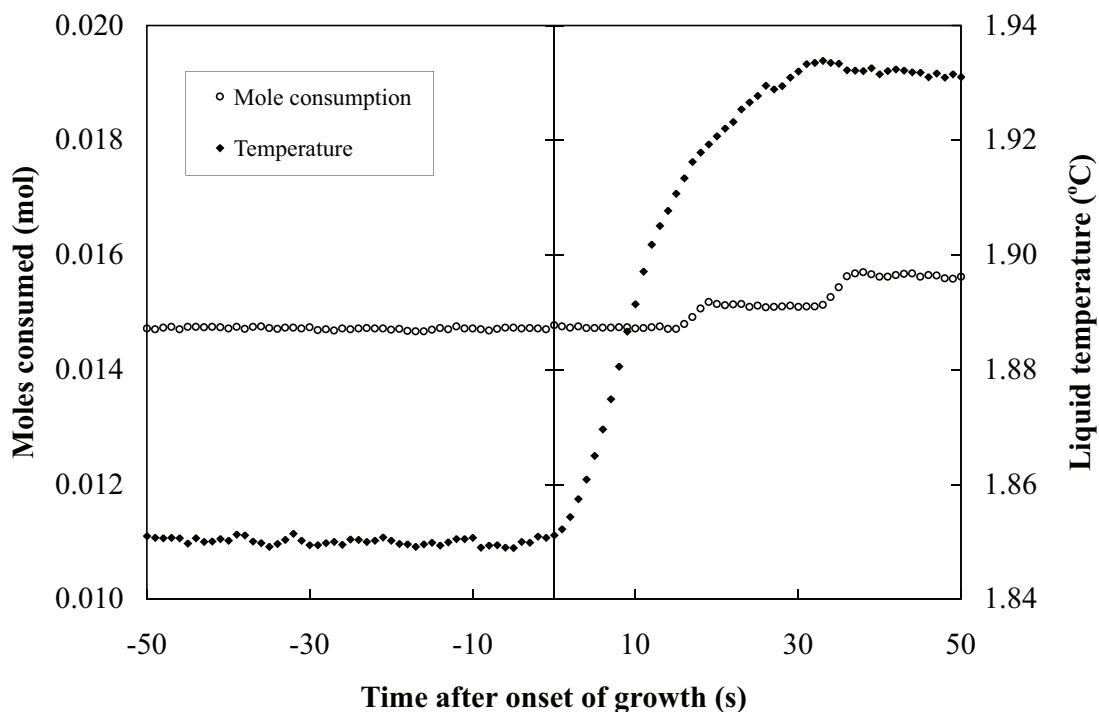
Figure 6.4: Increase in the liquid phase temperature at the onset of methane hydrate growth at 275.1 K and 4,458 kPa.

While both the experimental and semitheoretical approaches yield reaction rate constants in the same order of magnitude, there is a difference of approximately one order of magnitude when comparing the theoretical values to the other two methods. The theoretical approach uses homogeneous nucleation theory to predict the size of the critical nuclei diameter, which is consistently smaller than what was measured experimentally. Homogeneous nucleation theory typically predicts a critical nuclei diameter below 50 nm, while average values as large as a few hundreds of nanometers were measured with the particle size analyzer depending on the experimental conditions. These sizes are in agreement with the work of Nerheim *et al.* (1992), who reported at the onset of hydrate formation an average diameter greater than 100 nm for the double methane-propane hydrate. As pointed out by Hashemi *et al.*

Table 6.1: Average reaction rate constant of CH_4 hydrate formation ($\times 10^{-8}$ m/s)

Average temperature (K)	Experimental k_r	Semitheoretical k_r	Theoretical k_r
275.1	8.3 $\pm$0.5	7.2 $\pm$0.7	0.64 $\pm$0.09
277.1	21.5 $\pm$3.9	9.5 $\pm$1.0	0.63 $\pm$0.05
279.1	61.5 $\pm$4.8	25.0 $\pm$5.9	1.9 $\pm$0.6

(2007b), it is very unlikely that conditions for homogeneous nucleation are attained experimentally in a semi-batch stirred tank crystallizer. On the other hand, it is plausible that impurities in the nanometer range act as nucleation sites. Heterogeneous nucleation theory predicts a lower critical nuclei diameter than homogeneous nucleation theory. However, the values measured experimentally comprised both the impurity, if any, and the hydrate layer covering the former, which could explain the higher than expected diameters. Also, due to a lack of experimental data, the surface energy for the hydrate-water system was assumed to be the same as the one for the ice-water system and taken from the work of Ketcham and Hobbs (1969). Since the critical nuclei diameter is directly proportional to the surface energy, as predicted by equation 6.8, a significant difference between the surface energy of the hydrate-water and ice-water systems would lead to a considerable change in the critical nuclei diameter predicted by homogeneous nucleation theory. As seen from equation 6.2, the initial number of hydrate particles is a strong function of the critical nuclei diameter. An underestimated value for the critical nuclei diameter would overestimate the number of particles and the second moment, resulting in a lower than expected reaction rate constant. Nevertheless, the tenfold difference between the theoretical approach and the other two methods is the smallest difference reported so far in the literature, as Hashemi *et al.* (2007b), while revisiting the work of Clarke and Bishnoi (2005), found an experimental reaction rate constant a thousand times larger than the theoretical one predicted by a population balance and homogeneous nucleation theory.

A closer look at Figure 6.5 also highlights a difference in the trend predicted by each method. The experimental approach, which is based on the second moment
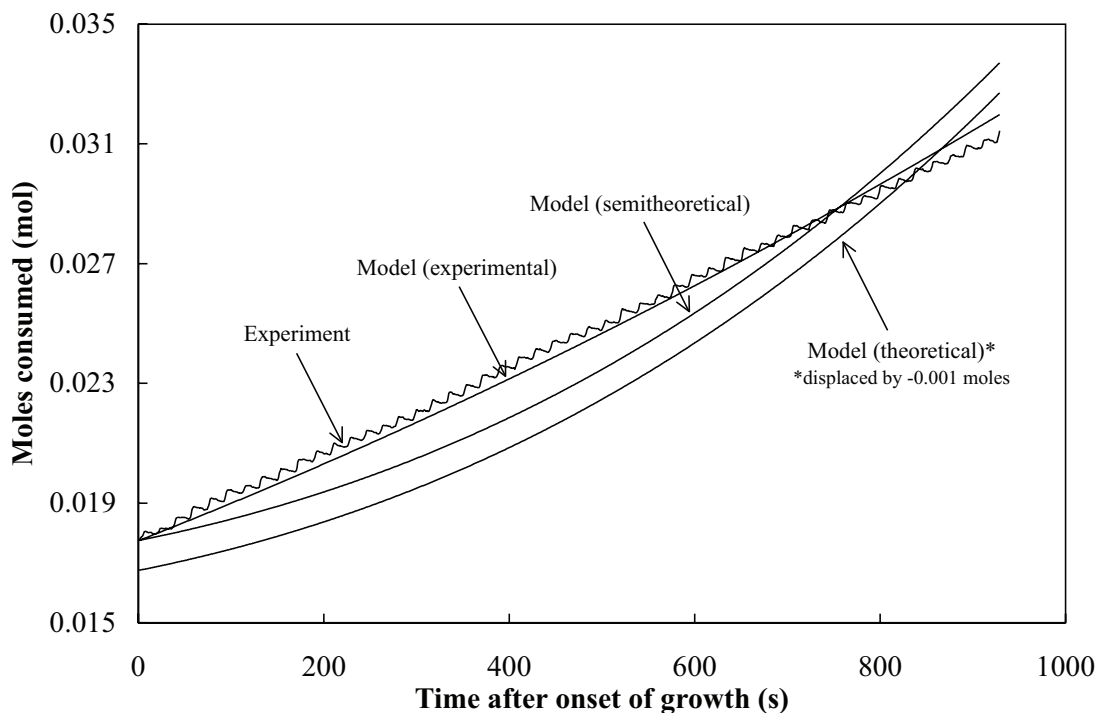
Figure 6.5: Experimental mole consumption and model predictions at 279.2 K and 5,519 kPa. The curve labeled 'Experiment' corresponds to data points recorded every second; due to the scale of the graph it appears to be a continuous line. The line labeled 'Model (experimental)' refers to the model predictions using the second moment obtained experimentally using the particle size analyzer. The line labeled 'Model (semitheoretical)' refers to the model predictions using a population balance and the critical nuclei diameter, the latter determined experimentally with the particle size analyzer. The line labeled 'Model (theoretical)' refers to the model predictions using a population balance and the critical nuclei diameter calculated using homogeneous nucleation theory. The 'Model (theoretical)' line has been intentionally displaced by -0.001 moles, otherwise it would overlap the semitheoretical line.

measured experimentally, predicts a similar trend to what is seen experimentally. The other two approaches predict a different trend. In both cases, the growth rate is assumed constant, as predicted by equation 6.6, and leads to a second moment that increases very rapidly. As a result, both the semitheoretical and theoretical trends display a different shape (pronounced curvature) than what is observed experimentally and predicted by the experimental approach. The assumption underlying equation 6.6 is that hydrate particles grow with the addition of a monolayer covering the entire surface, whereas the experimental method uses the second moment measured experimentally.

As it can be seen from Figure 6.6, the experimental reaction rate constant of methane hydrate formation increases with temperature, following an Arrhenius-type relationship. This is in agreement with the trend reported for the reaction rate constant of carbon dioxide hydrate formation from the work of Bergeron and Servio (2008a), as seen in Figure 6.6. It is also clear that methane seems to have faster intrinsic kinetics than carbon dioxide for the range of temperatures investigated. Even though the temperature dependence of the reaction rate constant of propane hydrate formation was not investigated by Bergeron and Servio (2008b), the value reported for propane at 274.2 K is larger than that for methane at 275.1 K. In other words, it appears that sII propane hydrates have faster intrinsic kinetics than sI methane hydrates, which have faster intrinsic kinetics than sI carbon dioxide hydrates. On the other hand, Malegaonkar *et al.* (1997) reported an inverse trend, with a reaction rate constant of carbon dioxide hydrate formation approximately one order of magnitude greater than that of methane.

It also appears as if pressure does not have a significant effect on the reaction rate constant of methane hydrate formation over the range of pressures investigated. At 277.1 K, an increase of 566 kPa did not yield a significant change in the reaction rate constant, as the value reported at 5,226 kPa (2.69×10^{-7} m/s) does not deviate significantly from the trend shown in Figure 6.6. A similar conclusion can be drawn at
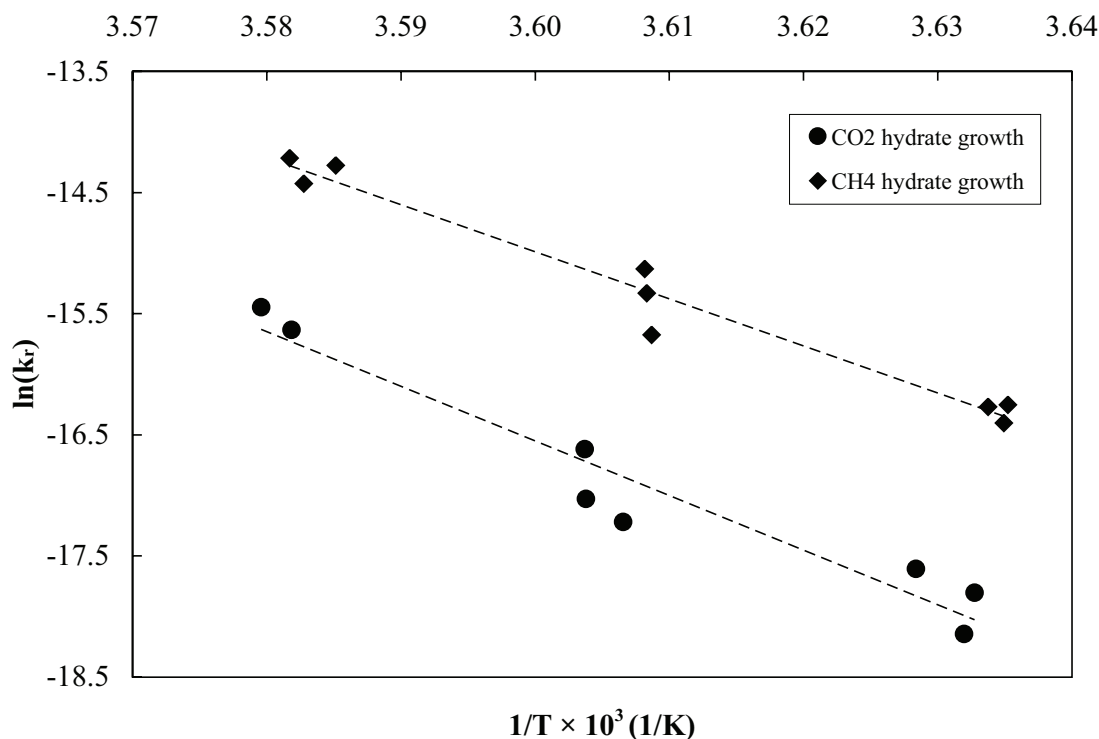
Figure 6.6: Experimental reaction rate constant of CH_4 hydrate formation over a 4-degree interval and comparison with the data of Bergeron and Servio (2008b) for CO_2 hydrate formation.

275.1 K, where an increase in pressure of 581 kPa yielded a value (7.5×10^{-8} m/s) in the vicinity of the other data points. Isaacs (1981) has suggested the following relationship for the effect of pressure on the reaction rate constant for an arbitrary chemical reaction:

$$\left(\frac{\partial ln\left(k_r\right)}{\partial P} \right)_T = -\frac{\Delta \bar{V}^+}{RT} \qquad (6.12)$$

where $\Delta \bar{V}^+$ is the difference in partial molar volumes between the transition state and the reagents. To the best of the authors' knowledge, no precise transition state has been proposed so far for hydrate growth and thus, the difference in partial molar volumes can not be calculated to predict the effect of pressure on the reaction

rate constant. On the other hand, the current work has demonstrated a negligible effect of pressure (566 and 581 kPa increase in pressure at 277.1 and 275.1 K respectively) on the reaction rate constant of methane hydrate formation. Based on such an observation and the work of Isaacs (1981), it would follow that the difference in partial molar volumes between the transition state (unknown) and the reagents during hydrate growth is negligible over this pressure range.

The activation energy for hydrate growth can also be determined from the Arrhenius relationship. Using the data of Bergeron and Servio (2008b) yields an activation energy of 375 kJ/mol for carbon dioxide hydrate growth, while the current work yields a value of 323 kJ/mol for methane hydrate growth. The authors speculate that different guests will have different activation energies analogous to different guests having different enthalpies of formation. The positive value for the activation energy implies that an energy barrier must be overcome for hydrates to grow. As a comparison, Freer *et al.* (2001) obtained a value of 171 kJ/mol from methane film growth kinetics, while Mullin (1997) reported a value of 40 - 60 kJ/mol for surface integration processes and 10 - 20 kJ/mol for diffusion processes. Interestingly, Vysniauskas and Bishnoi (1983) reported a value of -106.204 kJ/mol for methane hydrate growth. However, caution must be taken regarding their negative value. In particular, both the temperature dependence of the reaction rate constant and that of the concentration of water and methane monomers at the interface, which they could not measure, were included in their Arrhenius expression (Vysniauskas and Bishnoi, 1983). Based on such a fact, the negative activation energy they obtained is not due only to the temperature dependence of the reaction rate constant. Moreover, even though the current work reports an increasing reaction rate constant with temperature, the overall rate of reaction (dn/dt) decreases with increasing temperature at a given pressure. This can be explained from the fact that the driving force contained in equation 6.1 decreases with temperature, as the mole fraction of methane in the bulk liquid phase decreases with temperature (Bergeron and Servio, 2009) and its solubility under hydrate-liquid water equilibrium increases

with temperature (Bergeron *et al.*, 2007).

6.2.7 Conclusion

The reaction rate constant of methane hydrate formation was determined over a 4-degree interval. The reaction rate constant determined experimentally was found to increase with temperature following an Arrhenius-type relationship, from 8.3×10^{-8} m/s to 6.15×10^{-7} m/s, over the 4-degree range investigated, resulting in an activation energy of 323 kJ/mol. Pressure was found to have a negligible effect on the reaction rate constant of methane clathrate formation over the range of pressures investigated.

6.2.8 Acknowledgements

Notation

Please refer to Chapter 9.

References

Please refer to the general bibliography found at the end of the thesis document.

Chapter 7

Effect of Temperature on Guest Solubility

7.1 Preface

The kinetic model developed in Chapter 3 and subsequently reformulated in Chapter 4 relies on a concentration driving force incorporating the solubility of the gas hydrate former in water under hydrate-liquid water $(H - L_w)$ equilibrium. Since hydrate growth is characterized by precise temperature and pressure conditions, knowledge of the temperature dependency of the guest solubility in water is desired for modeling purposes, particularly when analyzing the driving force for clathrate hydrate formation. As pointed out in Chapter 2, several authors have confirmed experimentally the temperature dependency of the guest solubility in water under both hydrate-liquid water and vapor-liquid water equilibrium. Semi-empirical models have also demonstrated such a trend but to the best of the author's knowledge, a derivation from fundamental principles has yet to be suggested. Consequently, the temperature dependency of the guest solubility in water under vapor-liquid water and hydrate-liquid water equilibrium was demonstrated using fundamental thermodynamics. Due to their numerous applications, methane-water and carbon dioxide-water systems were investigated.

7.2 Theoretical temperature dependency of gas hydrate former solubility under hydrate-liquid water equilibrium

Sébastien Bergeron[a], Arturo Macchi[b], Phillip Servio[a]

[a]*Department of Chemical Engineering, McGill University, Canada*
[b]*Department of Chemical Engineering, University of Ottawa, Canada*

7.2.1 Abstract

Available experimental data and current semi-empirical models suggest a positive trend for the gas hydrate former solubility in the bulk liquid phase as a function of temperature under hydrate-liquid water equilibrium. Such a trend has been widely reported without theoretical explanation. This work proposes a comprehensive derivation, based on fundamental thermodynamics, of the gas hydrate former solubility dependency on temperature for any binary system under two-phase equilibrium.

7.2.2 Introduction

Gas hydrates are crystalline solids that form when gas or volatile liquid molecules suitable for hydrate formation are enclosed in a cage consisting of water molecules linked through hydrogen bonding. The presence of the hydrate-forming gas molecules leads to stabilization of the water lattice through physical bonding via week van der Waals forces. Three common structures have been reported, including structure I (sI), structure II (sII) and structure H (sH) (Englezos, 1993). Naturally occurring hydrates can be found below the permafrost and in sub-sea sediments where the pressure and temperature conditions allow them to be stable (Sloan, 1998b). Potential applications include methane hydrates as an alternate energy source (Chatti *et al.*, 2005), carbon dioxide sequestration as a means to mitigate the global warming effect (Brewer *et al.*, 1999) and transportation and storage of natural gas hydrates

over more conventional methods such as liquefied natural gas and compressed natural gas (Thomas and Dawe, 2003). Consequently, vapor-liquid water ($L_w - V$), vapor-liquid water-hydrate ($H - L_w - V$) and hydrate-liquid water ($H - L_w$) equilibrium are important concepts when dealing with such applications. Associated with these notions is the concept of solubility, which is the maximum amount of gas that can be dissolved in a liquid in equilibrium with its gaseous-rich phase, at a certain temperature and pressure. Under hydrate-liquid water equilibrium, there is no gaseous phase and thus, the concept of solubility is not directly applicable. The amount of gas dissolved in the bulk liquid phase is the equilibrium concentration of the gas hydrate former. Nevertheless, many authors refer to the term solubility even under hydrate-liquid water equilibrium and for clarity purposes, the same approach will be used in the present work. Various papers reported solubility measurements under hydrate-liquid water equilibrium. In particular, Servio and Englezos (2002), as well as Yang *et al.* (2001) and Kim *et al.* (2003), performed solubility measurements for methane-water systems. Similarly, Yang *et al.* (2000), as well as Servio and Englezos (2001) and Someya *et al.* (2005), performed solubility measurements for carbon dioxide-water systems. These studies have shown that the gas hydrate former solubility under hydrate-liquid water equilibrium decreases with decreasing temperature, whereas the trend is reversed under vapor-liquid water equilibrium. More recently, Hashemi *et al.* (2006) have proposed a semi-empirical model with newly optimized parameters that depicts a positive trend for the gas hydrate former solubility dependency on temperature under hydrate-liquid water equilibrium. Similarly, the model showed an opposite trend under vapor-liquid water equilibrium. Even though such trends have been widely reported, no comprehensive explanation has been given based on fundamental principles. Based on Tester and Modell (1997), this work will thus present a detailed derivation using fundamental thermodynamics to explain and confirm the reported dependency of the gas hydrate former solubility on temperature for both hydrate-liquid water and vapor-liquid water equilibrium.

7.2.3   Theory

For any binary mixture (components A and B) coexisting as α and β phases, the basic equations for the equilibrium condition are:

$$\mu_A^\alpha = \mu_A^\beta \tag{7.1}$$

$$\mu_B^\alpha = \mu_B^\beta \tag{7.2}$$

$$T^\alpha = T^\beta \tag{7.3}$$

$$P^\alpha = P^\beta \tag{7.4}$$

An equivalent criterion to equations 7.1 and 7.2 above is the equality of the fugacity of each component in each phase present, given by the following:

$$f_A^\alpha = f_A^\beta \text{ or } \ln f_A^\alpha = \ln f_A^\beta \tag{7.5}$$

$$f_B^\alpha = f_B^\beta \text{ or } \ln f_B^\alpha = \ln f_B^\beta \tag{7.6}$$

where f_i denotes the fugacity of a component in the mixture. Based on equations 7.3 and 7.4, no phase designation is required for both T and P. In order to obtain differential equations involving T, P, and phase compositions, we take the total derivatives of both equations 7.5 and 7.6. Thus, supposing that T, P and x_A are the $(n+1)$ variables in each phase, we have for component A:

$$d\ln f_A^\alpha = \left(\frac{\partial \ln f_A^\alpha}{\partial T}\right)_{P,x^\alpha} dT + \left(\frac{\partial \ln f_A^\alpha}{\partial P}\right)_{T,x^\alpha} dP + \left(\frac{\partial \ln f_A^\alpha}{\partial x_A^\alpha}\right)_{T,P} dx_A^\alpha$$

or

$$d \ln f_A^\alpha = -\frac{\bar{H}_A^\alpha - H_A^*}{RT^2} dT + \frac{\bar{V}_A^\alpha}{RT} dP + \left(\frac{\partial \ln f_A^\alpha}{\partial x_A^\alpha} \right)_{T,P} dx_A^\alpha \tag{7.7}$$

and

$$d \ln f_A^\beta = \left(\frac{\partial \ln f_A^\beta}{\partial T} \right)_{P,x^\beta} dT + \left(\frac{\partial \ln f_A^\beta}{\partial P} \right)_{T,x^\beta} dP + \left(\frac{\partial \ln f_A^\beta}{\partial x_A^\beta} \right)_{T,P} dx_A^\beta$$

or

$$d \ln f_A^\beta = -\frac{\bar{H}_A^\beta - H_A^*}{RT^2} dT + \frac{\bar{V}_A^\beta}{RT} dP + \left(\frac{\partial \ln f_A^\beta}{\partial x_A^\beta} \right)_{T,P} dx_A^\beta \tag{7.8}$$

where H_A^* denotes the enthalpy of component A in an ideal gas state at the temperature of the system. Using the same intensive variables, equations 7.7 and 7.8 can be rewritten for component B as follows:

$$d \ln f_B^\alpha = -\frac{\bar{H}_B^\alpha - H_B^*}{RT^2} dT + \frac{\bar{V}_B^\alpha}{RT} dP + \left(\frac{\partial \ln f_B^\alpha}{\partial x_A^\alpha} \right)_{T,P} dx_A^\alpha \tag{7.9}$$

$$d \ln f_B^\beta = -\frac{\bar{H}_B^\beta - H_B^*}{RT^2} dT + \frac{\bar{V}_B^\beta}{RT} dP + \left(\frac{\partial \ln f_B^\beta}{\partial x_A^\beta} \right)_{T,P} dx_A^\beta \tag{7.10}$$

Equating differentials of $\ln f_i$ based on equations 7.5 and 7.6:

$$-\frac{\bar{H}_A^\alpha - \bar{H}_A^\beta}{RT^2} dT + \frac{\bar{V}_A^\alpha - \bar{V}_A^\beta}{RT} dP + \left(\frac{\partial \ln f_A^\alpha}{\partial x_A^\alpha} \right)_{T,P} dx_A^\alpha - \left(\frac{\partial \ln f_A^\beta}{\partial x_A^\beta} \right)_{T,P} dx_A^\beta = 0 \tag{7.11}$$

$$-\frac{\bar{H}_B^\alpha - \bar{H}_B^\beta}{RT^2} dT + \frac{\bar{V}_B^\alpha - \bar{V}_B^\beta}{RT} dP + \left(\frac{\partial \ln f_B^\alpha}{\partial x_A^\alpha} \right)_{T,P} dx_A^\alpha - \left(\frac{\partial \ln f_B^\beta}{\partial x_A^\beta} \right)_{T,P} dx_A^\beta = 0 \tag{7.12}$$

For a binary system of phase π, the Gibbs-Duhem equation states that:

$$x_A^\pi \left(\frac{\partial \ln f_A^\pi}{\partial x_A^\pi} \right)_{T,P} + x_B^\pi \left(\frac{\partial \ln f_B^\pi}{\partial x_A^\pi} \right)_{T,P} = 0 \tag{7.13}$$

Consequently, multiplying equation 7.11 by x_A^α and equation 7.12 by x_B^α, then adding the two equations and applying equation 7.13 to each phase, we get:

$$-\frac{x_A^\alpha \left(\bar{H}_A^\alpha - \bar{H}_A^\beta \right) + x_B^\alpha \left(\bar{H}_B^\alpha - \bar{H}_B^\beta \right)}{RT^2} dT + \frac{x_A^\alpha \left(\bar{V}_A^\alpha - \bar{V}_A^\beta \right) + x_B^\alpha \left(\bar{V}_B^\alpha - \bar{V}_B^\beta \right)}{RT} dP$$

$$- \left(x_A^\alpha - \frac{x_A^\beta x_B^\alpha}{x_B^\beta} \right) \left(\frac{\partial \ln f_A^\beta}{\partial x_A^\beta} \right)_{T,P} = 0 \tag{7.14}$$

Solving for dP:

$$dP = \frac{1}{T} \frac{x_A^\alpha \left(\bar{H}_A^\alpha - \bar{H}_A^\beta \right) + x_B^\alpha \left(\bar{H}_B^\alpha - \bar{H}_B^\beta \right)}{x_A^\alpha \left(\bar{V}_A^\alpha - \bar{V}_A^\beta \right) + x_B^\alpha \left(\bar{V}_B^\alpha - \bar{V}_B^\beta \right)} dT + \frac{RT \left(x_A^\alpha - \frac{x_A^\beta x_B^\alpha}{x_B^\beta} \right) \left(\frac{\partial \ln f_A^\beta}{\partial x_A^\beta} \right)_{T,P}}{x_A^\alpha \left(\bar{V}_A^\alpha - \bar{V}_A^\beta \right) + x_B^\alpha \left(\bar{V}_B^\alpha - \bar{V}_B^\beta \right)} dx_A^\beta \tag{7.15}$$

For a binary mixture under two-phase equilibrium (2 degrees of freedom), T and x_A^β form an independent set for P under conditions of equilibrium. Thus, equation 7.15 is an exact differential equation and it follows that:

$$\left(\frac{\partial P}{\partial T} \right)_{x_A^\beta,[\alpha,\beta]} = \frac{1}{T} \frac{x_A^\alpha \left(\bar{H}_A^\alpha - \bar{H}_A^\beta \right) + x_B^\alpha \left(\bar{H}_B^\alpha - \bar{H}_B^\beta \right)}{x_A^\alpha \left(\bar{V}_A^\alpha - \bar{V}_A^\beta \right) + x_B^\alpha \left(\bar{V}_B^\alpha - \bar{V}_B^\beta \right)} \tag{7.16}$$

$$\left(\frac{\partial P}{\partial x_A^\beta} \right)_{T,[\alpha,\beta]} = \frac{RT \left(x_A^\alpha - \frac{x_A^\beta x_B^\alpha}{x_B^\beta} \right) \left(\frac{\partial \ln f_A^\beta}{\partial x_A^\beta} \right)_{T,P}}{x_A^\alpha \left(\bar{V}_A^\alpha - \bar{V}_A^\beta \right) + x_B^\alpha \left(\bar{V}_B^\alpha - \bar{V}_B^\beta \right)} \tag{7.17}$$

where $[\alpha, \beta]$ denotes conditions for which both phases α and β coexist at equilibrium. Applying the triple product rule to equation 7.17, it follows that:

$$\left(\frac{\partial T}{\partial x_A^\beta}\right)_{P,[\alpha,\beta]} \left(\frac{\partial P}{\partial T}\right)_{x_A^\beta,[\alpha,\beta]} \left(\frac{\partial x_A^\beta}{\partial P}\right)_{T,[\alpha,\beta]} = -1 \tag{7.18}$$

Combining equations 7.16, 7.17 and 7.18:

$$\left(\frac{\partial T}{\partial x_A^\beta}\right)_{P,[\alpha,\beta]} = -RT^2 \frac{\left(x_A^\alpha - \frac{x_A^\beta x_B^\alpha}{x_B^\beta}\right)\left(\frac{\partial \ln f_A^\beta}{\partial x_A^\beta}\right)_{T,P}}{x_A^\alpha \left(\bar{H}_A^\alpha - \bar{H}_A^\beta\right) + x_B^\alpha \left(\bar{H}_B^\alpha - \bar{H}_B^\beta\right)} \tag{7.19}$$

Rearranging equation 7.19:

$$\left(\frac{\partial x_A^\beta}{\partial T}\right)_{P,[\alpha,\beta]} = -\frac{x_A^\alpha \left(\bar{H}_A^\alpha - \bar{H}_A^\beta\right) + x_B^\alpha \left(\bar{H}_B^\alpha - \bar{H}_B^\beta\right)}{RT^2 \left(x_A^\alpha - \frac{x_A^\beta x_B^\alpha}{x_B^\beta}\right)\left(\frac{\partial \ln f_A^\beta}{\partial x_A^\beta}\right)_{T,P}} \tag{7.20}$$

Equation 7.20 is valid for any binary mixture under two-phase equilibrium. For discussion purposes, equation 7.20 can be written in terms of hydrate-liquid water or vapor-liquid water equilibrium for the methane-water system using the following designations:

α: hydrate (H) or vapor phase (V)
β: liquid phase (L)
A: methane (CH_4)
B: water (H_2O)
$H_A^\alpha - H_A^\beta$: heat of vaporization $(\Delta H_{vap})_A$, or heat of formation $(\Delta H_{form})_A$ of component A, depending on the phases present

Hence, in the case of hydrate-liquid water equilibrium, equation 7.20 becomes:

$$\left(\frac{\partial x_{CH_4}^L}{\partial T}\right)_{P,[H,L]} = -\frac{x_{CH_4}^H (\Delta H_{form})_{CH_4} + x_{H_2O}^H (\Delta H_{form})_{CH_4}}{RT^2 \left(x_{CH_4}^H - \frac{x_{CH_4}^L x_{H_2O}^H}{x_{H_2O}^L}\right) \left(\frac{\partial \ln f_{CH_4}^L}{\partial x_{CH_4}^L}\right)_{T,P}} \tag{7.21}$$

Similarly, in the case of vapor-liquid water equilibrium, equation 7.20 becomes:

$$\left(\frac{\partial x_{CH_4}^L}{\partial T}\right)_{P,[V,L]} = -\frac{x_{CH_4}^V (\Delta H_{vap})_{CH_4} + x_{H_2O}^V (\Delta H_{vap})_{CH_4}}{RT^2 \left(x_{CH_4}^V - \frac{x_{CH_4}^L x_{H_2O}^V}{x_{H_2O}^L}\right) \left(\frac{\partial \ln f_{CH_4}^L}{\partial x_{CH_4}^L}\right)_{T,P}} \tag{7.22}$$

7.2.4 Discussion

In hydrate-liquid water equilibrium, hydrate crystals start to decompose as the temperature increases resulting in a transfer of gas to the liquid phase and an increase in solubility. This trend continues up to the point where the vapor, liquid water and hydrate phases are at equilibrium and a further increase in temperature results in complete decomposition of the hydrate phase. In vapor-liquid water equilibrium, the gas hydrate former solubility decreases as temperature increases since more gas will enter the vapor phase. This solubility dependency on temperature can be seen in the work of Hashemi *et al.* (2006) and is represented in Figure 7.1 for a methane-water system.

Equation 7.22 applies to vapor-liquid water equilibrium. The numerator is always positive since the heat of vaporization is always a positive value. In the denominator, the term $\partial \ln f_{CH_4}^L / \partial x_{CH_4}^L$ is always positive since the fugacity of a component is proportional to its mole fraction. Similarly, based on the work of Hashemi *et al.* (2006), the term $x_{CH_4}^V - x_{CH_4}^L x_{H_2O}^V / x_{H_2O}^L$ is always positive. The gas hydrate former solubility in the bulk liquid phase $\left(x_{CH_4}^L\right)$ is very small, as seen in Figure 7.1, while its mole fraction in the vapor phase $\left(x_{CH_4}^V\right)$ is considerably greater than that of water. It follows that the expression contained in equation 7.22 is always negative.

As a result, equation 7.22 correctly predicts the gas hydrate former solubility dependency on temperature and is in agreement with the reported trend. A similar reasoning can be applied to the carbon dioxide-water system and is in agreement with the reported trend, as seen in Figure 7.2.

Figure 7.1: Comparison of calculated methane solubility in liquid water by the model of Hashemi *et al.* (2006) with the experimental data of Servio and Englezos (2002).

Equation 7.21 applies to hydrate-liquid water equilibrium. It can be seen that the numerator is always negative since the heat of hydrate formation is always negative. As in the case of vapor-liquid water equilibrium, the term $\partial \ln f_{CH_4}^L / \partial x_{CH_4}^L$ is always

positive. The sign of the term $x_{CH_4}^H - x_{CH_4}^L x_{H_2O}^H / x_{H_2O}^L$ depends on the occupancy of the gas hydrate. It has been shown that structure I hydrate (*e.g.* pure-component
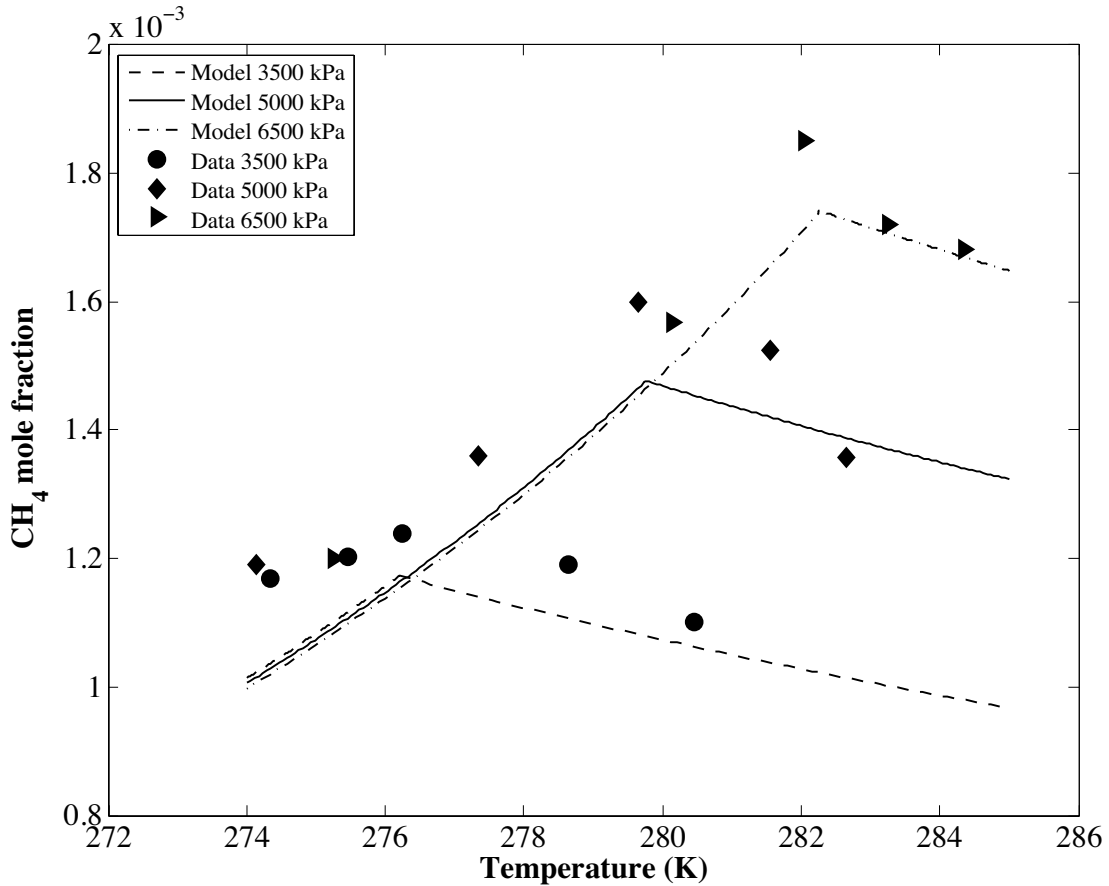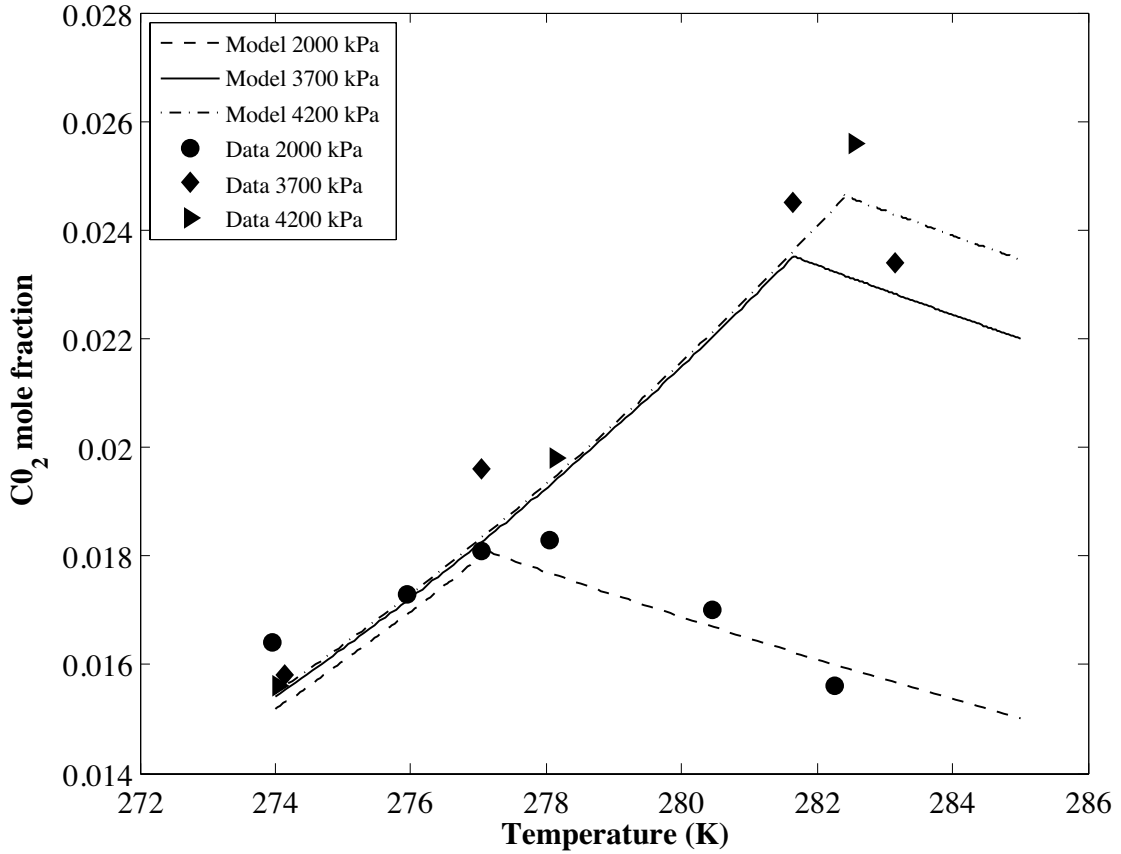

Figure 7.2: Comparison of calculated carbon dioxide solubility in liquid water by the model of Hashemi *et al.* (2006) with the experimental data of Servio and Englezos (2001).

methane and carbon dixoide hydrates) has 2 small cavities and 6 large cavities per unit cell, while each cell contains 46 water molecules (Holder *et al.*, 1980). Accordingly, the mole fraction of each component depends on the occupancy of those cavities. Similarly as in the case of vapor-liquid water equilibrium, the solubility of both methane and water in the liquid phase $\left(x_{CH_4}^L \text{ and } x_{H_2O}^L\right)$ can be determined

using the model proposed by Hashemi *et al.* (2006). Both terms $\left(x_{CH_4}^H \text{ and } x_{H_2O}^H\right)$ can be determined using the occupancy of the cavities of structure I hydrate. Consequently, in order for the term $x_{CH_4}^H - x_{CH_4}^L x_{H_2O}^H / x_{H_2O}^L$ to be positive, a minimum overall occupancy of 0.56 % and 0.86 % for the 8 cavities is required at 274 K and 3,500 kPa and 280 K and 6,500 kPa respectively. Holder *et al.* (1980) have reported that the average occupancy of structure I hydrate is greater than 80 %. Collins *et al.* (1990) experimentally found an average occupancy of 95 % for structure I methane hydrate. As a result, the expression contained in equation 7.21 is always positive and equation 7.21 correctly predicts the gas hydrate former solubility dependency on temperature under hydrate-liquid water equilibrium. Again, an analogous reasoning can be made for the carbon dioxide-water system. In order for equation 7.21 to correctly predict the carbon dioxide solubility dependency on temperature under hydrate-liquid water equilibrium, as seen in Figure 7.2, a minimum overall occupancy of 8.86 % and 12.68 % for the 8 cavities is required at 274 K and 2,000 kPa and 280 K and 4,200 kPa respectively. Such minima occupancies are still significantly smaller than those reported. In addition, the difference between the required minimum occupancy for methane and that for carbon dioxide is due to the greater solubility of carbon dioxide in liquid water compared to methane, as seen in Figures 7.1 and 7.2.

7.2.5 Conclusion

The current work has shown that the gas hydrate former solubility dependency on temperature can be proven using fundamental thermodynamics for both hydrate-liquid water and vapor-liquid water equilibrium. The predicted trend is in agreement with the reported experimental data and current semi-empirical models.

7.2.6 Acknowledgements

program (CRC).

Notation

Please refer to Chapter 9.

References

Please refer to the general bibliography found at the end of the thesis document.

Chapter 8

Conclusion

8.1 Comprehensive conclusion

Chapter 3 introduced a novel kinetic model for accurate predictions of the growth stage of hydrate formation, from which the reaction rate constant of propane hydrate formation was obtained. Measurements of the carbon dioxide and methane mole fraction in the bulk liquid phase at the onset of hydrate growth and thereafter, as detailed in Chapter 4, provided insights on the supersaturation of the bulk liquid phase. It was confirmed that the guest mole fraction in the bulk liquid phase increases with pressure, decreases with temperature and remains constant during at least the first 13 minutes of the growth stage in a semi-batch stirred tank crystallizer. These studies also permitted an alternate formulation of the aforementioned model independent of the dissolution rate at the vapor-liquid water interface, following which the reaction rate constant of both carbon dioxide (Chapter 5) and methane (Chapter 6) hydrate formation was obtained. The reaction rate constant of carbon dioxide and methane hydrate formation was found to increase with temperature, following an Arrhenius-type relationship, while pressure did not have a significant effect over the range investigated (~ 600 kPa increase for methane). The temperature trend of the reaction rate constant of hydrate formation yielded positive activation energies for carbon dioxide and methane hydrate growth. Chapter

7 confirmed the carbon dioxide and methane solubility dependency on temperature in water under hydrate-liquid water and vapor-liquid water equilibrium using fundamental thermodynamics.

8.2 Recommendations for future work

The present work provides data and modeling required to better understand and quantify the intrinsic kinetics of pure-component hydrates. Extension to multi-component systems represents an important step for the design of safe, economical and environmentally acceptable processes and facilities to deal with hydrate forming systems. As such, the following points should be considered in future studies.

- The addition of an infrared camera to study the spatial distribution of localized hot spots during the growth stage, if any, could highlight preferential site for hydrate growth, as well as the possibility for true secondary nucleation.

- Measurement of the guest mole fraction in the bulk liquid phase at the onset of hydrate growth and thereafter for multi-component systems is needed for modeling the growth stage of such mixtures. The use of a gas chromatographer, in addition to a gasometer, is essential for accurate determination of the mole fraction of each component in the bulk liquid phase.

- Extension of the current kinetic model to multi-component systems is readily feasible. The availability of the reaction rate constant for both methane and carbon dioxide hydrate formation, as presented in the present thesis, in addition to the bulk measurements highlighted above, will provide the necessary data to validate the extension of the model to the methane-carbon dioxide-water system.

- Additional studies using the carbon dioxide-nitrogen-water system should be initiated to determine the intrinsic kinetics of a multi-component hydrate system known to form both structure I and structure II hydrates.

Chapter 9

Notation

9.1 List of symbols

a = vapor-liquid interfacial area per unit volume of dispersion, 1/m

A = area, m^2

A_c = crystal-liquid interface, m^2

A_{LV} = vapor-liquid interfacial area, m^2

$B(r)$ = net birth term

C = concentration in liquid phase, mol/m^3

Cp = heat capacity, J/(kg K)

D = binary diffusion coefficient, m^2/s

$D(r)$ = net death term

f = fugacity, MPa

G = growth rate, m/s

H = enthalpy, J/mol, or Henry's law constant, MPa

J_b = nucleation rate in the bulk liquid phase, nuclei/(m^3 s)

J_{int} = nucleation rate at the vapor-liquid water interface, nuclei/(m^3 s)

k = mass transfer coefficient, m/s

k' = coverage factor

K = kinetic constant, mol/(m^2 s MPa)

k_r = reaction rate constant, mol/(m² s MPa) or m/s

K_{OL} = vapor-liquid interfacial conductance, m³/s

L = diameter, m

L_c = critical hydrate diameter, m

L_R = height, m

m = mass, kg

MW = molecular weight, g/mol

n = moles, mol, or arbitrary variable

P = pressure, MPa or kPa

P_g = power consumption, J/s

r = radius, m

r_c = critical hydrate radius, m

R = resistance, s/m³, or universal gas constant, kPa cm³/(mol K)

R_g = global reaction rate, mol/(m³ s)

Re = Reynolds number

Sc = Schmidt number

Sh = Sherwood number

t = time, s

T = temperature, K

u = standard uncertainty

U_x = expanded uncertainty

v = molar volume, m³/mol

v_{sg} = superficial gas velocity, Nl/min

V = volume, m³ or cm³

V_L = volume of liquid, m³

w = uncertainty

x = mole fraction

y = coordinate

y_L = film thichness, m

Z = compressibility factor

ΔH_{form} = heat of hydrate formation, J/mol

ΔH_{vap} = heat of vaporization, J/mol

Δg = change in free energy per unit volume of product formed, J/m^3

ΔG = change in free energy, J

ΔG_{crit} = maximum excess free energy, J

ΔG_s = change in free energy due to the formation of a bounday, J

ΔG_v = change in free energy due to the appearance of a new phase, J

9.2 List of Greek letters

α, β = phase designation

α_H = volumetric fraction of hydrate in the solution-hydrate mixture

α_2 = secondary nucleation rate, nuclei/(m^2 s)

η = moles of gas per mole of hydrate

γ = cumulative oversize particle distribution, 1/m^3

λ = number between 0 and 1

μ = chemical potential, J/mol

μ_0 = zeroth moment of the particle size distribution, 1/m^3

μ_1 = first moment of the particle size distribution, 1/m^2

μ_2 = second moment of the particle size distribution, 1/m

π = Pi or phase designation

ρ = density, g/m^3

σ = interfacial tension, J/m^2

φ = particle density distribution, 1/m^4

ζ = Hatta number

9.3 List of subscripts and superscripts

$\bar{H}$ = partial molar property

atm = atmospheric

$b =$ bulk liquid phase

$exp =$ experimental

$eq =$ equilibrium

$gm =$ gasometer

$HLV =$ hydrate-liquid water-vapor equilibrium

$H =$ hydrate

$HL =$ hydrate-liquid water equilibrium

$i =$ component

$l =$ liquid film

$L =$ liquid

$LV =$ vapor-liquid water equilibrium

$p =$ hydrate particle

$tb =$ turbidity

$V =$ vapor

$w =$ water

Bibliography

Benesh M.E. (1942) *The use of gas hydrates in improving the load factor of gas supply systems*, United States Patent Office, 2270016.

Bergeron S., Servio P. (2008a) *Reaction rate constant of CO2 hydrate formation and verification of old premises pertaining to hydrate growth kinetics*, AIChE Journal, 54:2964–2970.

Bergeron S., Servio P. (2008b) *Reaction Rate Constant of Propane Hydrate Formation*, Fluid Phase Equilibria, 265:30–36.

Bergeron S., Servio P. (2009) *CO2 and CH4 mole fraction measurements during hydrate growth in a semi-batch stirred tank reactor and its significance to kinetic modeling*, Fluid Phase Equilibria, 276:150–155.

Bergeron S., Macchi A., Servio P. (2007) *Theoretical Temperature Dependency of Gas Hydrate Former Solubility under Hydrate-Liquid Water Equilibrium*, Journal of Chemical Thermodynamics, 39:737–741.

Bishnoi P.R., Gupta A.K., Englezos P., Kalogerakis N. (1989) *Multiphase equilibrium flash calculations for systems containing gas hydrates*, Fluid Phase Equilibria, 53:97–104.

Bollavaram P., Devarakonda S., Selim M., Sloan E. (2000) *Growth Kinetics of Single Crystal sII Hydrates Elimination of Mass and Heat Transfer Effects*, Annals of the New York Academy of Sciences, 912:533–543.

Bonnefoy O., Gruy F., Herri J.M. (2005) *A priori calculation of the refractive index of some simple gas hydrates of structures I and II*, Materials Chemistry and Physics, 89:336–344.

Brewer P.G., Friederich G., Peltzer E.T., Jr. F.M.O. (1999) *Direct experiments on the ocean disposal of fossil fuel CO2*, Science, 284:943–945.

Buffett B.A. (2000) *Clathrate Hydrates*, Annu. Rev. Earth Planet. Sci., 28:477–507.

Callister W.D. (2003) *Materials Science And Engineering An Introduction*, sixth ed., John Wiley Sons, Inc.

Chapoy A., Mohammadi A.H., Chareton A., Tohidi B., Richon D. (2004a) *Measurement and Modeling of Gas Solubility and Literature Review of the Properties for the Carbon Dioxide-Water System*, Ind. Eng. Chem. Res., 43:1794–1802.

Chapoy A., Mokraoui S., Valtz A., Richon D., Mohammadi A.H., Tohidi B. (2004b) *Solubility measurement and modeling for the system propane-water from 277.62 to 368.16 K*, Fluid Phase Equilibria, 226:213–220.

Chatti I., Delahaye A., Fournaison L., Petitet J.P. (2005) *Benefits and drawbacks of clathrate hydrates: a review of their areas of interest*, Energy Conversion and Management, 46:1333–1343.

Chirico R.D., Frenkel M., Diky V.V., Marsh K.N., Wilhoit R.C. (2003) *ThermoML - An XML-Based Approach for Storage and Exchange of Experimental and Critically Evaluated Thermophysical and Thermochemical Property Data. 2. Uncertainties*, J. Chem. Eng. Data, 48:1344–1359.

Chun M.K., Lee H. (1996) *Kinetics of formation of carbon dioxide clathrate hydrates*, Korean J. Chem. Eng., 13(6):620–626.

Clarke M., Bishnoi P. (2000a) *Determinaiton of the Intrinsic Rate of Gas Hydrate Decomposition Using Particle Size Analysis*, Annals of the New York Academy of Sciences, 912:556–563.

Clarke M., Bishnoi P. (2000b) *Determination of the intrinsic rate of ethane gas hydrate decomposition*, Chemical Engineering Science, 55:4869–4883.

Clarke M., Bishnoi P. (2001a) *Determination of the Activation Energy and Intrinsic Rate Constant of Methane Gas Hydrate Decomposition*, The Canadian Journal of Chemical Engineering, 79:143–147.

Clarke M., Bishnoi P. (2001b) *Measuring and modelling the rate of decomposition of gas hydrates formed from mixtures of methane and ethane*, Chemical Engineering Science, 56:4715–4724.

Clarke M., Bishnoi P. (2004) *Determination of the intrinsic rate constant and activation energy of CO2 gas hydrate decomposition using in-situ particle size analysis*, Chemical Engineering Science, 59:2983–2993.

Clarke M., Bishnoi P. (2005) *Determination of the intrinsic kinetics of CO2 gas hydrates formation using in situ particle size analysis*, Chemical Engineering Science, 60:695–709.

Claussen W. (1951) *Suggested Structures of Water in Inert Gas Hydrates*, The Journal of Chemical Physics, 19:259–260.

Collins M.J., Ratcliffe C.I., Ripmeester J.A. (1990) *Nuclear Magnetic Resonance Studies of Guest Species in Clathrate Hydrates: Line-Space Anisotropies, Chemical Shifts, and the Determination of Cage Occupancy Ratios and Hydration Numbers*, J. Phys. Chem., 94:157–162.

Darbouret M., Cournil M., Herri J.M. (2005) *Rheological study of TBAB hydrate slurries as secondary two-phase refrigerants*, International Journal of Refrigeration, 28:663–671.

Davy H. (1811) *On Some of the Combinations of Oxymuriatic Gas and Oxygene, and on the Chemical Relations of These Principles, to Inflammable Bodies*, Philosophical Transactions of the Royal Society of London, 101:1–35.

Deaton W., Frost E. (1946) *Gas Hydrates and Their Relation fo the operation of Natural-Gas Pipe Lines*, United States Department of the Interior, Monograph 8.

Deen W.M. (1998) *Analysis of Transport Phenomena*, Oxford University Press, New York.

Durham W.B., Stern L.A., Kirby S.H. (2003) *Ductile flow of methane hydrate*, Can. J. Phys., 81:373–380.

Dyadin Y., Larionov , Aladko E., Manakov A., Zhurko F., Mikina T., Komarov V., Grachev E. (1999) *Clathrate formation in water-noble gas (hydrogen) systems at high pressures*, Journal of Structural Chemistry, 40:790–795.

Englezos P. (1993) *Clathrate Hydrates*, Ind. Eng. Chem. Res., 32:1251–1274.

Englezos P., Kalogerakis N., Dholabhai P.D., Bishnoi P.R. (1987a) *Kinetics of Formation of Methane and Ethane Gas Hydrates*, Chemical Engineering Science, 42(11):2647–2658.

Englezos P., Kalogerakis N., Dholabhai P.D., Bishnoi P.R. (1987b) *Kinetics of Gas Hydrate Formation from Mixtures of Methane and Ethane*, Chemical Engineering Science, 42(11):2659–2666.

Florusse L.J., Peters C.J., Schoonman J., Hester K.C., Koh C.A., Dec S.F., Marsh K.N., Sloan E.D. (2004) *Stable Low-Pressure Hydrogen Clusters Stored in a Binary Clathrate Hydrate*, Science, 306:469–471.

Freer E.M., Selim M.S., Jr. E.D.S. (2001) *Methane hydrate film growth kinetics*, Fluid Phase Equilibria, 185:65–75.

Gaudette J., Servio P. (2007) *Measurement of Dissolved Propane in Water in the Presence of Gas Hydrate*, J. Chem. Eng. Data, 52(4):1449–1451.

Gentzis T. (2000) *Subsurface sequestration of carbon dioxide - an overview from an Alberta (Canada) perspective*, International Journal of Coal Geology, 43:287–305.

Giavarini C., Maccioni F., Santarelli M.L. (2003) *Formation Kinetics of Propane Hydrates*, Ind. Eng. Chem. Res., 42:1517–1521.

Gudmundsson J.S., Parlaktuna M., Khokhar A. (1994) *Storing Natural Gas as Frozen Hydrate*, SPE Production Facilities, February:69–73.

Gupta A.K., Bishnoi P.R., Kalogerakis N. (1991) *A method for the simultaneous phase equilibria and stability calculations for multiphase reacting and non-reacting systems*, Fluid Phase Equilibria, 63:65–89.

Hammerschmidt E. (1934) *Formation of Gas Hydrates in Natural Gas Transmission Lines*, Industrial And Engineering Chemistry, 26:851–855.

Handa Y.P. (1990) *Effect of Hydrostatic Pressure and Salinity on the Stability of Gas Hydrates*, J. Phys. Chem., 94:2652–2657.

Harrison W.J., Wendlandt R.F., Sloan E.D. (1995) *Geochemical interactions resulting from carbon dioxide disposal on the seafloor*, Applied Geochemistry, 10:461–475.

Hashemi S., Macchi A., Bergeron S., Servio P. (2006) *Prediction of Methane and Carbon Dioxide Solubility in Water in the Presence of Hydrate*, Fluid Phase Equilibria, 246:131–136.

Hashemi S., Macchi A., Servio P. (2007a) *Dynamic Simulation of Gas Hydrate Formation in an Agitated Three-Phase Slurry Reactor*, in *2007 ECI Conference on The 12th International Conference on Fluidization - New Horizons in Fluidization Engineering*, Vancouver, Canada, pp. 329–336.

Hashemi S., Macchi A., Servio P. (2007b) *Gas Hydrate Growth Model in a Semibatch Stirred Tank Reactor*, Industrial And Engineering Chemistry Research, 46:5907–5912.

Hayduk W., Laudie H. (1974) *Prediction of Diffusion Coefficients for Nonelectrolytes in Dilute Aqueous Solutions*, AIChE Journal, 20(3):611–615.

Herri J., Gruy F., Pic J., Cournil M., Cingotti B., Sinquin A. (1999a) *Interest of in situ turbidimetry for the characterization of methane hydrate crystallization: Application to the study of kinetic inhibitor*, Chemical Engineering Science, 54:1849–1858.

Herri J., Pic J., Gruy F., Cournil M. (1999b) *Methane Hydrate Crystallization Mechanism from In-Situ Particle Sizing*, AIChE Journal, 45(3):590–602.

Hirai H., Tanaka T., Kawamura T., Yamamoto Y., Yagi T. (2004) *Structural changes in gas hydrates and existence of a filled ice structure of methane hydrate above 40 GPa*, Journal of Physics and Chemistry of Solids, 65:1555–1559.

Holder G.D., Corbin G., Papadopoulos K.D. (1980) *Thermodynamic and Molecular Properties of Gas Hydrates from Mixtures Containing Methane, Argon and Krypton*, Ind. Eng. Chem. Res., 19:282–286.

Holder G.D., Cugini A.V., Warzinski R.P. (1995) *Modeling of clathrate hydrate formation during carbon dioxide injection into the ocean*, Environ. Sci. Technol., 29:276–278.

Isaacs N.S. (1981) *Liquid Phase High Pressure Chemistry*, Jon Wiley Sons Inc.

IUPAC-NIST (various years) *Solubility Data Series*, Journal of Physical and Chemical Reference Data.

Jean-Baptiste P., Ducroux R. (2003) *The role of CO2 capture and sequestration in mitigating climate change*, C.R. Geoscience, 335:611–625.

Jensen L., Thomsen K., Solms N.v. (2008) *Propane hydrate nucleation: Experimental investigation and correlation*, Chemical Engineering Science, 63:3069–3080.

Kane S., Evans T., Brian P., Sarofim A. (1974) *Determination of the Kinetics of Secondary Nucleation in Batch Crystallizers*, AIChE Journal, 20:855–862.

Kang S.P., Lee H., Ryu B.J. (2001) *Enthalpies of dissociation of clathrate hydrates of carbon dioxide, nitrogen, (carbon dioxide + nitrogen), and (carbon dioxide + nitrogen + tetrahydrofuran)*, Journal of Chemical Thermodynamics, 33:513–521.

Karpinski P.H. (1980) *Crystallization as a mass transfer phenomenon*, Chemical Engineering Science, 35:2321–2324.

Kelland M.A. (2006) *History of the Development of Low Dosage Hydrate Inhibitors*, Energy Fuels, 20(3):825–847.

Kennet J.P., Cannariato K.G., Hendy I.L., Behl R.J. (2002) *Methane Hydrates in Quaternary Climate Change: The Clathrate Gun Hypothesis*, American Geophysical Union, Washington, DC.

Ketcham W., Hobbs P. (1969) *An Experimental Determination of the Surface Energies of Ice*, Philosophical Magazine, 19:1161–1173.

Kim H., Bishnoi P., Heidemann R., Rizvi S. (1987) *Kinetics of methane hydrate decomposition*, Chemical Engineering Science, 42:1646–1653.

Kim Y.S., Ryu S.K., Yang S.O., Lee C.S. (2003) *Liquid water-hydrate equilibrium measurements and unified predictions of hydrate containing phase equilibria for methane, ethane, propane, and their mixtures*, Ind. Eng. Chem. Res., 42:2409–2414.

Klauda J.B., Sandler S.I. (2005) *Global Distribution of Methane Hydrate in Ocean Sediment*, Energy Fuels, 19:459–470.

Kluytmans J., Wachem B.v., Kuster B., Schouten J. (2003) *Mass transfer in sparged and sittred reactors: influence of carbon particles and electrolyte*, Chemical Engineering Science, 58:4719–4728.

Koh C.A., Sloan E. (2007) *Natural Gas Hydrates: Recent Advances and Challenges in Energy and Environmental Applications*, AIChE Journal, 53(7):1636–1643.

Kvamme B. (2000) *A Unified Nucleation Theory for the Kinetics of Hydrate Formation*, Annals of the New York Academy of Sciences, 912:496–501.

Kvenvolden K.A. (1995) *A review of the geochemistry of methane in natural gas hydrate*, Org. Geochem., 23:997–1008.

Lackner K.S. (2003) *A Guide to CO2 Sequestration*, Science, 300:1677–1678.

Lee H., Lee J.w., Kim D.Y., Park J., Seo Y.T., Zeng H., Moudrakovski I.L., Ratcliffe C.I., Ripmeester J.A. (2005) *Tuning clathrate hydrates for hydrogen storage*, Nature, 434:743–746.

Lekvam K., Bishnoi P.R. (1997) *Dissolution of methane in water at low temperatures and intermediate pressures*, Fluid Phase Equilibria, 131:297–309.

Long J., Sloan E. (1996) *Hydrates in the Ocean and Evidence for the Location of Hydrate Formation*, International Journal of Thermophysics, 17:1–13.

Lu W., Chou I.M., Burruss R.C. (2008) *Determination of methane concentrations in water in equilibrium with sI methane hydrate in the absence of a vapor phase by in situ Raman spectrocospy*, Geochimica et Cosmochimica, 72:412–422.

Makogon Y. (1987) *Gaseous hydrates: the frozen energy*, La Recherche, 18(192):1192–1200.

Malegaonkar M.B., Dholabhai P.D., Bishnoi P.R. (1997) *Kinetics of Carbon Dioxide and Methane Hydrate Formation*, The Canadian Journal of Chemical Engineering, 75:1090–1099.

Mao W.L., Koh C.A., Sloan E. (2007) *Clathrate hydrates under pressure*, Physics Today, (October):42–47.

Mark T.C., McMullan R.K. (1965) *Polyhedral Clathrate Hydrates. X. Structure of the Double Hydrate of Tetrahydrofuran and Hydrogen Sulfide*, The Journal of Chemical Physics, 42:2732–2737.

McMullan R.K., Jeffrey G. (1965) *Polyhedral Clathrate Hydrates. IX. Structure of Ethylene Oxide Hydrate*, The Journal of Chemical Physics, 42:2725–2732.

Milkov A.V. (2004) *Global estimates of hydrate-bound gas in marine sediments: how much is really out there?*, Earth-Science Reviews, 66:183–197.

Monfort J., Nzihou A. (1993) *Light scattering kinetics study of cyclopropane hydrate growth*, Journal of Crystal Growth, 128:1182–1186.

Mori T., Mori Y. (1989) *Characterization of gas hydrate formation in direct-contact cool storage process*, Rev. Int. Froid, 12:259–265.

Mork M., Gudmundsson J.S. (2002) *Hydrate Formation Rate in a Continuous Stirred Tank Reactor: Experimental Results and Bubble-to-Crystal Model*, in *Proceedings of the Fourth International Conference on Gas Hydrates*, Yokohama, pp. 813–818.

Mullin J. (1997) *Crystallization*, 3rd ed., Butterworth-Heinemann, Oxford.

Natarajan V., Bishnoi P.R., Kalogerakis N. (1994) *Induction Phenomena in Gas Hydrate Nucleation*, Chemical Engineering Science, 49(13):2075–2087.

Nerheim A.R., Svarlaas T.M., Sammuelsen E.K. (1992) *Investigation of hydrate kinetics in the nucleation and early growth phase by laser light scattering*, in *Second International Offshore and Polar Engineering Conference*, San Francisco, pp. 620–627.

Ohmura R., Mori Y.H. (1999) *Comments on Solubility of Liquid CO2 in Synthetic Sea Water at Temperatures from 278 K to 293 K and Pressures from 6.44 MPa to 29.49 MPa, and Densities of the Corresponding Aqueous Solutions*, J. Chem. Eng. Data, 44:1432–1433.

Parrish W.R., Prausnitz J.M. (1972) *Dissociation Pressures of Gas Hydrates Formed by Gas Mixtures*, Ind. Eng. Chem. Res., 11:26–34.

Peng D.Y., Robinson D.B. (1976) *A New Two-Constant Equation of State*, Ind. Eng. Chem. Fundam., 15:59–64.

Perry R.H., Green D.W. (1997) *Perry's Chemical Engineer's Handbook*, seventh ed., McGraw-Hill.

Phillips J.B., Nguyen H., John V.T. (1991) *Protein Recovery from Reversed Micellar Solutions through Contact with a Pressurized Gas Phase*, Biotechnol. Prog., 7:43–48.

Redlich O., Kwong J. (1949) *On The Themodynamics of Solutions. V: An Equation of State. Fugacities of Gaseous Solutions*, Chemical Review, 44:233–244.

Ribeiro C.P., Lage P.L. (2008) *Modelling of hydrate formation kinetics: State-of-the-art and future directions*, Chemical Engineering Science, 63:2007–2034.

Ripmeester J.A., Tse J.S., Ratcliffe C.I., Powell B.M. (1987) *A new clathrate hydrate structure*, Nature, 325:135–136.

Schroeder W. (1927) *Die Geschichte der Gas Hydrate*, Sammlung. Chem. Tech. Vortrage, 29:98.

Seo Y., Lee H. (2002) *Hydration number and two-phase equilibria of CH4 hydrate in deep ocan sediments*, Geophysical research letters, 29:85–1–85–4.

Servio P., Englezos P. (2001) *Effect of temperature and pressure on the solubility of carbon dioxide in water in the presence of gas hydrate*, Fluid Phase Equilibria, 190:127–134.

Servio P., Englezos P. (2002) *Measurement of Dissolved Methane in Water in Equilibrium with its Hydrate*, J. Chem. Eng. Data, 47:87–90.

Skovborg P., Rasmussen P. (1994) *A Mass Transport Limited Model for the Growth of Methane and Ethane Gas Hydrates*, Chemical Engineering Science, 49(8):1131–1143.

Sloan E. (1998a) *Clathrate Hydrates of Natural Gases*, 2nd ed., Marcel Dekker Inc., New York.

Sloan E. (1998b) *Gas Hydrates: Review of Physical/Chemical Properties*, Energy Fuels, 12:191–196.

Sloan E., Koh C.A. (2007) *Clathrate Hydrates of Natural Gases*, 3rd ed., CRC Press.

Sloan E.D. (2003) *Fundamental principles and applications of natural gas hydrates*, Nature, 426:353–359.

Someya S., Bando S., Chen B., Song Y., Nishio M. (2005) *Measurement of CO2 solubility in pure water and the pressure effect on it in the presence of clathrate hydrate*, International Journal of Heat and Mass Transfer, 48:2503–2507.

Stoll R.D., Bryan G.M. (1979) *Physical Properties of Sediments Containing Gas Hydrates*, Journal of Ceophysical Research, 84:1629–1634.

Suess E., Bohrmann G., Greinert J., Lausch E. (1999) *Flammable Ice*, Scientific American, (November):76–83.

Takaoki T., Hirai K., Kamei M., Kanda H. (2005) *Study of natural gas hydrate (NGH) carriers*, in *Proceedings of the Fift International Conference on Gas Hydrates*, Trondheim, Norway.

Teng H., Yamasaki A. (1998) *Solubility of Liquid CO2 in Synthetic Sea Water at Temperatures from 278 K to 293 K and Pressures from 6.44 MPa to 29.49 MPa, and Densities of the Corresponding Aqueous Solutions*, J. Chem. Eng. Data, 43:2–5.

Tester J.W., Modell M. (1997) *Thermodynamics and Its Applications*, 3rd ed., Prentice-Hall, New Jersey.

Thomas S., Dawe R.A. (2003) *Review of ways to transport natural gas energy from countries which do not need the gas for domestic use*, Energy, 28:1461–1477.

Trebble M., Bishnoi P. (1987) *Development of a new four-parameter cubic equation of state*, Fluid Phase Equilibria, 35:1–18.

Trebble M., Bishnoi P. (1988) *Extension of the Trebble-Bishnoi Equation of State to Fluid Mixtures*, Fluid Phase Equilibria, 40:1–21.

Villard P. (1895) *Acetylene and its Hydrate*, Comptes Rendus, 120:1262–1265.

Vysniauskas A., Bishnoi P. (1983) *A kinetic study of methane hydrate formation*, Chemical Engineering Science, 38(7):1061–1072.

Vysniauskas A., Bishnoi P. (1985) *Kinetics of ethane hydrate formation*, Chemical Engineering Science, 40(2):299–303.

Waals J.V.d., Platteeuw J. (1959) *Clathrate Solutions*, Advances in Chemical Physics, 2:1–57.

Warren S.G. (1984) *Optical constants of ice from the ultraviolet to the microwave*, Applied Optics, 23(8):1206–1225.

Werezak G.N. (1969) *Aqueous solution concentration by a clathrate type of gas hydrate formation*, Chemical Engineering Progress Symposium Series, 65:6–18.

Wilke C., Chang P. (1955) *Correlation of diffusion coefficients in dilute solutions*, AIChE Journal, 1(2):264–270.

Wilson P., Lester D., Haymet A. (2005) *Heterogeneous nucleation of clathrates from supercooled tetrahydrofuran (THF)/water mixtures, and the effect of an added catalyst*, Chemical Engineering Science, 60:2937–2941.

Yang S., Yang I.M., Kim Y.S., Lee C.S. (2000) *Measurement and prediction of phase equilibria for water + CO2 in hydrate forming conditions*, Fluid Phase Equilibria, 175:75–89.

Yang S., Cho S., Lee H., Lee C. (2001) *Measurement and prediction of phase equilibria for water + methane in hydrate forming conditions*, Fluid Phase Equilibria, 185:53–63.

Zatsepina O.Y., Buffett B.A. (1997) *Phase equilibrium of gas hydrate: Implications for the formation of hydrate in the deep sea floor*, Geophysical research letters, 24(13):1567–1570.